Year : 2018

COMBINING FLUORESCENCE AND ELECTROPHYSIOLOGY MEASUREMENTS TO STUDY ASIC FUNCTION

Vullo Sabrina

UNIL | Université de Lausanne

Faculté de biologie
et de médecine

Département de Pharmacologie et Toxicologie

**COMBINING FLUORESCENCE AND ELECTROPHYSIOLOGY
MEASUREMENTS TO STUDY ASIC FUNCTION**

Thèse de doctorat ès sciences de la vie (PhD)

présentée à la

Faculté de biologie et de médecine
de l'Université de Lausanne

par

Sabrina VULLO

Master en Biologie, Università degli Studi di Pavia

Jury

Prof., Luc Tappy, Président
Dr. Stephan Kellenberger, Directeur de thèse
Dr. Ruud Hovius, expert
Dr. Michael Pusch, expert

Lausanne 2018

Imprimatur

Vu le rapport présenté par le jury d'examen, composé de

Président·e	Monsieur	Prof. Luc **Tappy**
Directeur·rice de thèse	Monsieur	Dr Stephan **Kellenberger**
Experts·es	Monsieur	Dr Ruud **Hovius**
	Monsieur	Dr Michael **Pusch**

le Conseil de Faculté autorise l'impression de la thèse de

Madame Sabrina Vullo
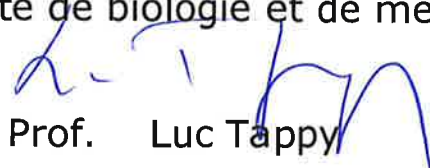
Master Università degli Studi di Pavia, Italie

intitulée

Combining fluorescence and electrophysiology measurements to study ASIC function

Lausanne, le 31 janvier 2019

pour le Doyen
de la Faculté de biologie et de médecine

Prof.   Luc Tappy

Table of Contents

Acknowledgments

I would like to express my warmest gratitude to all those persons whose comments, questions, ideas, criticism, suggestions, have contributed immensely to my personal and scientific growth.

First and foremost, I wish to express my deepest gratitude to my supervisor, Dr. Stephan Kellenberger, for his excellent guidance and continuous support throughout this journey for the past years. Thank you for providing a pleasant research environment, intellectually stimulating and professionally rewarding. Thank you for always having your door open, for "illuminating a path through the fog", for your wise advice, and for your precious help during the writing of my thesis. Thank you for everything. It has been a great pleasure to be under your wings during my PhD.

I would also like to thank my thesis committee members: Prof. Luc Tappy, Dr. Ruud Hovius and Dr. Michael Pusch, for their time, interest, and for helpful comments.

Special thanks go to Gaetano for his support and encouragement when I took the first steps of my PhD. The few months we spent together in the lab have probably been the most important of my PhD. Thank you for revealing me all the secrets of the VCF!

I am also very grateful to Sophie, Omar, Karolina, Anand, Zhong, Nicolas and Olivier. Thank you for providing skillful help and for making time in the lab enjoyable. Thank you for your friendships as well as good advice and for the nice moments spent together, also outside the lab.

I would like to thank all the members of the Department of Pharmacology and Toxicology of Lausanne, especially Prof. Laurent Schild, Dr. Miguel van Bemmelen and Ivan Gautschi for their technical and scientific support, and all people I had the pleasure to know during these years.

I am especially grateful to my family and close friends. To my parents, for all their love and never-ending support over these years. To my Dad, Calogero, a great source of wisdom and knowledge, thank you for always believing in me; and to my Mom, Maria Giovanna, my pillar of strength and faith, thank you for your continous encouragements and for always bringing a sense of calmness.
Special thanks to my brother, Giuseppe, and his girlfriend, Roberta. Thank you for your support during these years and for the very nice moments we spent together.

I reserve my greatest gratitude for the most constant presence of this journey, my "photonic" love Ivan. Thank you for having been always by my side since the first day of my PhD. For your unbelievable support, help, patience and encouragement. You, more than anyone else, experienced joys and pitfalls of my PhD. Thank you for being always there when I needed you, and for sharing with me your knowledge in many discussions about the physics of fluorescence! My gratitude to you is beyond words.

Abstract

Acid-Sensing Ion Channels (ASICs) are trimeric proton-gated and sodium-conducting channels widely expressed in neurons of the central and peripheral nervous systems. They contribute as pH sensors to a number of physiological and pathological conditions, such as learning, neurodegeneration after ischemia, and pain sensation. ASICs open transiently upon a lowering of the extracellular pH, before they enter a non-conductive desensitized state. Chicken ASIC1a structures have been solved in the closed, open and desensitized states. Despite the large amount of available information on the structure and function of ASICs, the precise proton binding sites and the mechanisms by which protonation promotes channel opening are still poorly defined. The acidic pocket, a cavity in the extracellular domain containing several negatively charged amino acids, has been proposed as the primary site for proton sensing. Concerning the molecular mechanisms, it is generally thought that protonation events on extracellular residues induce conformational changes that transmit the "activation signal" to the pore to control the opening of the channel gate. In the first part of this project, we asked whether protonation in the acidic pocket and palm domain is required for channel activation. We found that combination of neutralizing mutations of a large number of titratable acidic pocket residues produced channels that retained their proton sensitivity, suggesting that the residues that are essential for proton sensing are located in other domains. Concomitant with these experiments, we employed the voltage-clamp fluorometry (VCF) technique to investigate the structural rearrangements in the acidic pocket. Our VCF analysis indicates that this region undergoes conformational changes during both activation and desensitization. In the palm, neutralizing mutations of several acidic residues impaired channel desensitization, leading, in some cases, to the disappearance of the transient ASIC component and to the appearance of a sustained current component. In the second part of the project, we elucidated the structural rearrangements occurring in key channel regions during ASIC1a activity. Our VCF experiments reveal the presence of conformational changes in the wrist and palm domain consistent with a role of these regions in channel activation and desensitization.

In summary, our studies suggest that the acidic pocket is not the primary site for proton sensing in ASIC1a, but has, rather, a modulatory role. We show, in addition, that proton binding to the extracellular domain of ASIC1a induces conformational changes in the palm and in the wrist regions most likely important for transmitting the transduction signal to the channel gate. Our findings provide new insights on the basic mechanisms controlling ASIC activity and may be relevant for other members of ENaC/DEG family, to which ASICs belong.

Résumé

Les canaux sensibles aux protons (ASICs) sont des canaux sodiques activés par les protons. Ils sont largement exprimés dans les neurones du système nerveux central et périphérique. Ils contribuent en tant que senseurs de pH à un certain nombre de conditions physiologiques et pathologiques, telles que l'apprentissage, la neurodégénérescence après l'ischémie et la sensation de douleur. Les ASICs s'ouvrent de manière transitoire lors d'un abaissement du pH extracellulaire, avant d'entrer dans un état désensibilisé non conducteur. Les structures d'ASIC1a de poulet ont été résolues dans des états fermés, ouverts et désensibilisés. Malgré la grande quantité d'informations disponible sur la structure et la fonction des ASIC, les sites précis de liaison des protons et les mécanismes par lesquels la protonation induit l'ouverture du canal ASIC sont encore très peu définis. La poche acide, une cavité dans le domaine extracellulaire contenant plusieurs acides aminés chargés négativement, a été proposée être le site primaire pour la détection des protons. En ce qui concerne les mécanismes moléculaires de l'activation des ASICs, on pense généralement que les évènements de protonation sur les résidus extracellulaires induisent des changements conformationnels qui transmettent le «signal d'activation» au pore afin de contrôler l'ouverture du canal. Dans la première partie de ce projet, nous avons investigué si la protonation dans la poche acide et dans le domaine de la paume était nécessaire pour l'activation du canal. Nous avons constaté que la combinaison de mutations neutralisantes d'un grand nombre de résidus titrables dans la poche acide produisait des canaux qui conservaient leur sensibilité aux protons, suggérant que les résidus essentiels à la détection de protons se situaient dans d'autres domaines. Parallèlement à ces expériences, nous avons utilisé la technique de "voltage-clamp fluorometry" (VCF) pour étudier les réarrangements structurels dans la poche acide. Notre analyse par VCF indique que cette région subit des changements conformationnels lors de l'activation et de la désensibilisation. Dans la paume, des mutations neutralisantes de plusieurs résidus acides ont altéré la désensibilisation des canaux, conduisant, dans certains cas, à la disparition de la composante transitoire du courant d'ASIC et à l'apparition d'une composante soutenue. Dans la deuxième partie du projet, nous avons élucidé les réarrangements structurels intervenant dans des régions clés pendant l'activité de ASIC1a. Nos expériences de VCF révèlent la présence de changements conformationnels dans les domaines du poignet et de la paume au cours de l'activation et la désensibilisation du canal.

En résumé, nos études suggèrent que la poche acide n'est pas le principal site de liaison de protons dans ASIC1a, mais joue plutôt un rôle de modulateur. Nous montrons, en outre, que la

liaison de protons au domaine extracellulaire de ASIC1a induit des changements de conformation dans la paume et dans les régions du poignet, probablement importants pour la transmission du signal d'activation au pore du canal. Nos résultats fournissent de nouvelles informations sur les mécanismes de base contrôlant l'activité des ASICs et peuvent être pertinents pour d'autres membres de la famille des canaux épithéliaux sodiques / dégénerines, à laquelle les ASICs appartiennent.

Résumé à un large public

Chaque cellule vivante est délimitée par une membrane plasmatique qui sépare le contenu interne de son environnement. La membrane cellulaire est nécessaire pour réguler les échanges de substances entre les deux compartiments. Pour traverser la membrane, les ions nécessitent la présence de protéines de transport spéciales, appelés canaux ioniques. Différents canaux ioniques peuvent être activés par différents ligands, c'est-à-dire des molécules qui se lient au canal pour l'activer. Les canaux ioniques sensibles aux protons (ASICs) représentent une classe importante de canaux ioniques présents dans les neurones et activés par les ligands les plus simples possibles : les protons ! L'ouverture de ces canaux permet le passage des ions sodium dans la cellule et facilite la communication avec d'autres neurones. De nombreuses études ont montré que ces canaux jouent un rôle important dans l'apprentissage, la dégénérescence neuronale et la sensation de douleur. Pour pouvoir influencer l'activité de ces canaux, il est donc très important de comprendre les mécanismes qui sont à la base de leur activité. Il a été proposé que les protons se lient à différents sites du canal et que cette liaison induit des changements de conformation qui sont transmis au pore pour ouvrir le canal. Où les protons se lient-ils pour activer les ASICs ? Et quels types de mouvements conduisent à l'ouverture ou à la fermeture du canal ? Dans mon projet, j'ai découvert qu'une région considérée comme importante pour activer les ASICs joue, en réalité, un rôle marginal dans l'ouverture de ces canaux, suggérant que les protons se lient à d'autres régions du canal pour l'ouvrir. De plus, j'ai utilisé une technique qui permet de détecter les mouvements du canal afin de pouvoir comprendre quelles régions sont importantes pour son activité. Grâce à cette technique, j'ai pu observer des changements de conformation dans différents domaines, qui pourraient être importants pour la transmission du message d'ouverture au pore du canal. Ces régions peuvent donc être des cibles potentielles pour des médicaments. Mes résultats fournissent également des indices sur la régulation d'autres canaux appartenant à la même famille que les ASICs.

List of abbreviations

ΔF= change in fluorescence signal
τ= time constant
AF488= alexa fluor® 488 C5-maleimide
APETx2: sea anemone peptide toxin 2
ASIC: acid-sensing ion channel
BASIC: bile acid-sensitive ion channel
BLINaC: brain liver intestine sodium channel
BNaC: brain sodium channel
cASIC1a: chicken ASIC1a
CF488A= CF^{TM} 488A maleimide
CNS: central nervous system
COX: cyclooxygenase
COVG: cut-open vaseline gap
cryoEM: cryogenic electron microscopy
DEG= degenerin
DRG: dorsal root ganglion
ECD: extracellular domain
EC_{50}: half maximal effective concentration
ENaC: epithelial sodium channel
EPSC: excitatory postsynaptic current
Fτ: fluorophore lifetime
FaNaC: FMRF-amide-gated sodium channel
fASIC1a: fish ASIC1a
FMRFamide: Phe-Met-Arg-Phe amide
fUAAs: fluorescent unnatural amino acids
GMQ: 2-guanidine-4-methylquinazoline
H^+-ATPase: proton adenosine triphosphatase
hASIC1a: human ASIC1a
hiNaC: human intestine sodium channel
IC_{50}: half maximal inhibitory concentration
KO: knockout
lASIC1: lamprey ASIC1
LRET: luminescence resonance energy transfer
LTD: long-term depression
LTP: long-term potentiation
MEC-4: mechanosensory abnormal
MCAO: middle cerebral artery occlusion
mRNA: messenger ribonucleic acid
MitTx: *Micrurus tener tener* toxin

MTSET= 2-(trimethylammonium)ethyl methanethiosulfonate, Bromide
Nav: voltage-gated sodium channel
nH: Hill coefficient
NMA: normal mode analysis
NMDA: N-Methyl-D-aspartic acid
NSAID: non-steroidal anti-inflammatory drug
PHA-1: pseudohypoaldosteronism type 1
PcTx1: psalmotoxin 1
pH_{50}: half maximal effective concentration of protons
PNS: peripheral nervous system
PPK: pickpocket
rASIC1a: rat ASIC1a
sASIC1b: shark ASIC1b
SSD: steady-state desensitization
TEVC= two-electrode voltage clamp
TM= transmembrane domain
TMRM= tetramethylrhodamine-5-maleimide
TRPV1: transient receptor potential vanilloid 1
VCF= voltage-clamp fluorometry
WT: wild type
xASIC1.1: *Xenopous* ASIC1.1
zASIC4: zebrafish ASIC4

1. Introduction

Every living cell is delimited by a plasma membrane consisting of a lipophilic lipid bilayer that separates the inner content of the cell from the surrounding environment. The cell membrane constitutes, thus, a protective barrier around the cell and it is necessary to regulate the exchange of substances between the two compartments. Small or liposoluble uncharged molecules, such as oxygen, carbon dioxide and small lipids, can easily cross the cell membrane, whereas ions, amino acids, or other big molecules require the presence of special transport proteins that allow this process. Ion channels are integral membrane proteins that form water-filled pores allowing the movements of inorganic ions, such as Na^+, K^+, Ca^{2+}, Cl^-, through the lipid bilayer. They can be classified based on two main properties: the ion selectivity and the mechanism of activation. The ion selectivity is determined by the diameter of the pore and by the electrical charge of the amino acids lining the pore at its narrowest part, which constitutes the selectivity filter. Therefore, it is possible to distinguish highly selective channels for a specific ion and nonselective channels that allow the passage of ions that share similar size and charge (Hille, 2001). The term "gating" refers to all mechanisms leading to the opening or closing of an ion channel. Based on this property, it is possible to distinguish channels that are constitutively open, channels regulated by chemical signals, for example binding of extracellular ligands or intracellular messengers, and channels that open in response to specific stimuli, such as change in the membrane potential or application of mechanical forces.

The Acid-Sensing Ion Channels (ASICs) represent an important class of ion channels activated by the simplest ligands possible: protons! Several studies suggest that they are importantly involved in numerous physiological processes, such as learning and memory, fear behaviour, pain sensation, and pathological conditions, such as neurodegeneration after ischemic stroke, epileptic seizures, multiple sclerosis, and tumor development. For these reasons, they have

drawn large attention as targets of novel therapeutic agents for the treatment of various neurological disorders.

1.1 Acid-Sensing Ion Channels (ASICs)

1.1.1 The Superfamily of DEG/ ENaC ion channels

The « Degenerin (DEG)/Epithelial Na$^+$ Channel (ENaC)» superfamily was discovered at the beginning of the 1990s. The members of this family are exclusively present in animals of the metazoan kingdom and differ in terms of gating mechanisms, ion selectivity and physiological functions. The DEG/ENaC family comprises three main subfamilies: degenerin channels, ENaC and ASICs, and several smaller subfamilies (Kellenberger and Schild, 2002).

The degenerin channels have been identified in *C. elegans* neurons where they open in response to mechanical stimuli and constitute an important component of the mechanotransduction machinery. The term "degenerin", attributed to these channels, derives from the observation that nematodes harboring gain-of-function mutations of the genes DEG-1 and MEC-4, encoding the channel parts of mechanosensitive protein complexes, produced constitutively open channels whose functional properties were dramatically perturbed, leading to a progressive degeneration of sensory neurons expressing these mutated channels (Chalfie and Wolinsky, 1990a).

The subfamily of ENaC channels includes four subunits: α-, β-, γ- and δ-ENaC. The α-ENaC subunit was cloned at about the same time as the identification of the degenerin channels in *C. elegans*, with which it shares high sequence homology, suggesting a common channel family (Canessa et al., 1993; Chalfie and Wolinsky, 1990b; Lingueglia et al., 1993). ENaCs are amiloride-sensitive, voltage independent and high Na$^+$-selective channels. In the distal nephron, they are expressed at the apical membrane of the epithelial cells where they play a crucial role in Na$^+$ reabsorption. Indeed, mutations of ENaC genes have been shown to dramatically impair

Na$^+$ homeostasis, leading to the development of renal diseases (Hansson et al., 1995; Inoue et al., 1998; Rossier et al., 2002).

The first acid-evoked ASIC current was recorded in the 1980s in neurons isolated from rat trigeminal ganglia (Krishtal and Pidoplichko, 1980). ASICs were cloned by sequence homology of about 25% to ENaC and were initially named Brain Na$^+$ Channels (BNaC), since their genes were found to be expressed mainly in the central and peripheral nervous systems (Garcia-Anoveros et al., 1997; Price et al., 1996). After the discovery of their activation by extracellular protons, these channels were named acid-sensing ion channels (ASICs) (Waldmann et al., 1997a). Mutagenesis and functional studies suggest that ASICs are conserved throughout the superphylum Deuterostome, being reported in all the three phyla Chordata, Echinodermata and Hemichordata (Coric et al., 2008; Lynagh et al., 2018). Binding of extracellular protons to several ASIC domains induces channel opening and allows Na$^+$ ions enter the channel. Sodium entry leads to membrane depolarization and generation of action potentials in neurons, suggesting that ASICs might be involved in the regulation of neuronal activity (Deval et al., 2003; Vukicevic and Kellenberger, 2004).

The DEG/ENaC family includes also other related smaller subfamilies, such as the mammalian hiNaC and its ortholog BLINaC in rodents, recently renamed BASIC (for «Bile Acid-Sensitive Ion Channel»); the FMRF-amide-gated sodium channel (FaNaC), an excitatory ion channel cloned from the mollusk *Helix aspersa*; and *Drosophila* ENaC/DEG channels, such as pickpocket (PPK) (Adams et al., 1998; Kellenberger and Schild, 2002; Lingueglia et al., 1995; Wiemuth et al., 2012).

1.1.2 ASIC subunits and their tissue distribution

ASICs are widely expressed in both central and peripheral nervous systems (CNS and PNS) where they act as proton sensors and contribute to several physiological and pathological

conditions. Four genes in mammals, including ACCN2, ACCN1, ACCN3 an ACCN4, encode at least six different ASIC subunits: ASIC1a, ASIC1b, ASIC2a, ASIC2b, ASIC3 and ASIC4. ASIC1a and ASIC1b are splice variants of the ACCN2 gene, while ASIC2a and ASIC2b are splice variants of the ACCN1 gene. In humans, ASIC3 has three splice variants: ASIC3a, -3b and -3c (Delaunay et al., 2012).

The tissue distribution differs among subunits: ASIC1a, -2a, and -2b have been detected in both central and peripheral nervous systems, while ASIC1b and ASIC3 have been found exclusively in the peripheral neurons so far (Kellenberger and Schild, 2015), except for human ASIC3 that has also been reported in the CNS (Delaunay et al., 2012). ASIC4 has been detected throughout the CNS, but shows strongest expression in the pituitary gland (Akopian et al., 2000; Gründer et al., 2000).

Individual ASIC subunits co-assemble into homo- or heterotrimeric functional channels. In neurons of the central nervous system, ASICs can assemble to form homomeric ASIC1a, heteromeric ASIC1a/2a or ASIC1a/2b. A recent study shows that in living cells heteromeric ASIC1a/2a channels may have a flexible stoichiometry: they can be composed of 2 ASIC1a and 1 ASIC2a subunit or vice versa (Bartoi et al., 2014).

ASICs are cation channels activated by acidic pH changes. However, homomeric ASIC2b and ASIC4 do not form functional homomeric proton-gated channels and their function requires further investigation (Akopian et al., 2000; Gründer et al., 2000; Lingueglia et al., 1997). There is evidence showing that ASIC4 can associate with ASIC1a and ASIC3 to down regulate their expression at the cell membrane (Donier et al., 2008; Lin et al., 2015). In contrast, ASIC2b can assemble with other ASIC channel subunits to form heteromeric channels with distinct functional properties (Deval et al., 2004; Lingueglia et al., 1997). It is unclear why these channels do not respond to extracellular protons. The large ASIC extracellular loop suggests the existence of other non-proton ligands. It is possible, thus, that homomeric ASIC2b and

ASIC4 have their own specific ligands. Surprisingly, unlike rat ASIC4, zebrafish ASIC4.1 (zASIC4), but not zASIC4.2, can form functional homomeric channels in zebrafish neurons that are gated by extracellular protons; the same study showed also that the post-TM1 domain is responsible for the different activation by protons of zASIC 4.1 and 4.2 (Chen et al., 2007). *In situ* hybridization studies have reported ASIC1 mRNA in several regions of the central nervous system, such as the olfactory bulb, the cerebral cortex, the hippocampus, the basolateral amygdaloidal nuclei, the subthalamic nuclei and the cerebellum (Garcia-Anoveros et al., 1997; Waldmann et al., 1997a). At the cellular level, immunohistochemistry studies have shown that in central neurons ASICs localize to the cell body and in the postsynaptic dendritic spines, a favorable position to detect pH fluctuations at the synapse (Wemmie et al., 2002). In contrast to these studies, De la Rosa *et al.* did not find a robust ASIC1 expression in the dendritic spines and axons, but predominantly on the plasma membrane of the soma (de la Rosa et al., 2003). Conclusions regarding the precise ASICs sub-cellular distribution are difficult to make since previous reports are not always in agreement. In peripheral neurons, ASICs have been observed on cell bodies and sensory nerve terminals where they likely contribute to pain and mechanosensations (Wemmie et al., 2003; Wemmie et al., 2002; Zha et al., 2006). Besides the expression in neurons, ASICs have also been detected in glia, cardiomyocytes and osteoclasts, suggesting that they are also likely involved in the physiology of non-neuronal cells (Feldman et al., 2008; Hu et al., 2017; Jahr et al., 2005).

1.1.3 Biophysical properties

Protons are the only physiological ASIC activators identified so far. The functional characteristics of ASICs, such as proton affinity, ion permeability and current kinetics, have been extensively described in heterologous expression systems, like *Xenopous laevis* oocytes and mammalian cell lines, and differ with subunit composition.

Depending on the extracellular pH, ASICs may exist in three different functional states. At physiological pH 7.4, the channel is in a closed (or resting) state, which is a non-conducting state; upon a rapid drop of the extracellular pH, it transiently opens and elicits an inward current due to the passage of Na^+ ions through the channel pore; in the continuous presence of an acidic pH, the channel enters the desensitized state where it fails to respond to additional increase of extracellular protons. This state lasts as long as the pH remains acidic and protects the channel from excessive loading with Na^+ during prolonged acidification. The subsequent application of a more alkaline pH (~7.4) allows the channel recovery within few seconds (Fig. 1A). Some ASICs, such as ASIC2a and ASIC3, display, in addition to their transient component, a sustained current, corresponding to the returning from desensitized to open state. All these channel transitions are summarized in a three-state kinetic scheme shown in Fig. 1B.

ASICs display fast channel activation followed by slower desensitization kinetics. Time constants (τ) of channel opening of ~6-10 ms have been measured for ASIC1a, ASIC1b and ASIC3 in patch-clamp recording with very rapid perfusion system, whereas higher τ values (~400 ms for ASIC1a) have been reported for kinetics of current desensitization at pH close to pH_{50}, reflecting a slow entry of the channel into the desensitized state (Table 1) (Bassler et al., 2001; Li et al., 2010b; Sutherland et al., 2001).
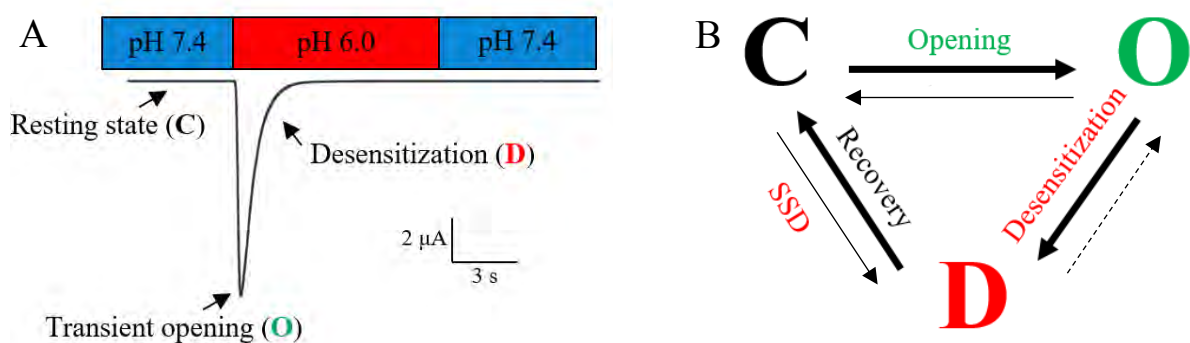
Figure 1. Schematic representation of ASIC gating. A. Representative trace of acid-evoked hASIC1a current measured on *Xenopous* oocytes showing three different functional states. B. ASIC gating scheme. Upon proton binding, ASICs can open generating a transient current and, after a certain time, enter the desensitized state while protons are still bound to the channel. The desensitized state can also be directly reached from the closed state without apparent opening, this transition is known as "steady state desensitization".

The pH_{50} of activation corresponds to the pH that induces half-maximal current and can be determined from a pH-response curve, fit by a Hill function. Among ASICs, ASIC1a and ASIC3 are the most sensitive to extracellular acidification showing a pH_{50} activation of approximately 6.5 (Table 1). In contrast, ASIC2a is less H^+-sensitive with a pH_{50} of ~4.5. For ASIC1a the Hill coefficient (nH) of channel activation is 3-4. nH >1 suggests cooperative binding of more than one proton during the channel activation.

Exposure to slightly acidic extracellular pH (between 7.4 and 6.9) promotes the direct channel transition from the closed to the desensitized state without apparent opening, a process known as «Steady-State Desensitization» (SSD) (Fig. 1B). SSD determines the fraction of channels that are available for opening. The pH_{50} of the SSD can also be fit by a Hill function. For hASIC1a the pH of half-maximal desensitization corresponds to ~7.2, with a Hill coefficient of approximately 10. The fact that the pH50 SSD curve is steeper than that of channel activation, with nH of 10 (compared to ~3 of activation), probably suggests that more residues are involved in the channel desensitization rather than in the activation (Liechti et al., 2010).

	pH$_{50}$ activation	pH$_{50}$ SSD	Desensitization time constant (s)	Sites of expression
ASIC1a	6.2-6.6	~7.2	~0.4	CNS, PNS
ASIC1b	5.9-6.3	~6.7	~0.9	PNS
ASIC2a	4.0-4.9	~5.6	~1.4	CNS, PNS
ASIC3	6.4-6.7	~7.1	~0.3	PNS

Table 1. Biophysical properties and sites of expression vary among different ASIC subunits. ASIC2b and ASIC4 have not been included in the table, as they do not form functional homomeric proton-gated channels. Desensitization time constants were measured at pH close to pH$_{50}$ (Kellenberger and Schild, 2015).

Mutagenesis studies have shown that several mutations affecting the pH dependence of activation were found to change also the pH dependence of the SSD (Bargeton and Kellenberger, 2010; Liechti et al., 2010; Sherwood and Askwith, 2008). A similar interaction between activation and desensitization is observed also in presence of different channel modulators; for example, lowering of extracellular Ca^{2+} concentration or application of the channel gating modifier PcTx1 induces a shift of both the activation and the SSD curves to more alkaline values (Babini et al., 2002; Chen et al., 2006), suggesting that these processes can be structurally coupled (the regions involved in ASIC modulation by Ca^{2+} are described in the paragraph *1.2.3*, subparagraph "*Ion conduction pathway and transmembrane domain*").

ASICs are mainly permeable to Na$^+$ ions. Homomeric ASIC1a and heteromeric ASIC1a/2b have also been reported to conduct Ca^{2+} ions (P$_{Na}$/P$_{Ca}$ ~10), suggesting a possible role of these channels in intracellular signaling and/or in some pathological conditions (Bassler et al., 2001; Samways et al., 2009; Sherwood et al., 2011; Waldmann et al., 1997b). In addition to Na$^+$, transient ASIC current conducts different monovalent cations (Na$^+ \simeq$ Li$^+ >>$ K$^+$; P$_{Na}$/P$_K$ = 10) (Kellenberger and Schild, 2002). ASICs are also highly permeable to H$^+$ (H$^+ >$ Na$^+$), however,

since the H$^+$ concentration is very small (~1 μM at pH 6), the contribution of protons to ASIC current is negligible (Chen and Grunder, 2007).

1.2 Structure

1.2.1 General architecture

The first ASIC crystal structure was solved in 2007 at high resolution (1.9 Å) from a truncated non-functional *Gallus gallus* (chicken) ASIC1a, which shares ~90% homology with the hASIC1a (Jasti et al., 2007). This structure corresponds most likely to the desensitized conformation of the channel since the crystallization was achieved at low pH (pH 5-6) and contains a constricted pore that would not allow the passage of ions. Crystallographic analysis reveals a channel composed of three identical subunits arranged around a central pore (Fig. 2B). Individual ASIC subunits consist of 500-560 amino acids and share a characteristic topology that includes a short intracellular amino- and carboxyl-termini domains (35-90 amino acids), which are however truncated in the structure, two transmembrane α-helices (TM1, TM2), and a large cysteine-rich extracellular loop (~370 amino acids) which is linked to the transmembrane domains (TMDs) via a flexible "wrist". The extracellular domain (ECD) of individual ASIC subunit resembles a clenched hand with five distinct domains, accordingly named: thumb, finger, knuckle, β-ball and palm (Fig. 2A). The structural aspects and functions of the different domains will be explained in more detail in the following subparagraphs.
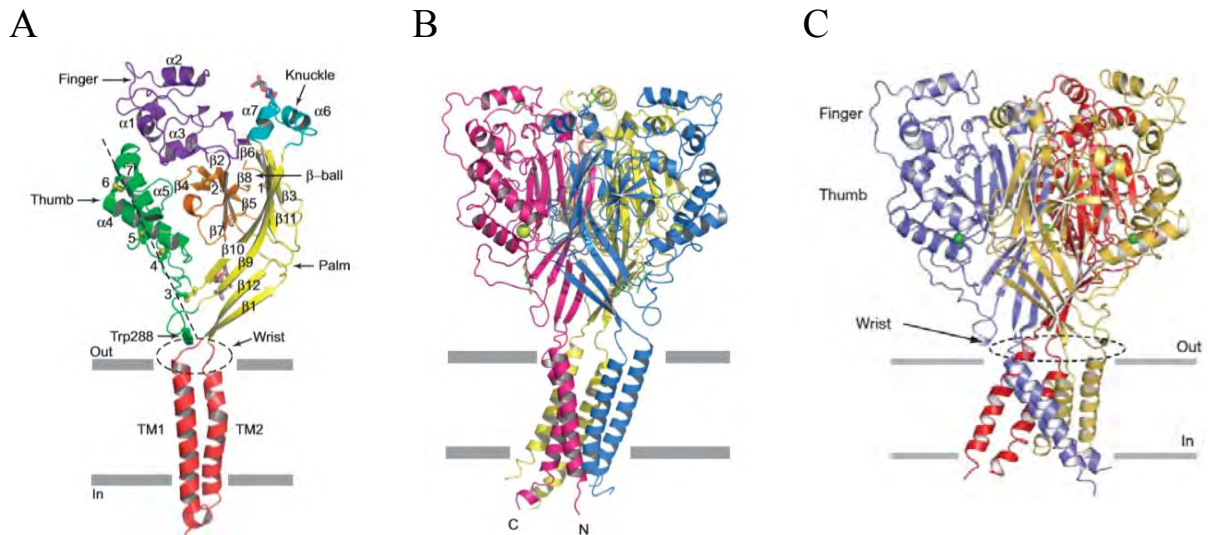
Figure 2. Structure of cASIC1a. A. Single ASIC subunit highlighting five distinct domains (Jasti et al., 2007). B. Crystal structure of cASIC1a desensitized state solved by Jasti *et al*. Three ASIC subunits are shown in different colors (Jasti et al., 2007). C. cASIC1a desensitized structure solved by Gonzales *et al*. (Gonzales et al., 2009). A single chloride ion per subunit is shown as a green sphere.

The second ASIC structure was obtained two years later from a cASIC1a construct that could produce a functional channel, in which only the C-terminus was deleted, whereas the N-terminus was included (Gonzales et al., 2009), thus preserving the crucial "gating" domain that is required for channel activation (Pfister et al., 2006). The structure was crystallized at lower resolution (3 Å) compared to the first one and at low pH (6.5). Also this structure likely captures the channel in the desensitized state (Fig. 2 C). The two structures show similar overall structural features; the main differences consist in their resolution and in the architecture of the transmembrane helices. In the structure solved by Gonzales, but not in that by Jasti, the transmembrane helices are arranged in a symmetric order (compare Fig. 2B and C). The electron density map of the transmembrane domain of the desensitized structure solved by Gonzales was later reinterpreted, showing a physical break of the α helix that separates this segment in two parts, TM2a and TM2b (Fig. 7).

Interestingly, in the desensitized structure but not in the open and closed structures, the residues Leu414 and Asn415 (corresponding to the human residues Leu415 and Asn416) show a swap in their sidechain orientation. The authors suggest that this structural change underlies the mechanism of desensitization (Baconguis et al., 2014; Gonzales et al., 2009; Yoder et al., 2018).

1.2.2 Closed, open and desensitized states: a structural comparison

After the publication of the ASIC crystal structures in the desensitized state, three other papers have come out reporting the crystal structure of cASIC1a in complex with two channel activators: the spider toxin Psalmotoxin-1 (PcTx1), and the heterodimeric snake toxin Mit-Toxin (MitTx) (Baconguis et al., 2014; Baconguis and Gouaux, 2012; Dawson et al., 2012). These structures elucidate the channel conformation in the open state. The open structure of the cASIC1a solved by Dawson and colleagues was obtained from a non-functional channel with truncated intracellular N- and C- termini, in complex with the gating modifier PcTx1, which activates cASIC1a by stabilizing the open conformation (Dawson et al., 2012). The structure was crystallized at pH 5.5 and at a resolution of 3.0 Å. It shows three independent PcTx1 molecules bound at the acidic pockets of the channel, as well as the molecular interactions between PcTx1 and cASIC1a.

At about the same time, another cASIC1a open structure in complex with the PcTx1 was solved by Baconguis and Gouaux at similar resolution as the one published by Dawson (~3.3 Å) (Baconguis and Gouaux, 2012). The structure was obtained from a functional channel construct with a small truncation of the N-terminus. Interestingly, crystals of the toxin-bound open structure were obtained at two different pH (pH 7.25 and 5.5, Fig. 3A and B) and, depending on the pH, they showed two different pore conformations with distinct selectivity properties! The high-pH open structure contains sparse inter-subunit and hydrophobic contacts between TM1 and TM2 domains that define and stabilize a symmetric pore. Compared to the

desensitized state, we observe a rotation of the cytoplasmic end of the TM2 by about 90° around the central axis, resulting in the disruption of the intra- and intersubunit contacts between TM1 and TM2 that define the occluded gate in the desensitized structure.

Surprisingly, the high-pH channel-PcTx1 complex contains a pore diameter of ~10-20 Å. Concomitant functional studies at pH 7.25 have shown that PcTx1-cASIC1a complex was unable to discriminate among monovalent cations, such as Na^+, K^+ and Cs^+, thus allowing the passage of bigger molecules, such as *N*-methyl-D-glucamine (NMDG), with a radius of ~4 Å (Fig. 3A). Moreover, application of 500 μM amiloride inhibited 95% of the peak current evoked at pH 7.25 in presence of 1 μM PcTx1, but only blocked 10% of the sustained current.
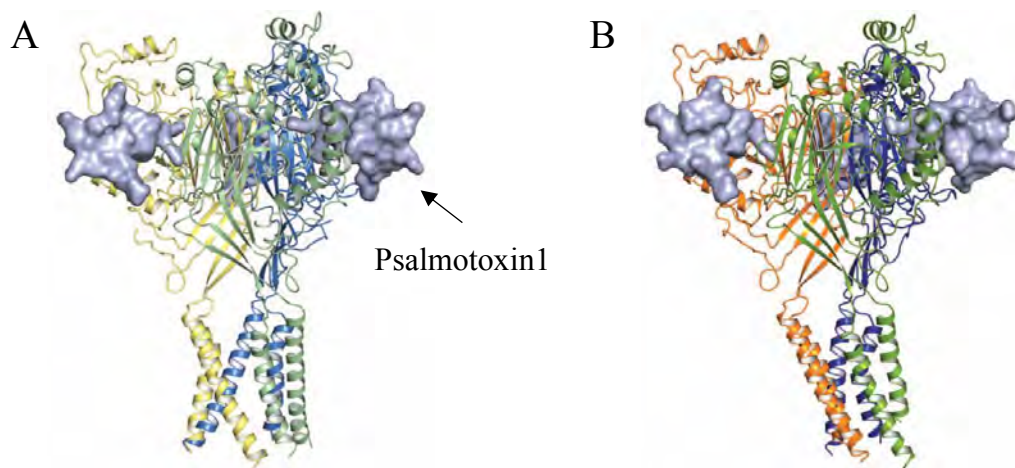
Figure 3. Structures of cASIC1a in complex with PcTx1. One toxin binds into the acidic pocket of each ASIC subunit. High-pH (A) and low-pH (B) channel-toxin complexes show marked differences in the architecture of the transmembrane domains (Baconguis and Gouaux, 2012).

In the low-pH structure, the TM2 of only one subunit adopts a straight α-helix, resulting in a shift of about four-residues toward the extracellulcar side relative to the other two subunits, thus conferring an asymmetrical geometry to the pore (Fig. 3B).

Apart from the pore architecture, another important difference between the high- and low-pH structure concerns the ion selectivity properties. In contrast to the non-selective high-pH gate, the low-pH pore remained selective for Na^+ over K^+ (10:1). The authors suggest that Na^+ ions

cross the pore in a hydrated state, and that the mechanism underlying ion selectivity can be simply described by a "barrier" model, which had been already proposed for Na^+-selective ion channel pores (Hille, 2001). According to this model, the pore discriminates ions by their size in complex with water molecules. Cross-section of the low-pH structure shows an elliptical pore with a diameter of ~4-10 Å, and thus, in agreement with the model, it would be large enough to allow the passage of Na^+ ions in complex with water molecules, but too small to allow hydrated potassium ions entering the channel (Baconguis and Gouaux, 2012).

The third and last cASIC1a open structure was crystallized in complex with the heterodimeric MitTx (Fig. 4A), which activates ASIC1a channels at nanomolar concentrations. The structure was obtained at pH 5.5 and at a resolution of approximately 2.3 Å. In contrast to the PcTx1 that binds exclusively into the acidic pocket, molecular interactions between the snake toxin and cASIC1a occur at the wrist, palm and thumb domains. The MitTx-bound open structure shows that the α helix of the TM2 domain is not continuous but it breaks at the level of the GAS motif (see Fig. 7 for clarity; refer to paragraph *1.2.3*, subparagraph *"Ion conduction pathway and transmembrane domain"* for more details about the GAS motif), which constitutes a belt that separates the TM2 domain in TM2a and TM2b and allows the TM2b to interact with the cytoplasmic side of the TM1 of an adjacent subunit (Baconguis et al., 2014).

It is difficult to say which of the available open structures better approximates the real open channel conformation. However, the cASIC1a-MitTx structure appears the most reliable, since it has been crystallized at high resolution, presents a plausible size of the pore diameter, and shows a three-fold symmetry channel which retains most of the main gating properties.

Very recently, the resting state structure of full length cASIC1a has been determined at high pH and at a resolution of 3.7 Å by both x-ray and cryo-EM (Yoder et al., 2018). The most striking feature of this structure is an expanded conformation of the acidic pocket, located between the thumb, the finger, and the β-ball domains (Fig. 4B). The structure shows some

similarities with both open and desensitized conformations. For instance, the overall TM domain is analogous between the resting and desensitized states, harboring a shut gate, whereas the conformation of the β1-β2 and β11-β12 linkers mimics that of the open state. In contrast to the desensitized state, the residues Leu414 and Asn415 (corresponding to the human residues Leu415 and Asn416) return to their original position.
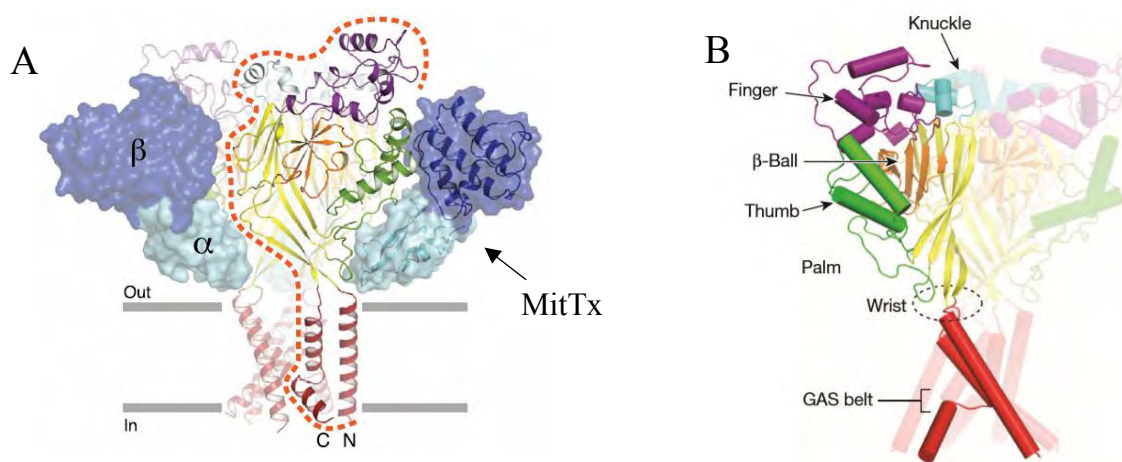
Figure 4. A. Structure of cASIC1a in complex with the heterodimeric MitTx (Baconguis et al., 2014). B. cASIC1a structure in the resting state (Yoder et al., 2018).

1.2.3 Structure-functional aspects of ASIC domains

The publication of ASIC structures has provided extremely important insights concerning the architecture, as well as the structural relations among different channel domains. In addition, mutagenesis and functional studies aided to evaluate the impact of structural changes on channel function. The most relevant features concerning the structure-function relationship of each ASIC domain are described below. For clarity, residue numbering follows the human protein.

A central role of the palm domain

The palm domain constitutes the core of ASIC extracellular domain. It is composed of four large β strands in each subunit that come together to form a central cavity of the channel and make direct interactions with all ASIC domains, except with the finger (Jasti et al., 2007). The lower part of the palm is directly connected to the TM1 and TM2 through the β strands 1 and 12, respectively, interactions that may have a crucial role in transmitting gating motions to the channel gate. The palm interacts also with the thumb and knuckle domains through β strands 9 and 10 and β strands 11 and 10, respectively, while the β1-β2 linker and β9 strand connect the palm to the β-ball domain (Fig. 2A).

A functional study combined with a computational approach identified residues in the palm domain that are critical for channel desensitization. Specifically, neutralizing mutations of the residues Glu413 and Glu418, respectively in the β11-β12 linker and in the β12 strand, induced an acidic shift of pH dependence of SSD, indicating these residues as potential sensors for SSD. The study provides also information about conformational changes in this region during channel gating. More specifically, functional analyses suggest that channel desensitization involves a movement of the palm domains toward the central axis (Liechti et al., 2010).

ASIC crystal structures have shown that residues located at the β1-β2 and β11-β12 linkers undergo critical structural changes during channel activity and their role in both activation and desensitization has been extensively investigated in several functional studies.

Coric and coworkers conducted a structure-functional study between fish and rat ASIC1a (f and rASIC1a), which share approximatively 76% of sequence homology. Most of the biophysical properties are similar between the two species, but not the rate of channel desensitization, which was found to be 25-fold faster in fASIC1 compared to rASIC1a. Functional studies using chimeric channels led to the identification of a short sequence formed by three residues Pro83-Leu84-Met85 (corresponding to human Ser83-Gln84-Leu85, Fig. 5) that is responsibile for the

different desensitization kinetics (Coric et al., 2003). This was the first evidence showing the importance of this segment in channel desensitization; after this, several other studies have followed.
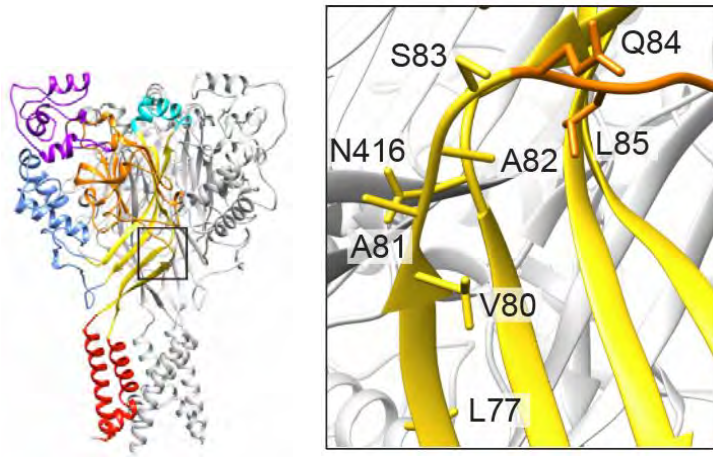
Figure 5. Close-up view of the β1-β2 linker connecting the palm (yellow) and β-ball (orange) domains. The residues Leu77 and Asn416 are located in the β1 strand and in the β11-β12 linker of the palm domain, respectively Figure adapted from (Baconguis et al., 2014).

Li et al. conducted a comparative study between the jawless fish lamprey ASIC1 (lASIC1), which does not respond to protons, and its proton-sensitive ortholog rASIC1, to identify potential residues that are responsible for the different proton sensitivity. The authors showed that mutation of two residues located in the β1 strand and in the β1-β2 linker of rASIC1, Q77L and T85L (corresponding to human Leu77 and Leu85, Fig. 5), was sufficient to convert lASIC1 into a highly sensitive proton-activated channel. This study, thus, suggests that lASIC1 is also proton-sensitive but channel opening is not evident probably because channels enter rapidly the desensitized state (Li et al., 2010c).

In a similar study, Li and coworkers compared the proton response between *Xenopous* ASIC1.1 (xASIC1.1), cloned from *Xenopous laevis* brain, and rASIC1a. Channels of both species responded with a transient current followed by a desensitized phase upon continue exposure to acidic pH, however, both rise and decay current phases were faster in xASIC1.1 than in rASIC1a. The origin of this distinct effect lies in the different amino acid composition at the β1-β2 linker. More specifically, xASIC1.1 contains the residues Pro83, Lys84, Met85, corresponding to Ser83, Gln84 and Leu85 (same as in human, Fig. 5). The triple mutant

xASIC1.1 P83S-K84Q-M85L (SQL) showed, indeed, a marked acidic shift of the pH_{50} SSD compared to the WT and a slower opening and desensitization. The authors suggest that mutations of these residues decrease the number of channels that transit from the closed to open state and from the open to desensitized state, resulting in a delayed and slow channel opening and in a decrease of pH_{50} SSD, respectively. These results highlight the functional importance of this segment ($\beta 1$-$\beta 2$ linker) during channel desensitization and provide also evidence for a role in channel activation (Li et al., 2010b). Mutation of the residue Asn416 (human) located in the $\beta 11$-$\beta 12$ linker was found to further slow down the desensitization rate in the double mutants M85L-N416L compared to the single mutation, generating an additive effect. However, no direct interaction was found between the two residues, suggesting that both residues in the $\beta 1$-$\beta 2$ and $\beta 11$-$\beta 12$ linkers indipendently contribute to the stabilization of the desensitized state (Li et al., 2010a). A functional interaction between these two linkers was shown in a comparative study between rASIC1a and shark ASIC1b (sASIC1b), which shows fast and incomplete desensitization kinetics, generating a sustained current that remains as long as acidification persists. Chimeras between the two channels allowed the identification of a triplet in the sASIC1b (Met109-Asp110-Ser111, corresponding to human Val80-Ala81-Ala82) responsible for the fast desensitization rate and the appearence of a sustained opening. Moreover, the authors found that cysteine residues introduced at the $\beta 1$-$\beta 2$ and $\beta 11$-$\beta 12$ linkers led to spontaneous formation of a disulfide bridge that trapped the channel in the desensitized state; the subsequent application of reducing agents dramatically increased current amplitude. These results suggest that the $\beta 1$-$\beta 2$ and $\beta 11$-$\beta 12$ linkers are dynamic and interact each other during desensitization. Moreover, introduction of amino acids with different properties at the $\beta 1$-$\beta 2$ linker destabilizes the desensitized state and leads to a channel reopening, given by the development of a sustained current (Springauf et al., 2011).

Together these studies support the notion that the palm domain plays a pivotal role in ASIC desensitization.

The palm domain is also an important binding site of some ASIC modulators. For example, the ASIC activator MitTx makes extensive contacts with residues Ala81 and Ser83 located in the β1-β2 linker (Baconguis et al., 2014). The first nonproton activator 2-guandine-4-methylquinazoline (GMQ) interacts with two acidic residues in the β1 and β12 strands to induce ASIC3 activation (Alijevic and Kellenberger, 2012; Yu et al., 2010; Yu et al., 2011).

In summary, these findings demonstrate a central role of the palm domain for channel gating and modulation.

The importance of the thumb domain

The thumb domain is a rigid structure composed of two α helices and stabilized by five disulfide bridges that provide structural integrity. Two loops connect the α helices 4 and 5 to the palm β strands 9 and 10, respectively. The loop that connects the β9 strand of the palm to the α4 helix of the thumb interacts with the post-TM1 domain via a flexible segment, named β-turn.

ASIC extracellular domain contains numerous intersubunit contacts and cavities. The most notable of these is represented by the "acidic pocket", a cluster of several acidic amino acids located 45 Å far from the TM domains. It consists of intra-subunit contacts among the finger, thumb and β-ball domains, together with the palm domain of an adjacent subunit (Jasti et al., 2007). Three pairs of acidic residues within a small space (~2.8 Å) form carboxyl-carboxylate interactions involving aspartates and glutamates side chains in the acidic pocket. Two pairs, Asp237-Asp351 and Glu238-Asp347, create connections between the finger and thumb domains; a third pair mediates interactions between Glu219 Asp409, located on the β-ball of one subunit and on the palm of an adjacent subunit, respectively. A fourth carboxyl-carboxylate pair makes intra-domain interactions between Glu79 and Glu418, both these residues are

located in the palm. All these pairs are conserved in almost all ASIC isoforms but not in other members of ENaC/DEG family (Jasti et al., 2007). Because of the presence of several negatively charged amino acids, the acidic pocket was proposed to be part of the ASICs proton-sensing machinery.

The thumb plays a role in mediating channel desensitization. It has been shown that swapping the thumb domain between ASIC1a and ASIC2a, which, despite the high sequence homology, display a remarkable difference in proton sensitivity, affected the channel desensitization kinetics. More specifically, ASIC1a channels containing the thumb domain of ASIC2a showed faster desensitization kinetics, suggesting that this domain contributes to the mechanism that controls channel desensitization (Krauson and Carattino, 2016).

The thumb domain is also an important site for channel modulation. X-ray structures of ASIC1a channels in open and desensitized states, but not in resting state, reveal the presence of three chloride ions bound to the channel at the interface between the β-ball and thumb domains of two different channel subunits (Baconguis et al., 2014; Gonzales et al., 2009; Jasti et al., 2007). More specifically, the canonical Cl^- binding site comprises two residues (Arg311 and Glu315) located in the α4 helix of the thumb domain and one residue (Lys211) in the β-ball domain of an adjacent subunit (Jasti et al., 2007). These residues are conserved among different ASIC isoforms, for this reason it has been suggested that this site might be important for channel gating and assembly. The importance of these residues for Cl^- binding and its modulation has been shown in a functional study where mutation of any of the three residues in ASIC1a produced channels that showed a marked increase of the rate of desensitization and a slowed rate of tachyphylaxis (decreased channel response after repeated acidic stimulations), without affecting channel pH dependence, suggesting that these residues are required to coordinate Cl^- binding and modulation. A similar effect on ASIC1a was also observed by replacing chloride ions with different extracellular anions. The authors showed that the effect on the

desensitization kinetics and tachyphylaxis dependend on the anion type (Kusama et al., 2010). This study suggests that chloride ions stabilize an open conformation of the channel by slowing the channel desensitization, and facilitates tachyphylaxis. In another study it was found that, similar to ASIC1a, different anions modulated the kinetics of desensitization of other ASIC channels. However, unlike ASIC1a, anions also modulated the pH dependence of activation of different ASIC isoforms and the anion modulation depended on the subunit composition (Kusama et al., 2013). Surprisingly, mutation of the three putative Cl⁻-binding sites in ASIC2a and ASIC3 had small or no effect on chloride modulation, suggesting the presence of other sites responsible for Cl⁻ modulation (Kusama et al., 2013). Modulation by extracellular chloride has also been observed in ENaC channels (Collier and Snyder, 2009).

Interestingly, Yoder and Gouaux have shown in a recent study that in the resting state chloride ions do not bind to their canonical site at the interface between β-ball and thumb domains, but they bind, rather, to an unusual site in the wrist, the portal used by ions to reach the ion channel pore. The significance of this non-canonical binding site is not clear, it may be involved in channel regulation or selectivity; further experiments will better clarify the importance of this site (Yoder and Gouaux, 2018).

Residues in the thumb domain are also involved in channel modulation by several toxins. A recent study reported the cryo-EM structure of cASIC1a in complex with the Mambalgin-1, a potent and reversible ASIC1a inhibitor. The structure shows that the toxin directly interacts with the α5 helix of the thumb domain of cASIC1a and initiates conformational changes that lead to channel inhibition (Sun et al., 2018). Binding of the gating modifier Psalmotoxin1 also involves primarily interactions with residues in the α5 of the thumb domain and, depending on the species and on the subunit composition, can either inhibit or activate ASIC1 (Er et al., 2017; Kellenberger and Schild, 2015). Together these studies further confirm the importance if this region in channel modulation and suggest that the thumb domain can serve as potential drug

target (Baconguis and Gouaux, 2012; Dawson et al., 2012). Refer to the paragraph *1.3.2.* for more details about ASIC modulation by Mambalgin-1 and PcTx1.

The finger, β-ball and knuckle domains

The finger is the region with the highest variability and lowest sequence conservation among DEG/ENaC family members. In the cASIC1a crystal structure, the finger is oriented toward the outside of the protein and is made up of three α helices (1-3) and several loops that make intra and inter-domains interactions. The finger is involved in a wide range of functions in ASICs. Mutations of residues located in the contact zone between the finger and β-ball domains led to a decrease in channel expression and maximal current (Bargeton and Kellenberger, 2010). Paukert *et al*. have shown that the residue Asp107 in the α1 helix (Fig. 6) plays an important role in proton sensitivity of ASIC1a activation (Paukert et al., 2008). Moreover, it has been shown that cleavage by trypsin decreases channel proton affinity by shifting ASIC1a pH dependence of both activation and SSD to more acidic values; the residue Arg145, located in the α2 finger helix (Fig. 6), is required for cleavage (Vukicevic et al., 2006).

It has been shown that Zn^{2+} modulates ASIC channels and that residues involved in this regulation are located at different positions within the finger. Only few nanomolar of this endogenous trace element are sufficient to inhibit homomeric ASIC1a and heteromeric ASIC1a/2a without affecting currents mediated by other homomeric ASICs. Mutation of Lys133 (Fig. 6) in ASIC1a extracellular domain abolished the high-affinity Zn^{2+} inhibition (Chu et al., 2004). However, at micromolar concentrations, Zn^{2+} has an opposite effect and potentiates currents mediated by homomeric ASIC2a, but not by homomeric ASIC1a. Mutagenesis studies have shown that the residue His163 is essential for Zn^{2+} potentiating effect (Fig. 6) (Baron et al., 2001).
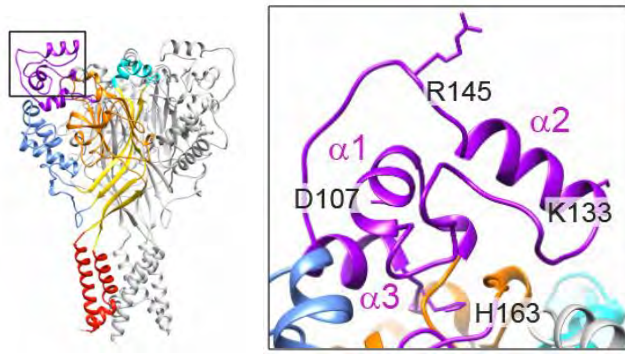
Figure 6. Close-up view showing three α helices of the finger domain (pink). Asp107 is involved in ASIC1a activation; Lys133 mediates Zn^{2+} inhibition in ASIC1a; His163 is involved in Zn^{2+} potentiation effect in ASIC2a; Arg145 is the cleavage site by trypsin in ASIC1a. Figure adapted from (Baconguis et al., 2014).

The finger, knuckle, thumb and palm domains surround a domain in the internal part of the channel: the β-ball. This domain is made up of five strands and several loops that make connections with the palm and finger domains (Jasti et al., 2007). Mutations of several acidic residues within this region have a marked effect on channel activation (Liechti et al., 2010). Higher up is located the knuckle domain, which consists of two α helices (6 and 7) that are connected to the β strands 10 and 11 of the palm domain, respectively (Fig. 2A).

Ion conduction pathway and transmembrane domain

Sodium ions are thought to access the channel pore through three oval-shaped fenestrations (~4-10 Å). These apertures are located in the wrist, a region that connects the ectodomain to the transmembrane domain of the channel. Due to its critical position, the wrist is considered a key region for transferring gating motions from the extracellular domain to the channel gate. Consistent with this hypothesis, experimental studies have shown that several residues in this region play a critical role in channel gating and modulation (Li et al., 2009; Lynagh et al., 2017b). A modulatory role of the wrist has also been observed in ENaC channels, where substitutions of residues located within this region reduced the Na^+ self-inhibition of the channel (Shi et al., 2012).

After entering the channel, ions travel through the transmembrane domain to reach the intracellular compartment. The transmembrane domain is composed of two α helices (TM1 and

TM2) contained in each channel subunit. The TM1 helix contacts the lipid bilayer but it also interacts with the TM2 of the same subunit and with the TM1 and TM2 of an adjacent subunit (Fig. 7). Together with the external end of the TM1, the TM2 domain lines the pore and contains the selectivity filter; residues within this segment are, thus, importantly involved in ion channel permeation. The ENaC selectivity filter is represented by the conserved G/S-x-S motif. This site corresponds to the residues Glycine 443-Alanine 444-Serine 445 (GAS motif) in ASICs. In the cASIC1a structure, this motif is located in the belt that separates the TM2 in TM2a and TM2b (Fig. 7).

Despite different gating properties, the TM2 domain is highly conserved between ASICs and ENaC. ENaC is a highly Na^+-selective channel (Na^+/K^+ >100) and it discriminates between cations based on their size. It has been shown that a single point mutation of a conserved Ser589, located in the TM2 of ENaC α subunit, has a profound effect on channel selectivity, with a direct correlation between permeation of larger ions and size of the mutants. This effect was explained by an enlargement of the pore when Ser589 was replaced by larger amino acids, suggesting that small differences in the amino acid composition lining the pore may confer to the channel distinct ion selectivity properties (Kellenberger et al., 1999).

Based on evidence on ENaC and on experimental studies showing that mutations of GAS residues had a profound effect on ion permeability and channel unitary conductance, it was initially concluded that the GAS motif was also the ASIC selectivity filter (Li et al., 2011; Yang et al., 2009). A conclusion, however, that turned out to be wrong. A recent study has indeed shown that there is no preference for sodium ions in the "GAS belt" and described that the ASIC selectivity filter is located in the lower end of the channel pore, including the two acidic residues Glu452 and Asp455 (Fig. 7) (Lynagh et al., 2017a).
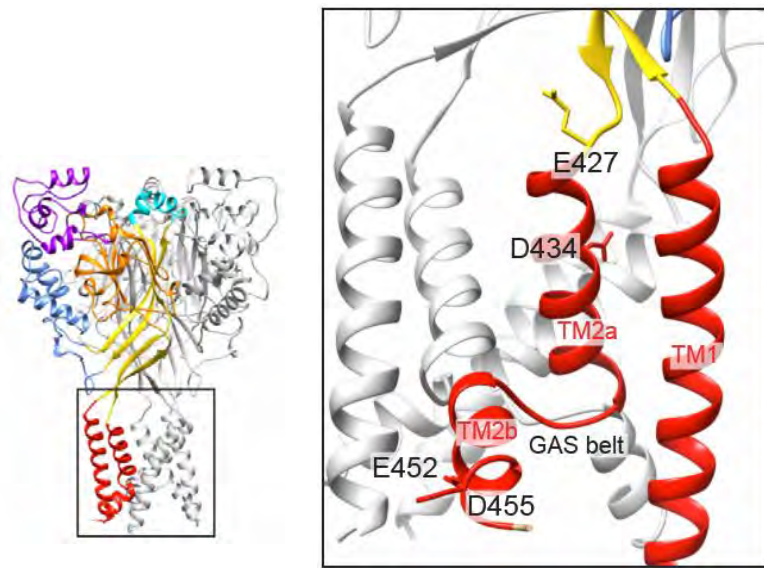
Figure 7. Close-up view of the pore formed by the TM domains. The α helix breaks at the level of the GAS belt, separating the TM2 domain in TM2a and TM2b. Glu427 and Asp434 constitute the calcium binding sites in ASIC1a. Asp434 is the "Deg site. The activation and desensitization gates are located in the TM2a. ASIC1a selectivity filter is represented by the residues Glu452 and Asp455, in the TM2b. Figure adapted from (Baconguis et al., 2014).

Together with the selectivity filter, one of the most important regions is represented by the channel gate. The "activation gate" is formed by residues located in the TM2a (Fig. 7) (Baconguis et al., 2014). The desensitized cASIC1a structure solved by Gonzales reveals the location of the "desensitized gate", an ~8 Å thick occlusion of the ion conduction pathway formed by the residues Asp434 and Gly437, located in the TM2a, resulting in a physical block of the transmembrane pore (Gonzales et al., 2009). The structural evidence for the location of the gate have been confirmed by a functional study that shows a tight rearrangement of the transmembrane domains given by different chemical modification rates of engineered cysteine located in this region (Li et al., 2011).

The Asp434 is also known as "Deg" site (Fig. 7), since mutation of the homologous site in *C. elegans*, DEG-1, produced constitutively open channels leading to degeneration of sensory neurons (Eastwood and Goodman, 2012).

Lowering extracellular calcium concentration increases ASIC proton sensitivity inducing an alkaline shift of the pH dependence of activation and SSD, and allowing opening of ASIC3 at physiological pH 7.4 (Babini et al., 2002; Immke and McCleskey, 2003; Zhang et al., 2006). In addition to this gating effect, calcium ions also modulate ASICs through a blocking effect, by

reducing the maximal current amplitude. The residues responsible for Ca^{2+} blocking effect in ASIC1a are Glu427 and Asp434, located at the entrance of the pore (Fig. 7) (Paukert et al., 2004). Immke et al. proposed a model in which a Ca^{2+} ion occludes the channel pore preventing ion permeation. Following this model, Ca^{2+} and proton ions compete for a common binding site in the pore, and the mechanism underlying channel activation would imply the release of Ca^{2+} block by a marked increase of extracellular protons without involving conformational changes of the channel (Immke and McCleskey, 2003). A recent study has shown that the residue Glu435 in rASIC3, located above the channel gate, contributes to the formation of the Ca^{2+} block site, since mutation of this residue to glycine, the equivalent residue in chicken ASIC1, diminished the rASIC3 Ca^{2+} block effect (Zuo et al., 2018). Different studies have shown that ASIC1a is not opened by the same mechanism as ASIC3 (*i.e.* relieving a pore-block by Ca^{2+}), since mutation of the two ASIC1a Ca^{2+} binding sites was not sufficient to constitutively open the channel (Paukert et al., 2004).

The intracellular domain

The intracellular ASIC domain comprises two short cytoplasmic N- and C-termini, unresolved in ASIC structures. The C-terminus region contains a PDZ domain, a structural domain formed by the last four residues of this segment. Its name derives from the first letters of the first three proteins discovered to share this domain: post synaptic density protein (PSD95), Drosophila disc large tumor suppressor (Dlg1), and zonula occludens-1 protein (Zo-1) (Kennedy, 1995). The C-terminus contains also phosphorylation and protein-protein interaction sites, which can be important for channel gating and/or regulation. A functional study has shown that crosslinking of cysteine residues in the cytoplasmic C-terminus favors the stabilization of ASIC1a homodimers (van Bemmelen et al., 2015).

The N-terminus contributes to the ion selectivity in ASIC2 and ASIC1a and to the Ca^{2+} permeability in ASIC1 (Bassler et al., 2001; Coscoy et al., 1999). This segment contains the conserved HG motif. Mutation of this site in ENaC resulted in a decreased open probability and surface expression leading to PHA-1 in humans, while mutation of the corresponding site in *C. elegans* disrupted touch sensitivity (Chang et al., 1996; Hong et al., 2000).

1.3 ASIC Pharmacology

1.3.1 Synthetic ASIC modulators

Due to the large site of its extracellular domain, we can easily imagine that many other ligands beside protons can bind to the ectodomain to modulate ASIC function. Currently, no drugs are clinically used as ASIC inhibitors or modulators. Several synthetic modulators have, however, been identified. Among them, the most relevant are described below.

Nonsteroidal anti-inflammatory drugs (NSAIDs) are medications widely used to relieve pain and reduce inflammation. Their principal mode of action consists in the inhibition of the activity of cyclooxygenase enzymes (COX-1 and/or COX-2). In cells, these enzymes are involved in the synthesis of prostaglandins, key biological mediators involved in inflammation. NSAIDs, such as aspirin, diclofenac and ibuprofen, directly inhibit ASICs in nociceptors but with relatively low potency (from 100 μM to 3 mM) (Voilley et al., 2001). A recent study has shown the mechanism of ibuprofen inhibition of ASIC1a and the putative ibuprofen binding site, which involves residues located near the wrist (Lynagh et al., 2017b).

Amiloride is a diuretic drug typically used to treat hypertension and congestive heart failure. Experimental evidence shows that ASIC current is blocked by a concentration of half maximal inhibition (IC_{50}) of about 10 to 100 μM, depending on ASIC subunit. Compared to ASIC, ENaC shows higher sensitivity to amiloride (IC_{50} of 100 nM) (Canessa et al., 1994; Garty and Palmer, 1997; Kellenberger and Schild, 2002). Functional studies suggest that amiloride inhibition

involves a pore-blocking mechanism via interaction with residues close to the desensitization gate and within the extracellular domain (Schild et al., 1997).

2-guanidine-4-methylquinazoline (GMQ) is a synthetic compound initially described as the first non-physiological ASIC activator. Mutagenesis studies have shown that GMQ induces sustained activation of ASIC3 channels at physiological pH and that this effect involves two glutamates residues located in the highly conserved lower palm domain (Yu et al., 2010; Yu et al., 2011). Mutations of these putative binding sites, indeed, abolished the activation by GMQ and affected the half maximal effective concentration (EC_{50}). A subsequent study clarified by which mechanism GMQ activates ASIC3: it induces a shift of the activation curve to more alkaline values, thus indicating that GMQ is not a genuine ASIC3 activator but rather a channel gating modifier. In contrast to its effect on ASIC3, the authors have also shown that GMQ induces in ASIC1a an acidic shift of the pH dependence of activation (Alijevic and Kellenberger, 2012).

Consistent with the role of ASIC3 nonproton ligand activator, animal studies have shown that injecting the synthetic compound into the mouse paw triggered pain behaviours in WT but not ASIC3^{-/-} mice (Yu et al., 2010). Moreover, another recent study has shown that injection of GMQ into mouse cheek induced itch and pain responses in WT animals; both physiological responses were however attenuated by genetic deletion of ASIC3, suggesting an important role of these channels in mediating itch and pain behaviour (Peng et al., 2015).

1.3.2 Animal toxins

 Several animal toxins have been found to either activate or inhibit ASICs with high potency. These molecules are thus considered important tools to explore the potential role of these channels in different diseases using animal models (Chu et al., 2011).

Psalmotoxin1 (PcTx1) is a 40-amino acids toxin isolated from the venom of the South American tarantula *Psalmopeus cambridgei.* To date, it is the most potent and selective inhibitor of ASIC1a. Nanomolar concentrations of this toxin are sufficient to inhibit homomeric ASIC1a and heteromeric ASIC1a/2b (IC_{50} of ~1 nM and ~2.5 nM, respectively) (Escoubas et al., 2000; Sherwood et al., 2011). PcTx1 has been considered as a gating modifier rather than a classical channel inhibitor, as the inhibition effect does not involve a pore-blocking mechanism but, rather, an alkaline shift of the pH dependence of both activation and SSD, thus promoting channel desensitization at physiological pH (Chen et al., 2005). Surprisingly, PcTx1 does not inhibit ASIC1b but, in contrast, potentiates it at physiological pH. This opposite effect can be simply explained by the fact that the SSD curve of ASIC1b is right shifted compared to that of ASIC1a (Chen et al., 2006). Surprisingly, PcTx1 activates cASIC1a at pH 7.4 (EC_{50} ~189 nM) probably by an increase of its apparent proton affinity, thus stabilizing its open conformation (Baconguis and Gouaux, 2012; Samways et al., 2009).

APETx2 is a toxin isolated from the sea anemone *Antopleura elegantissima*. It reversibly inhibits both homo- and heteromeric ASIC3 channels (IC_{50} from ~63 nM to 2 μM) (Diochot et al., 2004), but its site of action is currently unknown. Interestingly, it has been shown that high concentrations of APETx2 inhibit also the $Na_v1.8$ current in DRG neurons (IC_{50} of ~2.6 μM) (Blanchard et al., 2012; Peigneur et al., 2012).

Mambalgins. Mambalgin-1 and -2 have been isolated from the venom of the african snake *Dendroaspis polylepis polylepis*, better known as black Mamba. These toxins inhibit ASIC1a, -1b as well as heteromeric ASIC1a channels with an IC_{50} between 11 and 250 nM (Diochot et al., 2012). Functional analyses have shown that these molecules induce a strong acidic shift of the activation curve, thus trapping the channel in the closed state (Diochot et al., 2012; Salinas et al., 2014; Schroeder et al., 2014). A recent study reported the cryo-EM structure of cASIC1a

in complex with the Mambalgin-1, showing that it binds to the α5 helix of the thumb domain (Sun et al., 2018).

Mit-Toxin (MitTx) was discovered as a non-physiological ASIC activator. Isolated from the venom of the Texas coral snake *Micrurus tener tener*, this toxin is a dimer composed of two peptides, α and β (Bohlen et al., 2011). The toxin induces a slow opening of ASIC1a, -1b, -3 at nanomolar concentrations (EC_{50} of 9, 23 and 830, respectively), but the mechanism of action is not known. A recent paper reported the structure of cASIC1a in complex with the MitTx (Fig. 4A) (Baconguis et al., 2014). Crystallographic analysis shows that three toxins bind to the channel; more precisely, MitTxβ makes interactions with residues located in the acidic pocket, while MitTxα interacts mainly with the wrist, palm, and thumb domains (refer to paragraph *1.2.2* for more details about the cASIC1a structure in complex with MiTx).

1.4 Physiological and pathological roles

1.4.1 Synaptic plasticity, learning and memory

The robust ASIC1a expression in hippocampal neurons suggests a possible involvement in the regulation of important neurophysiological processes. Consistent with this hypothesis, studies conducted in hippocampal slices have reported that genetic deletion of ASIC1a in mice abolished most of the acid-evoked current in CNS neurons, impaired long-term potentiation (LTP) and induced a deficit in spatial memory, suggesting that homo- and heteromeric ASIC1a channels are the primary acid-sensors in neurons and contribute to the development or maintenance of LTP (Kellenberger and Schild, 2015; Quintana et al., 2015; Wemmie et al., 2013). Another study employed an *in vitro* multi-electrode array system to investigate synaptic plasticity in hippocampal slices from WT and ASIC KO mice. This study showed that genetic ablation or pharmacological blockade of ASIC1a strongly reduced the hippocampal LTP induction without affecting the long-term depression (LTD), another form of synaptic plasticity,

confirming an important role of these channels in promoting synaptic plasticity (Liu et al., 2016). In contrast to these observations, only one study reported that ASIC1a KO mice exhibited normal hippocampal LTP and spatial memory. The origin of this discrepancy might be due to the different approach utilized to generate KO animals or to different experimental conditions (Wu et al., 2013).

Two recent studies investigated the physiological role of proton-mediated ASIC signaling in neurotransmission in the lateral amygdala pyramidal neurons and in the nucleus accumbens core neurons. Protons released during presynaptic stimulations induce ASIC excitatory postsynaptic current (EPSC). These studies have shown that, compared with glutamate receptor current, ASIC current makes a small but important contribution to the EPSC. Indeed, presynaptic high-frequency stimulation (HFS) is accompanied by a progressive lowering of the extracellular pH, which can in turn activate ASICs while inhibiting NMDA receptors. The authors suggest that ASIC1a is a postsynaptic proton receptor required to sustain and enhance synaptic transmission over time (Du et al., 2014; Kreple et al., 2014).

There is evidence showing that ASIC1a modulates the number and length of dendritic spines. More specifically, an increase in dendritic spines density has been observed when ASIC1a was overexpressed in hippocampal pyramidal neurons, whereas an opposite effect was observed in neurons where ASIC1a expression was decreased, further supporting a potential involvement of these channels during learning and memory processes (Zha et al., 2006).

1.4.2 Fear-related behaviour

The amygdala constitutes a key component of the neural circuitry underlying fear learning (Duvarci and Pare, 2014). Consistent with the high expression of ASIC1a in this region, several studies have been performed to explore a possible role in fear-related behaviour.

Wemmie and colleagues have shown that overexpression of ASIC1a in transgenic mice increased fear behaviour, whereas deletion of the ASIC1a gene induced deficits in cue and context fear-conditioning (Coryell et al., 2007; Wemmie et al., 2003; Wemmie et al., 2004). The amygdala acts in the brain as a chemosensor that detects carbon dioxide (CO_2). An increase in inhaled CO_2 reduced brain pH and evoked fear behavior in mice (Ziemann et al., 2009). Interestingly, it was shown that removal or inhibition of ASIC1a function significantly reduced the CO_2-mediated effect, while restoring ASIC1a expression in the basolateral nuclei in the amygdala of ASIC1a KO mice rescued the CO_2-induced fear deficit, demonstrating an important role of ASIC1a in this brain region (Ziemann et al., 2009).

It was shown that ASIC1a has also a role in anxiety-like behaviour. Coryell and colleagues have shown that inhibition of ASIC1a in mice reduces anxiety in behavioural tests, suggesting that ASIC1a might be a potential target for antidepressant-like drugs (Coryell et al., 2009).

1.4.3 Nociception

Nociception refers to detection of harmful stimuli and translation into neuronal signals. Several pain-related conditions (*e.g.* inflammation) are associated with a decrease of the extracellular pH. This suggests the presence of some proton sensor receptors that can be activated to mediate pain sensation. Transient receptor potential vanilloid 1 (TRPV1) and ASIC channels are responsible for generating most of the acid-induced current in the peripheral nervous system, particularly in sensory neurons (Boscardin et al., 2016). TRPV1 is a nonselective cation channel activated by a large variety of physical and chemical stimuli, such as noxious heat (>42°C) and capsaicin. TRPV1 is also activated and modulated by extracellular protons (pH_{50} of ~5.4). Several studies conducted with animal models have demonstrated the importance of both ASIC and TRPV1 channels in detecting noxious stimuli. Specifically, mice lacking TRPV1 gene showed an impaired behavioral response to noxious thermal stimuli and a marked reduced

response to extracellular proton compared with WT mice (Caterina et al., 2000). Similarly, genetic deletion of ASIC3 in mice significantly reduced tissue inflammation and chronic pain (Sluka et al., 2009). Several other studies have confirmed the importance of ASIC3 in pain sensation. Local injection of the synthetic compound 2-guanidine-4-methylquinazoline (GMQ) into the mouse paw induced pain sensation in wild-type mice but not in ASIC3 null mice (Yu et al., 2010). How could a channel with fast and transient gating sense acidosis-induced pathological states, which are persistent and can last hours or days? One hypothesis is that ASICs can manifest a sustained current, which is normally present in ASIC3 and may occur in other ASIC isoforms in presence of different modulators (Wemmie et al., 2006).

Due to the specific expression of ASIC1b in nociceptors, a potential role in pain sensation has been investigated. Intraplantar injection of the snake toxin Mambalgin-1 evoked peripheral analgesic effect mediated by ASIC1b-contaning channels, strongly suggesting a role of ASIC1b in nociception and hyperalgesia (Diochot et al., 2012).

There are also evidence showing an ASIC-mediating pain sensation in the CNS. Intrathecal administration of PcTx1, or Mambalgin-1, inhibited pain behaviour through specific action on homomeric ASIC1a and probably heteromeric ASIC1a/2b (Diochot et al., 2012; Duan et al., 2007; Mazzuca et al., 2007).

Together these findings support the notion that ASIC channels are among the principal acid-sensors involved in the "pain pathway" and importantly contribute to acid-evoked nociception.

1.4.4 Neurodegeneration after ischemia

The occurrence of a brain ischemia is due to a reduction of the blood flow. In this condition, a lack of oxygen or glucose in neurons leads to an increase of the anaerobic metabolism and a subsequent raising of lactic acid concentrations up to 12-20 mM, instead of ~1 mM in physiological conditions (Immke and McCleskey, 2001; Schurr, 2002). Severe ischemic stroke

results in dramatic pH decrease to ~6 or below (Smith et al., 1986). Moreover, Ca^{2+} accumulation in neurons, mostly due to glutamate receptors, causes toxicity and leads to ischemic neuronal injury (Choi, 1988). Homomeric ASIC1a channels are slightly permeable to Ca^{2+} and the acidic environment generated during a brain ischemia seems suitable to activate these channels.

Studies conducted in animal models have shown that ASICs could contribute to the cell damage during cerebral ischemia. For instance, animal experiments have reported that up to five hours after transient middle cerebral artery occlusion (MCAO)-induced ischemia, the infarct volume in rats decreased by >60% after deletion of ASIC1a gene or pharmacological blockade, suggesting that ASIC1a represents a potential new target for the treatment of stroke (Xiong et al., 2004). In a similar study the infarct volume was reduced by >50% after intracerebroventricular injection of ASIC1a blockers, amiloride and PcTx1 (Pignataro et al., 2007).

Interestingly, a recent study shows a potential role of ASIC2 in neuronal ischemia. Jiang and coworkers have shown that ASIC2 gene deletion significantly attenuated ischemia-induced neuronal injury in hippocampal slices and protected mice brain from ischemic damage, suggesting a critical contribution of ASIC2 to neuronal injury in the brain (Jiang et al., 2016). How could we explain the contribution of calcium impermeable channels like ASIC1a/2a heteromers to neuronal injury? A reasonable explanation is that it occurs through a secondary mechanism. Previous studies have reported that ASIC2a facilitates ASIC1a surface trafficking and enhances its expression (Harding et al., 2014; Zha et al., 2009). Thus, ASIC2 deletion reduces ASIC1a expression and eliminates all ASIC1a/2a heteromeric channels leading to a reduction of acid-induced current and, consequently, to neuronal protection (Jiang et al., 2016).

1.5 Fluorescence and fluorescence quenching

The term "luminescence" comes from the Latin word *lumen*, for «light», and refers to the emission of light from any substance. In principle, in order to observe this phenomenon, a system has to receive from an external source a certain amount of energy sufficient to trigger a light emission. Different types of energy source, therefore, define different types of luminescence, such as electroluminescence, radioluminescence, chemiluminescence, and photoluminescence. In this last form of luminescence, energy is provided by the absorption of electromagnetic radiation between the ultraviolet and infrared wavelengths, which represent the two extremities of the visible spectrum (400-700 nm). Photoluminescence is commonly divided into two different processes: fluorescence and phosphorescence.

Fluorescence is a physical process that occurs in certain molecules, called for this reason fluorophores or fluorochromes, which become excited after absorption of a certain light. A given atom can exchange electromagnetic energy in discrete units, or fundamental quanta (singular *quantum*, Latin for «how much») of energy, called "photons". A photon is an elementary particle without mass, with an energy $E=h\nu$, where E is the photon energy, h is the Planck constant, and ν is the frequency of radiation. Thereby, a photon is associated to a specific frequency, which is inversely proportional to wavelength. As frequency increases (with a corresponding decrease in wavelength), the photon energy increases, and vice versa.

The processes that occur between the absorption and emission of light are best illustrated by the Jablonski diagram (Fig. 8). The diagram shows that absorption of a photon at a particular wavelength allows the fluorophore to pass from a ground state to high energy singlet states (S_1 and/or S_2). This process is extremely fast, in the order of 10^{-15} seconds. Following the excitation, the fluorophore remains in the high energy level for a defined time prior to return to the ground state. This time defines the lifetime of a given fluorophore ($F\tau$). Fluorescence lifetimes are usually close to 10 ns. From the excited state, the fluorophore relaxes within the excited state

through a non-radiative loss of energy that typically occurs in ~10^{-10} seconds, bringing the molecule to an intermediate state. Finally, the excess energy from this state is dissipated by releasing a photon at a specific wavelength, which allows the return of the fluorophore to the ground state. The emission of a photon generates a fluorescence light.
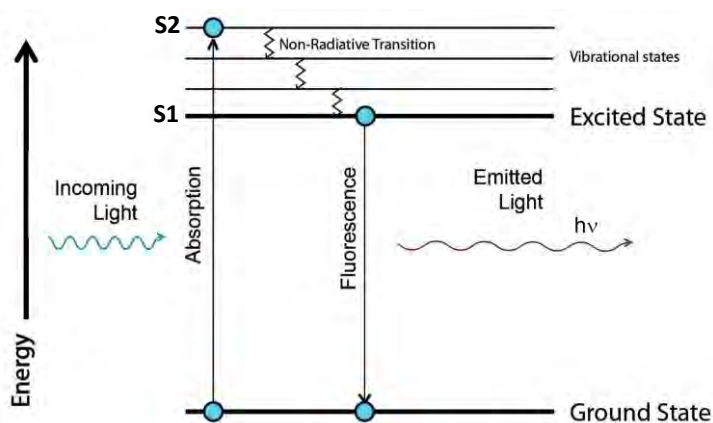
Figure 8. Illustration of the Jablonski diagram showing the processes following absorption of light by the fluorophore. S1 and S2 represent two different high energy levels.

Importantly, due the dissipation of energy that occurs during the permanence of the fluorophore in the excited state, the energy of the emitted photon is typically less than that of the absorbed photon, and, consequently, the emitted light is always of longer wavelength than the absorbed light. This phenomenon is commonly known as "Stokes shift" and represents one of the fundamental properties of a fluorophore.

1.5.1 Quantum yield and fluorescence quenching

Another important property that characterizes a fluorophore is the fluorescence quantum yield (ϕ), which gives the efficiency of a fluorescence process. The quantum yield is defined by the ratio of the number of photons emitted to the number of photons absorbed.

$$\Phi = \frac{\text{Number of photons emitted}}{\text{Number of photons absorbed}}$$

The maximum possible fluorescence quantum yield is 1.0 (100%): each photon absorbed results in a photon emitted. However, due to Stokes losses, the fluorescence quantum yield is always less than unity. Substances with high quantum yield values display brighter fluorescence emissions (Lakowicz, 2006).

Fluorescence quenching refers to each phenomenon that decreases the fluorescence intensity of a given substance. This process can occur either during the excited state, such as collisional quenching, energy transfer, or it may occur in the ground state after formation of non-fluorescent complexes. Common fluorescence quenchers include molecules such as oxygen, heavy atoms, like iodide or bromide, amino acids, such as Tryptophan, Tyrosine, Histidine, and Methionine, and many others. Fluorescence quenching can occur by different mechanisms. Typically, there are two kinds of quenching and both of them require a molecular contact between fluorophore and quencher: dynamic and static quenching (Lakowicz, 2006).

During the excited state, a collisional or dynamic quenching occurs if the fluorophore is sufficiently close to the quencher molecule. If this happens, the quencher facilitates the transition of the fluorescent molecule from the excited to the ground state. Fluorophores that are dynamically quenched show indeed a reduced fluorescence intensity and a shorter lifetime (Mansoor et al., 2010). Unlike dynamic quenching, in static quenching the fluorescent probe and the molecular quencher form a complex before light absorption, thus in the ground state. The resulted statically quenched complexes are, thus, non-fluorescent; they do not contribute to the emission intensity and do not affect the fluorescence lifetime (Mansoor et al., 2010).

1.5.2 Voltage-clamp fluorometry: principle and functional applications

In response to ligand binding or membrane depolarization, ion channels undergo conformational changes that are required to open the ion conduction pathway. Understanding the gating motions and the channel domains mainly involved, may help to modulate the channel

response and, consequently, the physiological and pathological processes in which they are involved.

Voltage-clamp fluorometry (VCF) is a powerful technique widely used to detect structural rearrangements during channel activity. VCF combines electrophysiology, molecular biology, chemistry and fluorescence into a single experimental approach.

The current is measured by a classic Two-electrode voltage-clamp (TEVC) setup, while detection of fluorescence signals requires additional optical components (*e.g.* excitation lamp, light band-pass filters and photodiode). To monitor channel conformational changes, VCF requires the use of environmental fluorescent probes, whose properties have been described in the previous paragraph. The VCF principle is as follows: a channel of interest is modified to include an engineered single cysteine residue at a strategic position. The cysteine is then selectively modified with an organic thiol-reactive fluorophore, which, in principle, specifically recognizes and reacts with the only available engineered cysteine of the channel (Gandhi and Olcese, 2008). The presence of structural rearrangements is assayed via differences in the fluorescence emission, which can be influenced by several factors, such as changes in the fluorophore exposure to the solvent and/or presence of nearby quenching molecules. Changes in the level of the emitted light indicate that conformational changes occur during channel gating. Therefore, VCF allows a correlation between changes in channel structure (given by the presence of specific fluorescence signals) with those occurring in channel function (current recording). Moreover, due to its high time resolution, the VCF technique does not only tell us that a specific movement takes place, but it also provides the timing at which a structural change occurs. However, the VCF does not provide any information about the direction of the observed movements.

To infer information on the relative direction of movements, the voltage-clamp fluorometry can be combined with the fluorescence quenching. The emission of fluorophores is sensitive to the

local environment (*i.e.* presence of a hydrophobic or hydrophilic environment) but also to the proximity of neighboring quenching groups. Imagine for example that a fluorophore is in close proximity to an endogenous Tryptophan (Trp) in a specific channel domain; depending on the changes in distance and orientation between fluorophore and quencher, the resulting fluorescence signal can be either positive, indicating an increased distance between them, or negative, suggesting that probe and quencher are approaching each other. The fluorescence signal is generally represented as a change relative to the total signal ($\Delta F/F$). Artificial addition or removal of a quencher can then be used as a reference to indicate the relative direction of fluorophore movement. Importantly, quenching by Tryptophan only occurs in a short range of distance (5-15 Å). This approach has already been successfully applied in several studies (Bonifacio et al., 2014; Gwiazda et al., 2015b; Mansoor et al., 2010; Pantazis and Olcese, 2012; Vullo et al., 2017).

Despite numerous advantages, the VCF technique shows, however, some limitations. Firstly, the fluorophore has its own length (usually from about 7 Å to 10 Å), which can perturb the structure of the protein and, consequently, limits the interpretation of fluorescence changes (ΔF) in terms of structural changes; secondly, commonly used fluorescent probes cannot cross the plasma membrane, precluding thus the detection of conformational changes in the intracellular channel domains; thirdly, cysteine residues better exposed to the solvent are more accessible to form covalent bonds with the fluorophore, compared to cysteine residues located deep inside the protein; finally, the time resolution of the VCF could not be sufficient to resolve conformational changes in channels that display rapid transition kinetics. These technical limitations can be overcome by several other methods (Chatterjee et al., 2013; Kalstrup and Blunck, 2013; Wulf and Pless, 2018).

Fluorimetric measurements can also be combined with the Cut-Open Vaseline Gap (COVG), which represents a variant of the classic voltage-clamp technique. Even though COVG is more

difficult to implement, it shows several advantages over the TEVC. The main benefits include a more rapid clamping, which is required to accurately record fast channel kinetics; improved signal-to-noise ratio, and the possibility to modulate the intracellular and extracellular milieu. For these reasons, recording with COVG in combination with VCF are particularly useful to study the properties of fast-activating ion channels and their gating motions (Rudokas et al., 2014; Stefani and Bezanilla, 1998).

VCF technique was first developed to investigate conformational changes of the S4 transmembrane segment of the *Shaker* K^+ channel expressed in *Xenopous* oocytes (Mannuzzu et al., 1996). In this study, the authors observed a decreased emission when the fluorophore tetramethylrhodamine-5-maleimide (TMRM) was attached at the extracellular end of the S3-S4 linker of the channels. The presence of negative fluorescence signals was interpreted as a movement from a hydrophobic to a polar environment during depolarization. Indeed, they found a correlation between the outward translocation of the S4 helix (as measured by changes in fluorescence emission) and channel gating currents. A similar study conducted by Cha and Bezanilla confirmed the presence of conformational changes in the S4 helix. The authors found that some of these structural changes correlated with the current kinetics of activation and inactivation (Cha and Bezanilla, 1997).

Since the first pioneer studies, VCF has been extended to many other ion channels, such as voltage-gated proton channels, Na^+-coupled P_i cotransporter, glycine receptor, proton-activated ion channels, P2X1 receptor (Bonifacio et al., 2014; Lorinczi et al., 2012; Smith and Gonzales, 2014; Virkki et al., 2006; Wang and Lynch, 2012).

2. Hypotheses and aims

Much progress has been made in the past years in the understanding of the structural and functional aspects of ASIC channels. Crystal ASIC structures have been solved in the closed, open and desensitized states, several putative proton-binding sites have been identified, and a large number of functional studies have provided invaluable insights into our understanding of ASIC gating. Despite this amount of research that has been conducted over the years, the molecular mechanisms leading to ASIC activation are still poorly understood. We hypothesize that proton binding to several ASIC extracellular domains initiates conformational changes that are probably propagated through the lower palm domain and the wrist to the transmembrane domains, where the pore and channel gates lie. It would be, therefore, very useful to investigate the type and the timing of these conformational changes to understand how these structural changes drive channel activity. For a better comprehension of the molecular mechanisms underlying channel activation, it is also very important to identify more accurately the proton-binding sites.

Specific aims

1) Determine whether pH sensing in the acidic pocket or in the palm domain is essential for ASIC activation by extracellular protons.

2) Describe conformational changes in the acidic pocket, which has been suggested to be the primary site for ASIC H^+ sensing.

3) Describe conformational changes in the palm and wrist, which are expected to transmit the structural changes induced by protonation of extracellular residues to the channel pore.

Strategies

To address the first two aims, we combined mutagenesis and VCF experiments to determine whether, and on which extent, channel activation depends on protonation events in the acidic pocket and palm domain, and whether conformational changes in the acidic pocket are compatible with a role in channel activation. This work is described in the published paper "Conformational dynamics and role of the acidic pocket in ASIC pH-dependent gating" (paragraph 3.1).

To address the third aim, we employed the VCF technique to investigate the structural rearrangements occurring in the lower palm and wrist during channel activity, and correlate them with a specific channel transition. This work is described in the prepared manuscript "Rapid and slow conformational changes in the lower palm and wrist region associated with ASIC1a gating transitions" (paragraph 3.2).

3. Results

3.1 Project 1: Role of the acidic pocket and palm domain in hASIC1a

Article: Conformational dynamics and role of the acidic pocket in ASIC pH-dependent gating

Authors: Sabrina Vullo, Gaetano Bonifacio, Sophie Roy, Niklaus Johner, Simon Bernèche and Stephan Kellenberger

In the first part of this project, we asked whether protonation events in the acidic pocket and palm domain are required for channel activation. We found that combination of neutralization mutations of a large number of titratable acidic pocket residues did not prevent the opening of the channel in response to an acidic stimulation, but, rather, fine-tuned its pH dependence. In the palm, neutralizing mutations of several acidic residues impaired channel desensitization, leading, in some cases, to the disappearance of the transient ASIC component and to the appearance of a sustained current component. Our results suggest that protonation in the acidic pocket is not essential for channel activation, whereas, protonation in the palm is required for normal desensitization. The second part of the project aimed at elucidating the structural rearrangements within the acidic pocket occurring during channel activity. Using the voltage-clamp fluorometry technique, we found conformational changes in the acidic pocket related to both activation and desensitization, and proposed a model that likely predicts the conformational changes in this region during ASIC activity.

Our study provides important insights on two key regions in the extracellular domain involved in ASIC1a pH-dependent gating.

My contribution to the manuscript:

The mutagenesis and functional test of potential pH sensing residues were carried out by Sophie Roy, technician in the laboratory. The screening of the cysteine mutants within the acidic pocket was performed by the former PhD student, Dr. Gaetano Bonifacio. I performed and analyzed most of the experiments for the voltage-clamp fluorometry, and all the experiments asked by the reviewers. I contributed to the writing of the manuscript.

Conformational dynamics and role of the acidic pocket in ASIC pH-dependent gating

Sabrina Vullo[a,1], Gaetano Bonifacio[a,1], Sophie Roy[a], Niklaus Johner[b,c], Simon Bernèche[b,c], and Stephan Kellenberger[a,2]

[a]Department of Pharmacology and Toxicology, Faculty of Biology and Medicine, University of Lausanne, 1011 Lausanne, Switzerland; [b]SIB (Swiss Institute of Bioinformatics), Biozentrum, University of Basel, 4056 Basel, Switzerland; and [c]Biozentrum, University of Basel, 4056 Basel, Switzerland

Acid-sensing ion channels (ASICs) are proton-activated Na$^+$ channels expressed in the nervous system, where they are involved in learning, fear behaviors, neurodegeneration, and pain sensation. In this work, we study the role in pH sensing of two regions of the ectodomain enriched in acidic residues: the acidic pocket, which faces the outside of the protein and is the binding site of several animal toxins, and the palm, a central channel domain. Using voltage clamp fluorometry, we find that the acidic pocket undergoes conformational changes during both activation and desensitization. Concurrently, we find that, although proton sensing in the acidic pocket is not required for channel function, it does contribute to both activation and desensitization. Furthermore, protonation-mimicking mutations of acidic residues in the palm induce a dramatic acceleration of desensitization followed by the appearance of a sustained current. In summary, this work describes the roles of potential pH sensors in two extracellular domains, and it proposes a model of acidification-induced conformational changes occurring in the acidic pocket of ASIC1a.

acid-sensing ion channel | conformational changes | voltage clamp fluorometry | pH sensing | kinetic model

Acid-sensing ion channels (ASICs) are Na$^+$-permeable channels (1) that participate in neuronal signaling under conditions involving pH changes, such as neuronal activity, ischemia, and inflammation. ASICs are involved in fear behaviors, learning, neurodegeneration after ischemic stroke, and pain sensation (2, 3). Functional ASICs are composed of three identical or homologous subunits (4, 5).

These channels respond to extracellular acidification with a transient current, because, after opening, they rapidly enter a nonconducting, so-called "desensitized" functional state. Crystal structures of chicken ASIC1 (~90% sequence homology to human ASIC1a) reveal presumably desensitized (5, 6) and toxin-opened conformations (7–9). Single ASIC subunits have a shape similar to that of a hand holding a small ball (5), and thus their domains have been named accordingly (Fig. 1A). The palm domain forms the internal scaffold of the channel along the central vertical axis. The thumb and the finger point toward the exterior of the channel and enclose, together with the β-ball, the "acidic pocket" (AcP), a region containing many acidic residues (Fig. 1A) (5).

Due to the presence of many acidic residues, the AcP was initially proposed as a pH sensor of ASICs (5). Although mutation of AcP Glu and Asp residues shifts the pH dependence of ASIC activation to more acidic values (5, 10–12), H$^+$-sensing residues have also been identified outside the AcP (10, 12, 13), indicating that the AcP is not the only extracellular pH-sensing domain. Its importance is, however, underlined by the fact that it constitutes the binding site of several ASIC-specific toxins (7, 14).

In the present study, we asked whether acid sensing in the AcP and the palm is required for ASIC activation and whether the timing of conformational changes in the AcP is compatible with a role in activation. We show that combined, conservative mutation of potential pH-sensing residues in the AcP changes the pH

dependences, but still allows ASIC opening and desensitization. Analogous mutations in the palm accelerated desensitization and led to the appearance of a secondary, sustained current. Voltage clamp fluorometry (VCF) analysis indicates the occurrence of rapid and slow conformational changes in the AcP, compatible with a role in both activation and desensitization, and allows us to propose a model of conformational changes in this domain.

Results

Acidic Residues in the Acidic Pocket Are Not Required for ASIC Activation. To determine the importance of pH sensing in the AcP for ASIC1a function, we combined neutralization mutations of all Asp, Glu, and His residues of the AcP to Asn or Gln (Fig. 1 A and B). When all of the protonable residues of the AcP were mutated, these channels, expressed in *Xenopus* oocytes, still produced transient currents upon extracellular acidification. Some mutants displayed up to twofold accelerated kinetics of current decay (Fig. S1A), in accordance with previous studies that described altered current kinetics of AcP mutants (15, 16). Some mutants showed a sustained current, which was, however, small in all mutants except AcP16b (Fig. S1B), indicating that desensitization is, in most mutants, complete at the end of an acidification.

The pH of half-maximal activation (pH50) was generally shifted by ~0.5 pH units to more acidic values compared with WT (green symbols and bars in Fig. 1 D and E). The Hill coefficient, a measure of the steepness of the pH-current relationship and of the cooperativity of the process, decreased from ~3 in WT to ~1.5 in most channels containing more than seven AcP mutations (gray

Significance

Many physiological processes are regulated by pH. The acid-sensing ion channels (ASICs) are neuronal pH sensors involved in learning, fear behavior, neurodegeneration after ischemic stroke, and pain sensation. The mechanism by which acidic pH activates ASICs is still poorly understood. We show here that the "acidic pocket," the binding site of several toxins, is not essential for channel function but has, rather, a modulatory role. Furthermore, we describe the structural rearrangements occurring in this domain during ASIC activity, and highlight the importance of the "palm" domain in channel opening and current decay. In this study, we provide insights on the molecular mechanisms controlling ASIC activity together with a rational basis for the development of ASIC-targeting drugs.
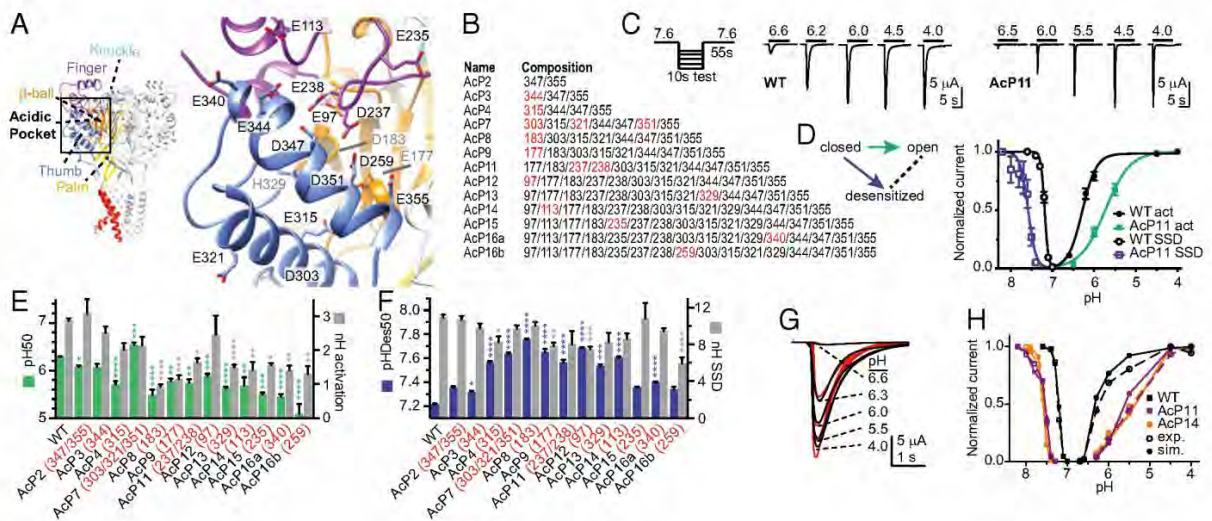
Fig. 1. Combined mutation of AcP residues preserves almost normal ASIC1a function. (*A*) Structural image, showing a human ASIC1a model based on the chicken ASIC1 structure (8). (*Left*) Trimer structure. Individual domains of one subunit are colored and labeled. (*Right*) Close-up view of the AcP formed by the thumb, the finger, and the β-ball. The residues that were mutated are indicated. (*B*) Mutant composition. Each number in the right column represents a neutralization mutation, Glu to Gln, Asp to Asn, and His to Asn. The new mutations from one construct to another are marked in red. (*C*) Representative current traces of WT and the mutant AcP11. The pH protocol is schematically indicated on the left. (*D*) The pH dependence of activation and SSD of WT and AcP11 (*n* = 4–6). Normalized current amplitudes are plotted as a function of stimulation pH for activation (filled symbols) and as a function of the conditioning pH for SSD (open symbols). The solid lines represent fits to the Hill equation (*SI Materials and Methods*). The kinetic scheme of ASIC functional states is shown, emphasizing, with a green arrow, the activation, and, with a blue arrow, the SSD transition. (*E*) The pH dependence of activation, plotting pH of half-maximal activation (pH50) values as green bars (left axis) and the Hill coefficient (nH) in gray (right axis). The conditioning pH in these experiments was 7.6 to 8.0, depending on the mutant, to ensure stable recordings without occurrence of SSD. For each mutant, the numbers in red indicate the residues mutated in addition to the mutations already present in the preceding mutant; *n* = 4–125. (*F*) The pH dependence of SSD, showing pH of half-maximal SSD, pHDes50 values as blue bars, and nH values of SSD in gray; *n* = 5–56. (*G*) Experimental current traces (black) of an activation curve of ASIC1a WT and corresponding traces generated by the 32-state model (red; *SI Materials and Methods*). (*H*) Activation and SSD curves of WT, AcP11, and AcP14 generated experimentally (filled symbols) or by the 32-state model (open symbols). (*P < 0.05; **P < 0.01; ***P < 0.001; ****P < 0.0001; different from WT.)

bars in Fig. 1*E*). The pH dependence of steady-state desensitization (SSD), the direct transition from the closed to the desensitized state (blue arrow in the scheme of Fig. 1*D*), was determined by exposing oocytes to a series of conditioning test pH solutions for 55 s, each followed by a short application of an acidic pH solution. The pH dependence of SSD was shifted to more alkaline values by the combination of AcP mutations (blue symbols and bars in Fig. 1 *D* and *F*), although the values are less alkaline for constructs containing >14 neutralization mutations.

As shown above, neutralization mutations of protonable residues in the AcP induced the following functional changes: (*i*) They shift the pH50 of activation to more acidic values; (*ii*) they shift the pH50 of SSD to more alkaline values; and (*iii*) they decrease the Hill coefficient of activation, but not of SSD. Neutralization mutations of Asp and Glu, mimicking protonated acidic residues, correspond to gain of function mutations, which are expected to lead to an alkaline shift in pH dependence as observed for neutralization mutations of key proton-sensing residues in the K+ channel KcsA (17). Although our mutagenesis approach does not indicate whether a mutated residue is a pH sensor or has other roles in conformational transitions, it is very likely that at least some of these residues are pH sensors. Because the observed effects of AcP mutations appear to be complex, we use kinetic models to illustrate how these mutations may affect pH dependence. Consider a four-state model as depicted in Fig. S1*C*, corresponding to a system with two protonation sites, either of which can be protonated or not. A neutralization mutation will correspond to having one of the sites always protonated, reducing the problem to a two-state model. We show that, if protonation of both sites is required for the transition to the state of interest (e.g., the open state), then a neutralization mutation will always lead to an increase in pH50 accompanied by a decrease of the Hill coefficient (*SI Materials and Methods* and Fig. S1*D*). However, if protonation of only one of the sites is required, then mutation of the other one can lead to both an increase or a decrease in pH50 and an increase or a decrease in the Hill coefficient (Fig. S1 *D* and *E* and *SI Materials and Methods*). The observed effects of AcP mutations therefore suggest a nonessential role of this domain in activation. To test this hypothesis, we built a kinetic model of ASIC comprising three sets of protonation sites: (*i*) sites in the AcP, (*ii*) other sites responsible for desensitization, and (*iii*) sites leading to activation (Fig. S1*F* and *SI Materials and Methods*). The model was fitted to traces of complete activation and SSD curves of ASIC1a WT and the mutants AcP11 and AcP14. The model reproduced the experimental data reasonably well if protonation of the AcP was considered accessory for activation, regardless of whether the same protonation events in the AcP were modeled as required or were accessory for desensitization (Fig. 1 *G* and *H* and Fig. S1*F*), but not if they were considered essential for activation. The parameters of the fitted models indicated that protonation of the AcP shows a negative cooperativity with protonation of activation sites, and a positive cooperativity with protonation of desensitization sites. The modeling suggests, therefore, that protonation-mimicking mutations of the AcP induced an acidic shift in activation pH dependence due to the negative cooperativity between these two types of protonation.

Combined Mutations of Potential pH Sensors in the Palm Accelerate Desensitization and Give Rise to a Nondesensitizing Current. To assess the role of pH sensing in the palm, we combined mutations

45

of the six acidic residues of the lower and middle palm (palm core, "PaC," bold in Fig. 2A), and subsequently, in addition, the two nearby β-ball residues D212 and E254 (Fig. 2 A and B). The most striking feature of these combined mutants is the appearance of a sustained current component and, with increasing number of mutations, a complete disappearance of the transient current (Fig. 2C and Fig. S2A). The disappearance of the peak current could be due to either loss of channel activation or very fast desensitization; to distinguish between these two possibilities, we measured the mutant channels at a lower temperature, which is known to strongly slow down desensitization but not activation (18). We uncovered a peak current in PaC6, and observed a strong increase of the PaC4 peak current amplitude relative to that of the sustained current (Fig. 2D and Fig. S2B). This demonstrates that the combined mutations such as PaC6 accelerate desensitization to an extent that the transient current disappears.

The slowly developing sustained current is only induced by cumulative palm mutations, as no single neutralization mutation of acidic residues of the palm, except for D78, induced any sustained currents (Fig. S2C). This sustained current is distinct from the transient current with regard to several properties. (i) In contrast to the WT peak current, the sustained current has almost completely lost its cation selectivity (Fig. S2 D–G; P_{Na}/P_K ratio of 9.8 ± 0.4, 5.2 ± 0.4, 2.5 ± 0.3 and 2.7 ± 0.9 for WT, PaC4 peak, PaC4, and PaC6 sustained current, respectively; $n = 3–11$, $P < 0.01$); (ii) it is not inhibited by the pore blocker

amiloride (Fig. S2 H and I); and (iii) its pH dependence of activation is shifted by two pH units to more acidic values (Fig. 2E).

Additional mutation of the two acidic palm residues pointing toward the wrist, D78 and E421, or the wrist residue H73 (Fig. S2J) in PaC mutants did not further change the current properties in most cases (Fig. S2 K–N). In two of these mutants, a transient current was reconstituted. The pH dependence of the tested palm mutants correlated with the type of current—transient vs. sustained—and not with the number of mutations (Fig. 2E and Fig. S3M). This correlation, together with the different current properties, further confirms that these nondesensitizing currents are profoundly different types of openings, and may be related to sustained ASIC currents induced by some chemical compounds and lipids (19, 20).

Conformational Changes in the Acidic Pocket. By which mechanisms do the palm and the AcP influence ASIC function? The comparison of toxin-opened and desensitized ASIC structures showed evidence for a centripetal movement of the three lower palm domains during desensitization (7). Accessibility studies combined with molecular dynamics simulations suggested that this conformational change in the palm is transduced into closure of the pore (21).

To obtain information on possible conformational changes in the AcP during gating, we applied VCF, which employs simultaneous measurement of ionic currents and of the fluorescence intensity of fluorophores placed at specific sites of the channel (Fig. 3A). Attachment of the fluorophores AlexaFluor488 (Fig. 3B) or CF488A to engineered Cys residues at different positions of the AcP did not, in most mutants, lead to measurable fluorescence changes (ΔF) during channel activity (Table S1). Changes in fluorescence intensity of fluorophores are due to alterations in the environment and/or quenching by nearby amino acid residues. Trp is known as a strong fluorescence quencher (22). To allow the measurement of ΔF signals in this domain, we have paired engineered Cys residues as fluorophore docking positions with engineered Trp residues as quenchers across the AcP (Fig. 3A and Fig. S3A).

Cys/Trp double mutants of the AcP produced transient acid-induced currents, and various types of ΔF signals. The ΔF of several Cys/Trp mutants contained two components, an initial rapid negative or positive ΔF that was followed by a slower ΔF of the opposite polarity, as illustrated by current and ΔF traces of the mutant D237C/D347W (Fig. 3C, lower traces). To associate ΔF signals with functional transitions, we compared the kinetics of the ΔF and the current signals, measured as rise time (the time to pass from 10 to 90% of the full amplitude). We measured the pH 6-induced ΔF and currents from approximately the same oocyte surface by using a recording chamber in which the solution flows under the oocyte (Fig. 3D and *SI Materials and Methods*). The onset kinetics of the fast ΔF component of the mutants D347C/T236W, D237C/D347W, D351C/D237W, and E355C match the kinetics of current appearance (Fig. 3E and Fig. S3B; see Table S2 for a correlation analysis). These ΔF signals started 100 ms to 250 ms before the current (Fig. 3 F and G), strongly suggesting that the monitored movements in these mutants are correlated with channel opening. The second ΔF components and the ΔF signals of all other mutants were slower than current appearance (Fig. 3E), and the difference in delay was smaller or absent. The ΔF onset was, in most mutants, faster than the current decay (Fig. 3H), and only two mutants, K343C/T236W and D351C/F257W, showed ΔF onset kinetics correlated with current desensitization. The transitions occurring after channel opening may thus be associated with desensitization or with its preparation.

The pH dependence of the ΔF signals was, in most mutants, close to that of SSD, and was more alkaline than the pH dependence of current activation (Fig. 3I); hence these conformational
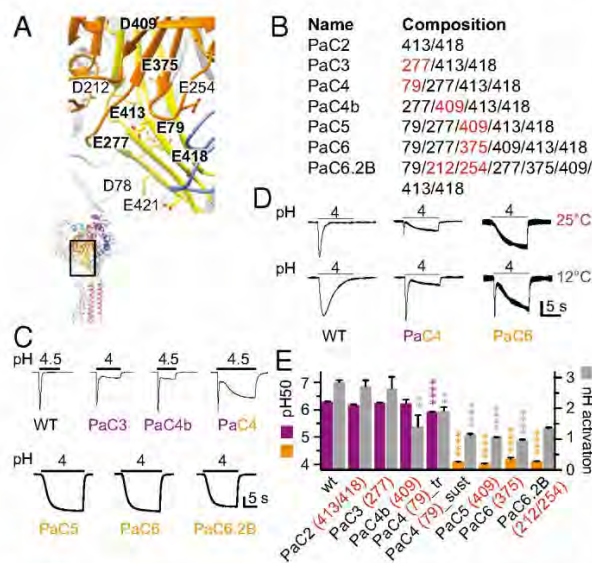
Fig. 2. Combined mutations of palm residues accelerate desensitization and induce a sustained current. (A) Structural image of the palm (yellow) and β-ball (orange) domains of one ASIC1a subunit, showing the acidic residues investigated here, with residues of the "palm core" (see *Results*) highlighted in bold. (B) Mutant composition. The new mutations from one construct to another (compared with the construct with lower number of mutations) are marked in red. B, β-ball; PaC, palm core. (C) Representative current traces of different palm mutants. The vertical bar corresponds to (in microamperes) 6 (WT), 3 (PaC3), 4 (Pa4b), 1 (PaC4), 1.25 (PaC5), 0.5 (PaC6), and 0.24 (PaC6.2B). (D) Representative current recordings of WT, PaC4, and PaC6 at the indicated temperatures. The vertical bar corresponds to (in microamperes) 4.6 (WT), 3.2 (PaC4), and 1 (PaC6). In C and D, the conditioning pH was 7.4. (E) The pH dependence of activation, pH50 values (colored bars), and nH of activation (gray bars); $n = 5–128$. The pH50 values of transient currents are shown in purple, and those of sustained currents are shown in orange. (*P < 0.05; **P < 0.01; ***P < 0.001; ****P < 0.0001; different from WT.)
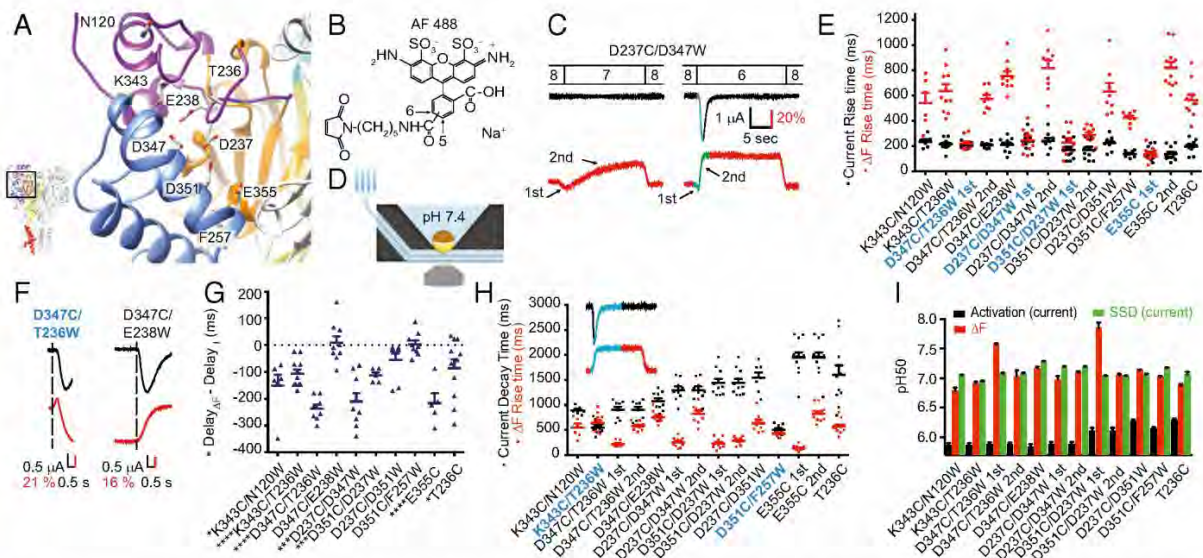
Fig. 3. Fluorescence changes in the AcP associated with channel opening and desensitization. (*A*) Close-up view of the AcP, showing the residues that were mutated to Cys (to dock fluorophores) and/or to the quenching residue Trp. (*B*) Structure of the fluorophore AlexaFluor488. (*C*) Representative current and ΔF traces at pH 7 and 6 of the mutant D237C/D347W, highlighting, in green and blue, the parts of the pH 6 traces used for kinetic analysis. Note that the ΔF trace has two components, as highlighted with the arrows. (*D*) Schematic view of the oocyte recording chamber used for measurements of current and ΔF kinetics (*SI Materials and Methods*). (*E*) Scatter graph comparing the rise time of the channel opening (black) and the ΔF onset (red) in response to acidification from the conditioning pH 7.4 to the stimulation pH 6 in paired experiments; $n = 6$–12. For mutants containing two ΔF components, the two are distinguished as first and second. Correlation between the ΔF and current signal is indicated by labeling in bold turquoise (see criteria in Table S2). (*F*) Representative current and ΔF traces showing (*Left*) a mutant in which the start of the ΔF signal precedes that of the current (D347C/T236W) and (*Right*) one in which the two signals start at the same time (D347C/E238W). The vertical dashed line indicates the beginning of the ΔF. (*G*) Scatter dot plot of the difference in the ΔF and current delay of appearance (delay$_{\Delta F}$ − delay$_I$) measured at pH 6; $n = 5$–11. (*H*) Scatter graph comparing the current decay time (black) and the fluorescence rise time (red) in response to acidification from pH 7.4 to pH 6 in paired experiments; $n = 6$–12. Bold turquoise labels indicate correlation between ΔF onset and current decay kinetics (Table S2). (*Inset*) In blue, the parts of current and ΔF traces whose kinetics were compared. (*I*) The pH of half-maximal amplitude (pH50) for current (black columns) and fluorescence activation (red), and the pH of current SSD (green); $n = 4$–16.

changes could be part of channel desensitization. The ΔF signals sharing the kinetics of current appearance also showed such a shifted pH dependence, indicating that they occur at more alkaline pH than channel opening. This observation does not rule out their possible implication in channel opening, but it indicates that there must be other conformational changes required for activation, which have a lower pH50 than those occurring in the AcP and would therefore govern the pH50 of activation. This shift in pH dependence is reminiscent of the leftward shift in voltage dependence of ΔF versus currents in voltage-gated K$^+$ channels (23, 24).

Hypothesized Movements Based on VCF Observations. The proximity of a quenching group decreases the total fluorescence (F) of a fluorophore, but may generate an activity-induced ΔF if there is a change in distance between the fluorophore and the quenching group. The specific ΔF signals of the single Cys mutants used in the Cys/Trp pairs were of very small amplitude compared with the ΔF signal of related Cys/Trp pairs (Table S1), indicating that the ΔF observed in double mutants is due to the additional presence of the engineered Trp. Control experiments showed that the only endogenous Trp residue in the proximity of the palm, W233, did not affect these signals (compare Fig. S3C and Fig. 4A). A positive ΔF indicates, therefore, an increase in distance between the Trp residue and the Cys-attached fluorophore, whereas a negative ΔF indicates a decrease in this distance. These ΔF signals do not exactly reflect the distance changes between the Cys and Trp of a given pair, because the fluorophore has itself a diameter of 7 Å to 10 Å and is attached to the Cys residue by a linker (Fig. 3B), with an estimated

distance between the docking site and the center of the fluorophore of 5 Å to 15 Å (from molecular dynamics trajectories, Corry research group, karri.anu.edu.au/handy/). This limitation has to be considered as a factor of imprecision in the following interpretation of the VCF data.

The nature of the ΔF signals of different Cys/Trp double mutants (Fig. 4A) is summarized in the ASIC structure (Fig. 4B) with dotted lines between the paired residues and with "+" indicating an increase, and "-" a decrease, in ΔF. The early, rapid ΔF signals suggest, therefore, a short-lived approach of D237 toward D347 and D351, and an increase of the T236–D347 distance, which occurs during or slightly before activation. The VCF analysis suggests that these movements are then followed by a decrease of the N120–K343 and T236–D347 distances, and by an increase of the D237–D347, D237–D351, and E238–D347 distances, and, with the time course of desensitization, an increase of the F257–D351 and a decrease of the K343–T236 distances.

We estimate that the higher amplitude of the slower ΔF components is due to a larger conformational change, because, in the ΔF signals composed of a rapid and a slow component, the ΔF of both components depends on the quenching by the engineered Trp, and rapid and slow signals were compared within the same Cys/Trp pair. Most likely, the conformational changes generating these ΔF signals are part of a continuous movement of the involved AcP domains. The initial, fast ΔF signals that are correlated with channel activation may represent a tilting of the finger loop that would bring D237 and E238, located at the lower end of the loop, closer to the α5 helix, and T236, which is higher up, farther away from the α5 helix (green arrows in Fig. 4C). The distance changes involving residues T236, D237, and E238 occurring
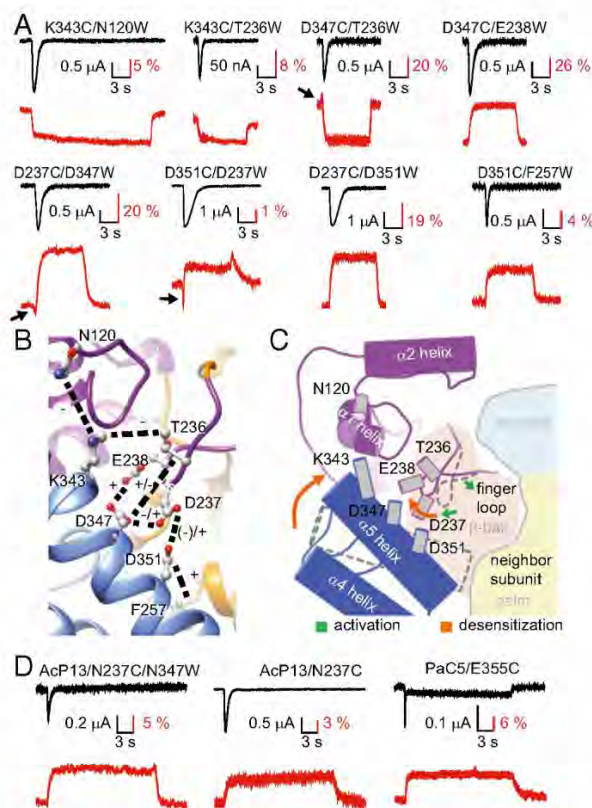
Fig. 4. Predicted conformational changes in the AcP. (*A*) Representative, paired current (black) and fluorescence (red) traces of double mutants in response to extracellular acidification to pH 6. Black arrows point to fast ΔF components. (*B*) View of the AcP with the mutated residues, indicating, by dashed black lines, the different Cys/Trp pairs. For each double mutant, the nature of the ΔF signal is indicated by "+" or "−" signs ("+" denotes increase in ΔF); for mutants with composite ΔF signal, the left sign represents the first component. (*C*) Scheme indicating the deduced conformational changes in the AcP during opening and steps preceding and correlated with desensitization, as discussed in the *Results*. The gray cylinders represent residues mutated for the VCF experiments. The dotted outlines of the finger loop and α5 thumb helix represent their hypothesized position in the closed state. Hypothesized conformational changes are illustrated by arrows, the green arrows standing for conformational changes occurring during activation, and the orange arrows standing for subsequent steps occurring before and during desensitization. (*D*) Representative current and ΔF traces of the mutants AcP13/N237C/N347C, AcP13/N237C, and PaC5/E355C. Note that not only the N237C/N347W pair, but also the single mutation N237C, induced measurable ΔF signals, indicating that, in the changed environment of the AcP13 mutant, the N237C ΔF did not depend on the presence of a nearby Trp residue and does not reflect a change in distance between the fluorophore and the Trp residue. The PaC5/E355C mutant showed, in approximately half of the experiments, a rapid transient and a sustained component and, in the other half, only a sustained current.

after activation are best explained by a movement of this finger loop toward the outside of the protein (right orange arrow in Fig. 4*C*). This movement may involve a partial rotation of the loop, thereby bringing T236 closer to K343 and D347, as well as moving D237 and E238 away from D347 and D351. The α5 helix likely undergoes a movement relative to the other domains that brings its outer end (K343) closer to the finger and its inner part (D351) farther away from the β-ball.

ΔF Signals in Mutants Containing Protonation-Impaired Domains. To determine whether conformational changes depend on protonation

events in the AcP and the palm, we introduced a fluorophore/quencher pair in the AcP mutant AcP13, and the E355C mutation in the palm mutant PaC5, thus two mutants in which a large number of acidic residues have been neutralized. In both, AcP13/N237C/N347W and PaC5/E355C, the slow, but not the fast, ΔF component was present (Fig. 4*D* and Fig. S4). The absence of a fast ΔF component in these mutants may be due to a requirement of protonation of AcP or palm residues for the rapid ΔF signal. We cannot, however, exclude the possibility that this absence is due to a changed environment, especially for AcP13/N237C/N347W. The fact that the slower ΔF signal is still present in the combined mutants indicates that neither protonation of AcP nor palm residues is required for the slower conformational changes occurring in the AcP. E355C showed, as expected, faster current decay kinetics in the PaC5 background, and this acceleration was also reflected in the ΔF onset kinetics ($P < 0.0001$ and <0.05, respectively; Fig. S4*D*).

Discussion

We show, in this study, that the presence of protonable residues in the AcP and the palm is not essential for ASIC activation but plays other roles: In the AcP, acidic residues allow the fine-tuning of ASIC pH dependence, whereas, in the palm, they control the desensitization kinetics and prevent the appearance of a sustained current. Our VCF analysis provides evidence of conformational changes in the AcP correlated to activation and desensitization, and proposes a likely sequence of conformational changes in the AcP upon extracellular acidification.

The observed acceleration of the desensitization kinetics in palm mutants was much stronger than kinetic changes of palm mutants investigated in previous studies (10, 21) and led to the disappearance of the transient current at room temperature. The fact that acceleration was induced by mutations that mimic protonated side chains suggests that protonation events in the palm lead to desensitization.

The AcP is the binding site of the two gating modifier toxins PcTx1 and Mambalgin (7, 9, 25–27). Nonconservative mutations in the AcP of ASICs have induced strong changes in the pH dependence (11, 28), whereas conservative mutations of Asp and Glu residues induced modest (5, 12) or no changes in activation pH dependence (10). The acidic residues E344, D347, D351, and E355 of the thumb α5 helix that are at the center of the interaction with the finger loop are better conserved between ASIC1a and ASIC2 (three of four) than between ASIC1a and ASIC3 (one of four), whose pH dependence is close to that of ASIC1a. These differences appear not to affect the conformational changes in the AcP, because at least the slow ΔF signals were still present after neutralization of many AcP residues (Fig. 4*D*). For ASIC2, it was shown that regions outside the AcP, mostly the first ~90 residues after the TM1, are critical for channel function (29, 30). These observations are consistent with an important regulatory, but not essential, role of the AcP in ASIC activation. The AcP also controls the kinetics and pH dependence of desensitization (15, 16, 27), a role that is underlined here by the slow ΔF signals, which may reflect conformational changes leading to desensitization. In ENaC, the AcP may also have a regulatory role, because it was shown to contain a binding site for Na$^+$ involved in channel inhibition (31).

Experimental evidence for conformational changes in the AcP was recently provided by luminescence resonance energy transfer (LRET) measurements showing that the distance between residues of the thumb and the finger is decreased in the desensitized compared with the closed state (28). We describe here the time course of this closing movement and suggest that it concerns, rather, the external end of the AcP, which opens on its inner side. Such a movement of the inner part of the AcP is supported by the recent observation that formation of a disulfide bond between the thumb residue E355C and R175C of the palm locks

48

the channel in the closed state (32). The slower conformational changes in the AcP do not depend on protonation events in the AcP or the palm, indicating that these conformational changes in the AcP are induced by protonation events occurring outside the AcP or the palm. Protonation of AcP residues, or binding of ligands to the AcP, may influence the kinetics and possibly the amplitude of these conformational changes and thereby modulate ASIC function.

Our observation of large ΔF signals occurring between opening and desensitization, suggesting conformational changes in the AcP, contradicts the findings with crystal structures of ASIC1, which show an almost identical conformation of the AcP in toxin-opened and desensitized channels (7). It is possible that the toxin-opened ASIC conformation studied in crystal structures is different from the H$^+$-opened conformation. Evidence for important conformational changes during ASIC desensitization comes from the observation that ASIC currents show a strong temperature dependence of desensitization. In contrast, the temperature dependence of activation is much weaker (18). These observations are consistent with the small-amplitude ΔF signals correlated to activation and the large-amplitude ΔF signals correlated to later events. The above-mentioned LRET experiments (28) and a recent Cys accessibility study (15) also suggest conformational changes in the AcP upon acidification. To affect channel activity, conformational changes in the AcP need to change the conformation of the ASIC pore. The downward movement of the internal end of the α5 helix during desensitization would likely be transmitted to the pore via the β-turn structure that is part of a palm–thumb loop and interacts with the external end of the transmembrane domain, or via the palm.

Materials and Methods

WT and mutant human ASIC1a were expressed in *Xenopus laevis* oocytes. All experiments with *Xenopus* were carried out in accordance with the Swiss federal law on animal welfare, following protocols that had been approved by the committee on animal experimentation of the Canton de Vaud. ASIC currents were measured by two-electrode voltage clamp, and VCF experiments were carried out as described previously (ref. 33; Table S3), with the exception that a different measuring chamber, allowing measurement of current and fluorescence from approximately the same oocyte surface, was used for the kinetics experiments. Kinetic models were fitted directly to the measured currents using the Data2Dynamics software (34). Data are presented as mean ± SEM. Individual experimental data points are provided in *Supporting Information*. Detailed material and methods are provided in *SI Materials and Methods*.

1. Yang L, Palmer LG (2014) Ion conduction and selectivity in acid-sensing ion channel 1. *J Gen Physiol* 144(3):245–255.
2. Wemmie JA, Taugher RJ, Kreple CJ (2013) Acid-sensing ion channels in pain and disease. *Nat Rev Neurosci* 14(7):461–471.
3. Kellenberger S, Schild L (2015) International Union of Basic and Clinical Pharmacology. XCI. Structure, function, and pharmacology of acid-sensing ion channels and the epithelial Na$^+$ channel. *Pharmacol Rev* 67(1):1–35.
4. Bartoi T, Augustinowski K, Polleichtner G, Gründer S, Ulbrich MH (2014) Acid-sensing ion channel (ASIC) 1a/2a heteromers have a flexible 2:1/1:2 stoichiometry. *Proc Natl Acad Sci USA* 111(22):8281–8286.
5. Jasti J, Furukawa H, Gonzales EB, Gouaux E (2007) Structure of acid-sensing ion channel 1 at 1.9 Å resolution and low pH. *Nature* 449(7160):316–323.
6. Gonzales EB, Kawate T, Gouaux E (2009) Pore architecture and ion sites in acid-sensing ion channels and P2X receptors. *Nature* 460(7255):599–604.
7. Baconguis I, Gouaux E (2012) Structural plasticity and dynamic selectivity of acid-sensing ion channel-spider toxin complexes. *Nature* 489(7416):400–405.
8. Baconguis I, Bohlen CJ, Goehring A, Julius D, Gouaux E (2014) X-ray structure of acid-sensing ion channel 1-snake toxin complex reveals open state of a Na$^{(+)}$-selective channel. *Cell* 156(4):717–729.
9. Dawson RJ, et al. (2012) Structure of the acid-sensing ion channel 1 in complex with the gating modifier Psalmotoxin 1. *Nat Commun* 3:936.
10. Krauson AJ, Rued AC, Carattino MD (2013) Independent contribution of extracellular proton binding sites to ASIC1a activation. *J Biol Chem* 288(48):34375–34383.
11. Li T, Yang Y, Canessa CM (2009) Interaction of the aromatics Tyr-72/Trp-288 in the interface of the extracellular and transmembrane domains is essential for proton gating of acid-sensing ion channels. *J Biol Chem* 284(7):4689–4694.
12. Liechti LA, et al. (2010) A combined computational and functional approach identifies new residues involved in pH-dependent gating of ASIC1a. *J Biol Chem* 285(21):16315–16329.
13. Paukert M, Chen X, Polleichtner G, Schindelin H, Gründer S (2008) Candidate amino acids involved in H$^+$ gating of acid-sensing ion channel 1a. *J Biol Chem* 283(1):572–581.
14. Mourier G, et al. (2016) Mambalgin-1 pain-relieving peptide, stepwise solid-phase synthesis, crystal structure, and functional domain for acid-sensing ion channel 1a inhibition. *J Biol Chem* 291(6):2616–2629.
15. Krauson AJ, Carattino MD (2016) The thumb domain mediates acid-sensing ion channel desensitization. *J Biol Chem* 291(21):11407–11419.
16. Kusama N, Harding AM, Benson CJ (2010) Extracellular chloride modulates the desensitization kinetics of acid-sensing ion channel 1a (ASIC1a). *J Biol Chem* 285(23):17425–17431.
17. Posson DJ, Thompson AN, McCoy JG, Nimigean CM (2013) Molecular interactions involved in proton-dependent gating in KcsA potassium channels. *J Gen Physiol* 142(6):613–624.
18. Askwith CC, Benson CJ, Welsh MJ, Snyder PM (2001) DEG/ENaC ion channels involved in sensory transduction are modulated by cold temperature. *Proc Natl Acad Sci USA* 98(11):6459–6463.
19. Marra S, et al. (2016) Non-acidic activation of pain-related Acid-Sensing Ion Channel 3 by lipids. *EMBO J* 35(4):414–428.
20. Yu Y, et al. (2010) A nonproton ligand sensor in the acid-sensing ion channel. *Neuron* 68(1):61–72.
21. Roy S, et al. (2013) Molecular determinants of desensitization in an ENaC/degenerin channel. *FASEB J* 27(12):5034–5045.
22. Pantazis A, Olcese R (2012) Relative transmembrane segment rearrangements during BK channel activation resolved by structurally assigned fluorophore-quencher pairing. *J Gen Physiol* 140(2):207–218.
23. Mannuzzu LM, Moronne MM, Isacoff EY (1996) Direct physical measure of conformational rearrangement underlying potassium channel gating. *Science* 271(5246):213–216.
24. Cha A, Bezanilla F (1997) Characterizing voltage-dependent conformational changes in the Shaker K$^+$ channel with fluorescence. *Neuron* 19(5):1127–1140.
25. Schroeder CI, et al. (2014) Chemical synthesis, 3D structure, and ASIC binding site of the toxin mambalgin-2. *Angew Chem Int Ed Engl* 53(4):1017–1020.
26. Salinas M, et al. (2014) Binding site and inhibitory mechanism of the mambalgin-2 pain-relieving peptide on acid-sensing ion channel 1a. *J Biol Chem* 289(19):13363–13373.
27. Chen X, Kalbacher H, Gründer S (2005) The tarantula toxin psalmotoxin 1 inhibits acid-sensing ion channel (ASIC) 1a by increasing its apparent H$^+$ affinity. *J Gen Physiol* 126(1):71–79.
28. Ramaswamy SS, MacLean DM, Gorfe AA, Jayaraman V (2013) Proton-mediated conformational changes in an acid-sensing ion channel. *J Biol Chem* 288(50):35896–35903.
29. Schuhmacher LN, Srivats S, Smith ES (2015) Structural domains underlying the activation of acid-sensing ion channel 2a. *Mol Pharmacol* 87(4):561–571.
30. Smith ES, Zhang X, Cadiou H, McNaughton PA (2007) Proton binding sites involved in the activation of acid-sensing ion channel ASIC2a. *Neurosci Lett* 426(1):12–17.
31. Kashlan OB, Blobner BM, Zuzek Z, Tolino M, Kleyman TR (2015) Na$^+$ inhibits the epithelial Na$^+$ channel by binding to a site in an extracellular acidic cleft. *J Biol Chem* 290(1):568–576.
32. Gwiazda K, Bonifacio G, Vullo S, Kellenberger S (2015) Extracellular subunit interactions control transitions between functional states of acid-sensing ion channel 1a. *J Biol Chem* 290(29):17956–17966.
33. Bonifacio G, Lelli CI, Kellenberger S (2014) Protonation controls ASIC1a activity via coordinated movements in multiple domains. *J Gen Physiol* 143(1):105–118.
34. Raue A, et al. (2015) Data2Dynamics: A modeling environment tailored to parameter estimation in dynamical systems. *Bioinformatics* 31(21):3558–3560.
35. Li P, et al. (2010) Site-specific fluorescence reveals distinct structural changes induced in the human rho 1 GABA receptor by inhibitory neurosteroids. *Mol Pharmacol* 77(4):539–546.
36. Hille B (2001) *Ion Channels of Excitable Membranes* (Sinauer Assoc, Sunderland, MA), 3rd Ed.
37. Pettersen EF, et al. (2004) UCSF Chimera—A visualization system for exploratory research and analysis. *J Comput Chem* 25(13):1605–1612.
38. Mukhtasimova N, Lee WY, Wang HL, Sine SM (2009) Detection and trapping of intermediate states priming nicotinic receptor channel opening. *Nature* 459(7245):451–454.
39. Krashia P, Lape R, Lodesani F, Colquhoun D, Sivilotti LG (2011) The long activations of α2 glycine channels can be described by a mechanism with reaction intermediates ("flip") *J Gen Physiol* 137(2):197–216.
40. Raue A, et al. (2013) Lessons learned from quantitative dynamical modeling in systems biology. *PLoS One* 8(9):e74335.

PHYSIOLOGY

Supporting Information

Vullo et al. 10.1073/pnas.1620560114

SI Materials and Methods

Molecular Biology. The human ASIC1a sequence was subcloned in a pSP65-derived expression vector containing 3′ and 5′ non-translated sequences of *Xenopus laevis* β-globin. Site-directed mutagenesis was done by using the Quikchange approach. All mutations were confirmed by sequencing (Synergen Biotech). Combined mutations were neutralization mutations, i.e., Asp to Asn, Glu to Gln, and His to Asn, except for D212, which was mutated to Gly. Mutation of D212 to Asn abolished channel function (no pH 5-induced membrane current in two series of experiments). Because all other ASIC subunits contain a Gly residue at the homologous position, D212 was mutated to Gly to disrupt a possible protonation of this side chain. The mutant channel D212G was functional. In vitro transcription was carried out with the mMessage mMachine SP6 kit (Ambion/Life Technologies).

Oocyte Handling and Injection. All experiments with *Xenopus* were carried out in accordance with the Swiss federal law on animal welfare, following protocols that had been approved by the committee on animal experimentation of the Canton de Vaud. Oocytes were isolated and cultured as described previously (12). Briefly, healthy stage V and VI oocytes of female *Xenopus laevis* frogs were treated with collagenase for isolation and defolliculation. They were subsequently injected with 50 nL to 100 nL of cRNA (0.02 μg/μL to 0.5 μg/μL). Oocytes were kept in modified Barth's saline (MBS) containing (in millimolars) 85 NaCl, 1 KCl, 2.4 NaHCO₃, 0.33 Ca(NO₃)₂, 0.82 MgSO₄, 0.41 CaCl₂, 10 Hepes, and 4.08 NaOH. For some experiments, oocytes were kept in an MBS containing 10 mM NaCl, with 75 mM NaCl replaced by *N*-methyl-D-glutamine. Oocytes that were later used for VCF were incubated after the injection for 1 h in MBS containing 10 mM 3-maleimidopropionic acid (Bachem) to modify free Cys residues of endogenous oocyte proteins at the cell surface. Measurements were done 24 h to 56 h after injection.

Solutions and Reagents. The standard recording solution was composed of (in millimolars) 110 NaCl, 2 CaCl₂, and 10 Hepes for pH values ≥ 6.8. Solutions with a pH < 6.8 contained Mes instead of Hepes. The pH was adjusted using NaOH. In some experiments, NaCl was replaced by *N*-methyl-glucosamine (120 mM) that is not conducted by ASICs. For measurement of the current–voltage relationship, the recording solution contained (in millimolars) 110 NaCl, 2 MgCl₂, and 10 Hepes (or 10 Mes for pH ≤ 6.7). To investigate the permeability to K⁺ and Cs⁺ ions, NaCl was substituted by the same concentration of KCl or CsCl. The pH was adjusted using NaOH, KOH, and CsOH, for solutions containing Na⁺, K⁺, and Cs⁺, respectively. For experiments performed at different temperatures, the extracellular solution contained Mops (which is less temperature-dependent) as pH buffer instead of Hepes or Mes; 10 mM stock solutions of AlexaFluor488 C-5 Maleimide (Alexa-Fluor488, Life Technologies) and CF488A (Biotium) were prepared in DMSO and stored in aliquots at −20 °C.

Electrophysiology. All experiments of the VCF part were carried out with oocytes that had been previously exposed to CF488 maleimide or AlexaFluor488 maleimide. Currents were recorded by two-electrode voltage clamp at −60 mV (−40 mV for VCF experiments) with a Dagan TEV-200 amplifier at a sampling rate of 1 ms and low-pass filtering at 2 kHz. Oocytes were impaled with two glass electrodes filled with 1 M KCl, with a resistance of <0.8 MΩ. The perfusion speed was set to 5 mL/min to 15 mL/min, and switching between different solutions was controlled by electrovalves. To generate activation and SSD curves, the recording chamber was perfused with conditioning pH solution, and, every minute, ASICs were activated with stimulation solution for 5 s to 10 s. For measurements of current–voltage relationship, the holding potential was −60 mV and 90-ms voltage ramps from −100 mV to +80 mV were applied every 200 ms. The conditioning pH was 7.4, and the stimulation pH was 5. For experiments performed at different temperatures, the temperature of the perfusion solution was monitored in the perfusion chamber with a temperature-sensitive probe (Th-10Km; Cell MicroControls) and changed by the perfusion solutions between 12 °C and 25 °C.

VCF. A total number of 30 engineered Cys–Trp pairs in the AcP were generated and tested by VCF. They had been chosen based on the following criteria: (*i*) The distance between their Cα atoms was ≤ 15 Å; (*ii*) one of the residues was on the thumb helix, the other on the other side of the AcP; (*iii*) the side chains of these residues were oriented toward each other; and (*iv*) the residue to be mutated to Cys appeared accessible from the solution as judged from the crystal structure. Only the eight pairs whose ΔF signal was specific according to the criteria shown in Table S3, and of which the corresponding Cys mutant alone did not induce a measurable ΔF, were included in the study. VCF experiments were mostly performed as described previously (33). Labeling was carried out in the dark with 5 μM CF488A maleimide or AlexaFluor488 C-5 maleimide at 19 °C for 15 min. The light source was an Intensilight lamp (C-HGFI; Nikon). The emitted signal was detected by a 40× Nikon objective and quantified by a photodiode (S1336-18BQ; Hamamatsu Photonics). The ΔF was normalized to the total fluorescence intensity F, as determined with a scalable offset device. A low-pass eight-pole Bessel filter was used to amplify and filter the signal at 50 Hz. On most mutants, we tested the two fluorophores CF488A and AlexaFluor488. We used the one with the higher signal amplitude and better apparent specificity for the experiments. As a measure of specificity, we determined the ΔF induced by acidification to pH 6 from the conditioning pH 7.4 and also from the conditioning pH of 6.8, at which the tested ASICs were desensitized and did not open. We considered the ΔF induced by the pH change from 6.8 to 6 as a potential pH effect on the fluorophore itself and determined the ratio ΔF (pH6.8→6)/ΔF (pH7.4→6) as a measure of the potentially nonspecific fraction of the signal. All mutants showed some ΔF in the pH 6.8-to-6 transition, which was, however, generally <30% of the ΔF amplitude measured in response to the pH drop from 7.4 to 6 (Table S3). For most measurements, oocytes were placed in an RC-25 recording chamber (Warner Instruments), as described previously (33). For kinetic measurements, we used a specially designed chamber to measure and compare the ΔF and current kinetics from similar oocyte surfaces (Fig. 3D). This chamber contained an upper compartment that was connected, by a hole of 0.85 mm diameter, to a lower channel. The oocyte was placed in the upper compartment in the hole, bathed in recording solution at the conditioning pH, e.g. pH 7.4, and impaled with the electrodes. The bottom side of the oocyte was exposed to the lower channel, allowing the solution to flow under the oocyte, as described previously (35). The chamber was made based on a prototype kindly provided by G. Akk, Washington University in St. Louis, St. Louis.

Data Analysis. Current recordings were controlled and recorded using Chartmaster and analyzed with Chartmaster or Fitmaster (HEKA Electronics). Normalized activation curves were fitted to the Hill equation [$(I = I_{max}/(1 + (10^{-pH50}/10^{-pH})^{nH}$], where I_{max}

is the maximal current, pH_{50} is the value at which the current amplitude is half-maximal, and nH is the Hill coefficient (GraphPad Prism). SSD curves were fitted to an analogous equation. The kinetics of ΔF and current signals were determined as rise times, the time to get from 10 to 90% of the maximal amplitude. The permeability ratio of two ions A and B was calculated from reversal potential (E_{rev}) values determined from voltage ramps obtained when the ASIC current was induced by acidification in an extracellular solution containing either the cation A or B, from the relationship $\Delta E_{rev} = E_{rev,B} - E_{rev,A} = (RT/zF)\ln(P_B[B]_o/P_A[A]_o)$, where R is the Gas constant (8.3145 J mol^{-1} K^{-1}), T is the absolute temperature (in K), z is the valence of the ions, F is the Faraday's constant (96485 C mol^{-1}), $P_{B(or\ A)}$ is the permeability of B (or A), and $[B]_o$ and $[A]_o$ are the extracellular concentrations of ions B and A (36). Structural images were made with Chimera (37) from a human ASIC1a homology model, based on the crystal structure of chicken ASIC1, which shares 90% sequence homology with human ASIC1a [PDB number 4NTW (8)].

Analysis of Two-Component ΔF Signals. For mutants with two ΔF components, it might be possible that, under certain pH conditions, the second component may decrease the apparent amplitude of the first component, which would lead to an underestimation of the rise time of the first component. This possible error was estimated and corrected as indicated in Fig. S3 *D* and *E*. In the mutants with a composite ΔF signal, the pH dependence of the first component was generally shifted to alkaline values with regard to the pH dependence of the second ΔF component and reached maximal amplitudes at pH 7. This difference in pH dependence allowed observation of the first signal alone at alkaline pH values; in these mutants, saturation of the amplitude of the first ΔF component occurred at pH values at which the amplitude of the second ΔF component was still small (Fig. S3*D*). If, at an acidic pH at which the second ΔF component had a high amplitude, the amplitude of the first component decreased (as illustrated in Fig. S3*D*), this probably indicated that the accelerated second component had cut a part of the first ΔF component. We observed, indeed, a decrease of the amplitude of the first ΔF component in the mutants D347C/ T236W and D351C/D237W. Such a decrease of the amplitude of the first ΔF component at more acidic pH was not observed with the mutant D237C/D347W (higher ΔF amplitude at pH 6.2 than at pH 7), and it was previously shown that this is not the case for the E355C mutant (33). In principle, if this decrease in the two double mutants reflects the partial suppression of the first ΔF component by the second one, it leads to an underestimation of rise time. We have therefore corrected the individual rise time values of the first ΔF component of these mutants measured at pH *x* by dividing the measured rise time by the ratio $\Delta F/F$ at pH *x*/$\Delta F/F$ at pH7 (Fig. S3*E*). An alternative would have been a double exponential fit for the two components. Due to the short duration of the first component, such fits were, however, not reliable.

Data Presentation and Statistics. Statistical comparison of two mean values was done with the *t* test. For statistical analysis of more than two mean values, we determined first the distribution of the experimental population, and used, for Gaussian distributions, ANOVA followed by Tukey's multiple comparisons test (Graphpad Prism 6). For non-Gaussian distributions, nonparametric tests (Kruskal-Wallis, followed by Dunn's multiple comparisons test) were used. The data are presented as mean ± SEM. Individual data points and numbers of experiments are provided in Dataset S1. The numbers correspond to the number of individual oocytes, from which measures were taken.

SI Kinetic Models

By using a four-state kinetic model, we first show how mutations that mimic a protonated pH sensor affect the midpoint and the steepness of the pH-dependent state when the protonation step

affected by the mutation is either (*i*) essential or (*ii*) accessory for reaching the state of interest (e.g., the open state).

A second, more complex model is then used to fit the experimental data to better understand the mechanism underlying the observed functional effects of AcP mutations.

Analytic Solutions for Four-State and Two-State Kinetic Models. We consider a four-state kinetic model (Fig. S1*C*) representing a channel with two protonation sites (indicated by subscript *a* and superscript *b*), both of which can be protonated or not (states C, C_a, C^b, and C_a^b). We use this simple four-state model to obtain analytic expressions for the pH50 and Hill coefficient of a transition of interest (e.g., to state C_a^b) and show how these are affected by mutation at one of the two sites in two situations: (*i*) both protonations are essential for the transition of interest (we observe C_a^b); (*ii*) only protonation of *b* is required for the transition of interest (we observe $C^b + C_a^b$).

Let $K_{A\to B}$ be the transition rate from state A to state B; then our model is given by

$$K_{C\to C_a} = k_a\left(\frac{[H]}{[H_{50}^a]}\right)^{n_a} \quad ; \quad K_{C_a\to C} = k_a$$

$$K_{C\to C^b} = k_b\left(\frac{[H]}{[H_{50}^b]}\right)^{n_b} \quad ; \quad K_{C^b\to C} = k_b$$

$$K_{C_a\to C_a^b} = \alpha k_b\left(\frac{[H]}{[H_{50}^b]}\right)^{n_b} \quad ; \quad K_{C_a^b\to C_a} = k_b$$

$$K_{C^b\to C_a^b} = \alpha k_a\left(\frac{[H]}{[H_{50}^a]}\right)^{n_a} \quad ; \quad K_{C_a^b\to C^b} = k_a.$$

[H] is the proton activity [pH $= -log_{10}([H])$], $[H_{50}^a]$ is the proton activity at which proton sensor *a* is protonated in half of the channels, and similarly for $[H_{50}^b]$. Here n_a and n_b correspond to the number of protons in sensors *a* and *b*, and α is the cooperativity between sensors *a* and *b* ($\alpha > 1$ corresponds to a positive cooperativity; i.e., protonation of *a* makes protonation of *b* easier, while $\alpha < 1$ corresponds to negative cooperativity). Finally k_a (respectively k_b) is the protonation rate for sensors *a* (respectively *b*) at $[H] = [H_{50}^a]$ (respectively $[H] = [H_{50}^b]$). These parameters do not influence the equilibrium state but only the rate at which the system reaches equilibrium at a given pH. Note that only the forward transitions (protonation) are pH-dependent, just as ligand binding depends on the concentration of ligands whereas unbinding does not.

At equilibrium, we have

$$\begin{cases} P(C_a) = \left(\frac{[H]}{[H_{50}^a]}\right)^{n_a} P(C) \\[4pt] P(C^b) = \left(\frac{[H]}{[H_{50}^b]}\right)^{n_b} P(C) \\[4pt] P(C_a^b) = \alpha\left(\frac{[H]}{[H_{50}^b]}\right)^{n_b} P(C_a) \\[4pt] P(C_a^b) = \alpha\left(\frac{[H]}{[H_{50}^a]}\right)^{n_a} P(C^b) \\[4pt] 1 = P(C) + P(C_a) + P(C^b) + P(C_a^b) \end{cases} \qquad \text{[S1]}$$

51

with $P(C_x)$ denoting probability of the channel being in state C_x. From this system of equations (Eq. **S1**), we can easily obtain the equilibrium probabilities

$$P(C) = \frac{1}{F([H])} \qquad \text{[S2]}$$

$$P(C_a) = \frac{\left(\frac{[H]}{[H_{50}^a]}\right)^{n_a}}{F([H])} \qquad \text{[S3]}$$

$$P(C^b) = \frac{\left(\frac{[H]}{[H_{50}^b]}\right)^{n_b}}{F([H])} \qquad \text{[S4]}$$

$$P(C_a^b) = \frac{\alpha\left(\frac{[H]}{[H_{50}^a]}\right)^{n_a}\left(\frac{[H]}{[H_{50}^b]}\right)^{n_b}}{F([H])} \qquad \text{[S5]}$$

with

$$F([H]) = 1 + \left(\frac{[H]}{[H_{50}^a]}\right)^{n_a} + \left(\frac{[H]}{[H_{50}^b]}\right)^{n_b} + \alpha\left(\frac{[H]}{[H_{50}^a]}\right)^{n_a}\left(\frac{[H]}{[H_{50}^b]}\right)^{n_b}. \qquad \text{[S6]}$$

For the remainder of this section, we will assume that both transitions correspond to single protonation sites ($n_a = 1$ and $n_b = 1$). Let us first consider the case where both protonations are needed for the transition of interest, so we define $[H_{50}]_{4state}$ as the proton concentration at which half the channels have both sites protonated, $P(C_a^b, [H_{50}]_{4state}) = 1/2$. It follows from Eq. **S5** that

$$[H_{50}]_{4state} = \frac{[H_{50}^a] + [H_{50}^b] + \sqrt{\left([H_{50}^a] + [H_{50}^b]\right)^2 + 4\alpha[H_{50}^a][H_{50}^b]}}{2\alpha}$$

$$> \frac{[H_{50}^a] + [H_{50}^b]}{\alpha}. \qquad \text{[S7]}$$

The Hill coefficient for this transition ($C \to C_a^b$) is given by

$$n_{4state} = \frac{d}{d\log([H])}\log\left(\frac{P(C_a^b)}{1 - P(C_a^b)}\right)\Bigg|_{[H]=[H_{50}]}$$

$$= [H]\frac{d}{d[H]}\log\left(\frac{\alpha[H][H]}{[H_{50}^a][H_{50}^b] + [H]([H_{50}^a] + [H_{50}^b])}\right)\Bigg|_{[H]=[H_{50}]}$$

$$= \frac{[H]}{\alpha[H][H]}\left(2\alpha[H] - \frac{\alpha[H][H]([H_{50}^a] + [H_{50}^b])}{[H_{50}^a][H_{50}^b] + [H]([H_{50}^a] + [H_{50}^b])}\right)\Bigg|_{[H]=[H_{50}]}$$

$$= 2 - \frac{[H]([H_{50}^a] + [H_{50}^b])}{[H_{50}^a][H_{50}^b] + [H]([H_{50}^a] + [H_{50}^b])}\Bigg|_{[H]=[H_{50}]}$$

$$= 1 + \frac{[H_{50}^a][H_{50}^b]}{[H_{50}^a][H_{50}^b] + [H]([H_{50}^a] + [H_{50}^b])}\Bigg|_{[H]=[H_{50}]} > 1. \qquad \text{[S8]}$$

Let us now consider how the pH50 and n would be affected by a neutralization mutation of one of the two protonation sites. For this, we consider that a neutralization mutation corresponds to one of the sites being always protonated (in this example, the site "a"), so that we are left with a two-state model (states C_a and C_a^b) for which it is easy to show that

$$P_{2state}(C_a^b) = \frac{\alpha\left(\frac{[H]}{[H_{50}^b]}\right)^{n_b}}{1 + \alpha\left(\frac{[H]}{[H_{50}^b]}\right)^{n_b}} \qquad \text{[S9]}$$

$$[H_{50}]_{2state} = \frac{[H_{50}^b]}{\alpha} \qquad \text{[S10]}$$

$$n_{2state} = 1. \qquad \text{[S11]}$$

From the comparison of Eq. **S7** with Eq. **S10** and Eq. **S8** with Eq. **S11**, it is clear that

$$[H_{50}]_{4state} > [H_{50}]_{2state} \Rightarrow pH50_{4state} < pH50_{2state}$$
$$n_{4state} > n_{2state},$$

so that, in this model (two protonation sites, both needed for the transition of interest), a protonation-mimicking mutation will always increase the pH50 while decreasing the Hill coefficient. This is exemplified in Fig. S1D showing simulated data with such a four-state model (red triangles and lines) and the impact of a neutralization mutation (black circles and line).

If, instead, we consider the first protonation ("a") as accessory to the transition of interest brought about by the second protonation (i.e., that in this case, both C^b and C_a^b are "states of interest"), we get, for the four-state model,

$$P\left(C_a^b, [H_{50}]_{4state}^{accessory}\right) + P\left(C^b, [H_{50}]_{4state}^{accessory}\right) = 1/2$$

$$[H_{50}]_{4state}^{accessory} = \frac{[H_{50}^a] - [H_{50}^b] + \sqrt{\left([H_{50}^a] - [H_{50}^b]\right)^2 + 4\alpha[H_{50}^a][H_{50}^b]}}{2\alpha}.$$

Let us now show that $[H_{50}]_{4state}^{accessory}$ can be both smaller and larger than $[H_{50}]_{2state}$, which is equivalent to the ratio $[H_{50}]_{4state}^{accessory}/[H_{50}]_{2state}$ being either smaller or larger than 1.

$$\frac{[H_{50}]_{4state}}{[H_{50}]_{2state}} = \frac{\alpha[H_{50}]_{4state}}{[H_{50}^b]} = \frac{1}{2}\left[\left(\frac{[H_{50}^a]}{[H_{50}^b]} - 1\right)\right.$$

$$\left. + \sqrt{\left(\frac{[H_{50}^a]}{[H_{50}^b]} - 1\right)^2 + 4\alpha\frac{[H_{50}^a]}{[H_{50}^b]}}\right]. \qquad \text{[S12]}$$

Eq. **S12** is plotted in Fig. S1E as a function of $[H_{50}^a]/[H_{50}^b]$ and α, clearly showing that $[H_{50}]_{4state}^{accessory}$ can be larger (red region in Fig. S1E) or smaller (blue region in Fig. S1E) than $[H_{50}]_{2state}$. This proves that a protonation-mimicking mutation of a site that is accessory to the transition of interest can either decrease or increase the pH50.

Similarly, we now calculate the Hill coefficient in the case of protonation a being accessory to the observed transition (transition to $C^b + C_a^b$). In this case, the Hill coefficient is defined as

$$n_{4state}^{accessory} = \frac{d}{d\log([H])} \log\left(\frac{P_{C_a^b} + P_{C^b}}{1 - P_{C_a^b} - P_{C^b}}\right)\Bigg|_{[H]=[H_{50}]}$$

$$= [H]\frac{d}{d[H]} \log\left(\frac{\alpha[H][H] + [H_{50}^b][H]}{[H_{50}^a][H_{50}^b] + [H][H_{50}^a]}\right)\Bigg|_{[H]=[H_{50}]}$$

$$= \frac{[H]}{\alpha[H][H] + [H_{50}^b][H]}\left(2\alpha[H] + [H_{50}^b] - \frac{(\alpha[H][H] + [H_{50}^b][H])[H_{50}^a]}{[H_{50}^a][H_{50}^b] + [H][H_{50}^a]}\right)\Bigg|_{[H]=[H_{50}]}$$

$$= 1 + \frac{\alpha[H][H]}{\alpha[H][H] + [H_{50}^b][H]} - \frac{[H][H_{50}^a]}{[H_{50}^a][H_{50}^b] + [H][H_{50}^a]}\Bigg|_{[H]=[H_{50}]}$$

$$= 1 + \frac{\alpha[H][H]([H_{50}^a][H_{50}^b] + [H][H_{50}^a]) - [H][H_{50}^a](\alpha[H][H] + [H_{50}^b][H])}{(\alpha[H][H] + [H_{50}^b][H])([H_{50}^a][H_{50}^b] + [H][H_{50}^a])}\Bigg|_{[H]=[H_{50}]}$$

$$= 1 + \frac{[H_{50}^a][H_{50}^b][H][H](\alpha-1)}{(\alpha[H][H] + [H_{50}^b][H])([H_{50}^a][H_{50}^b] + [H][H_{50}^a])}\Bigg|_{[H]=[H_{50}]}. \qquad \text{[S13]}$$

Note that the second term in Eq. **S13** will be positive for $\alpha > 1$ and negative for $\alpha < 1$ (α is always positive, so the denominator is always positive). So it is clear that a mutation mimicking the protonation of an accessory site will lead to a decrease in Hill coefficient for positive cooperativity (if $\alpha > 1$, then $n_{4state}^{accessory} > 1 = n_{2state}$), and an increase in Hill coefficient in case of negative cooperativity (if $\alpha < 1$ then $n_{4state}^{accessory} < 1 = n_{2state}$). These results are exemplified in Fig. S1D showing the equilibrium probabilities for such a four-state model (blue triangles and lines) and the impact of a neutralization mutation on its pH50 and Hill coefficient (black circles and line), thus illustrating that the pH50 shift of such a mutation can be alkaline or acidic.

Kinetic Model for Fitting Experimental ASIC1a Data. The kinetic model of ASIC1a, illustrated in Fig. S1F, is composed of 32 states corresponding to three sets of protonation sites (o = activation, d = desensitization, and a = AcP) and four conformations [C = closed, O = open, D = closed-desensitized, and (OD) = open-desensitized]. For computational reasons (see below), the protonation of closed channels toward opening and desensitization is represented by two steps each ($C\rightarrow C^o \rightarrow C^O$, $C\rightarrow C^d \rightarrow C^D$), which does not mean that exactly two protonation steps are involved. Opening and desensitization involve a final pH-independent transition ($C^O \rightarrow O^O$, $C^D \rightarrow D^D$). Evidence for such a ligand-independent transition before opening comes from several studies with ligand-gated ion channels (38, 39). Each of these 16 states can exist with the proton sensor in the AcP protonated or not (e.g., C and ^aC), yielding a total of 32 states.

Protonation transitions are described by their pH50 (or the equivalent proton concentration $[H_{50}]$) at which the protonation and deprotonation rates are equal, the Hill coefficient n, and their transition rate at pH = pH50, k. For example, protonation of the AcP

$$K_{C\rightarrow {}^aC} = k_a\left(\frac{[H]}{[H_{50}^a]}\right)^{n_a} = k_a 10^{-n_a(\text{pH}-\text{pH}_{50}^a)}, \qquad \text{[S14]}$$

whereas the reverse transition is given by

$$K_{{}^aC\rightarrow C} = k_a.$$

Similar expressions were also used for the protonations of activation and desensitization sites, except that these transitions were split into two identical transitions ($C\rightarrow C^o \rightarrow C^O$, $C\rightarrow C^d \rightarrow C^D$); this was done because these transitions have large Hill coefficients (we found values of ~11 for desensitization and 3 for activation), which led to difficulties in the simulation. Splitting these transitions decreases the corresponding Hill coefficient by a factor of 2, which allowed for easier integration of the equations.

$$K_{C\rightarrow C_d} = k_d 10^{-n_d(\text{pH}-\text{pH}_{50}^d)}; \quad K_{C_d\rightarrow C} = k_d \qquad \text{[S15]}$$

$$K_{C_d\rightarrow C_D} = k_d 10^{-n_d(\text{pH}-\text{pH}_{50}^d)}; \quad K_{C_D\rightarrow C_d} = k_d$$

$$K_{C\rightarrow C^o} = k_o 10^{-n_o(\text{pH}-\text{pH}_{50}^o)}; \quad K_{C^o\rightarrow C} = k_o \qquad \text{[S16]}$$

$$K_{C^o\rightarrow C^O} = k_o 10^{-n_o(\text{pH}-\text{pH}_{50}^o)}; \quad K_{C^O\rightarrow C^o} = k_o.$$

The rates of the pH-independent transitions to the open and desensitized states are

$$K_{C^O\rightarrow O^O} = f_O; \quad K_{O^O\rightarrow C^O} = b_O \qquad \text{[S17]}$$

$$K_{C_D\rightarrow D_D} = f_D; \quad K_{D_D\rightarrow C_D} = b_D. \qquad \text{[S18]}$$

We included cooperativity between protonation of the AcP and the other protonations, as well as with channel opening and desensitization.

$$K_{{}^aC\rightarrow {}^aC_d} = \alpha_D K_{C\rightarrow C_d} \qquad \text{[S19]}$$

$$K_{{}^aC\rightarrow {}^aC^o} = \alpha_O K_{C\rightarrow C^o} \qquad \text{[S20]}$$

$$K_{{}^aC_D\rightarrow {}^aD_D} = \beta_D K_{C_D\rightarrow D_D} \qquad \text{[S21]}$$

$$K_{{}^aC^O\rightarrow {}^aO^O} = \beta_O K_{C^O\rightarrow O^O}. \qquad \text{[S22]}$$

The four cooperativity parameters ($\alpha_D, \alpha_O, \beta_D$, and β_O) are always positive, with values below 1 indicating negative cooperativity (e.g., if $\alpha_D < 1$, protonation of AcP will make the protonation of the desensitization sites harder), and values above 1 corresponding

to positive cooperativity (e.g., if $\alpha_D > 1$, protonation of AcP will make the protonation of the desensitization sites easier). To respect microscopic reversibility, Eqs. **S19–S22** also lead to cooperativity between the other transitions and protonation of the AcP,

$$K_{C_d \to {}^aC_d} = \alpha_D K_{C \to {}^aC}; \quad K_{C_D \to {}^aC_D} = \alpha_D \alpha_D K_{C \to {}^aC}$$

$$K_{C_o \to {}^aC_a} = \alpha_O K_{C \to {}^aC}; \quad K_{C_O \to {}^aC_O} = \alpha_O \alpha_O K_{C \to {}^aC}$$

$$K_{C_d^O \to {}^aC_d^O} = \alpha_D \alpha^O K_{C \to {}^aC}; \quad K_{C_D^o \to {}^aC_D^o} = \alpha_D \alpha_D \alpha^O K_{C \to {}^aC}$$

$$K_{C_d^O \to {}^aC_d^O} = \alpha_D \alpha^O \alpha^O K_{C \to {}^aC}; \quad K_{C_D^O \to {}^aC_D^O} = \alpha_D \alpha_D \alpha^O \alpha^O K_{C \to {}^aC}$$

$$K_{D_D \to {}^aD_D} = \alpha_D \alpha_D \beta_D K_{C \to {}^aC}; \quad K_{D_D^o \to {}^aD_D^o} = \alpha_O \alpha_D \alpha_D \beta_D K_{C \to {}^aC};$$
$$K_{D_D^O \to {}^aD_D^O} = \alpha_O \alpha_O \alpha_D \alpha_D \beta_D K_{C \to {}^aC}$$

$$K_{O^o \to {}^aO^o} = \alpha_O \alpha_O \beta^O K_{C \to {}^aC}; \quad K_{O_d^o \to {}^aO_d^o} = \alpha_D \alpha_O \alpha_O \alpha_O \beta^O K_{C \to {}^aC};$$

$$K_{O_D^o \to {}^aO_D^o} = \alpha_D \alpha_D \alpha_O \alpha_O \beta^O K_{C \to {}^aC}$$

$$K_{(OD)_D^O \to {}^a(OD)_D^O} = \alpha_O \alpha_O \alpha_D \alpha_D \beta_D \beta^O K_{C \to {}^aC}.$$

The remaining rates are all equivalent to one of the rates defined above. For the reverse reactions, all rates for reactions shown with the same color in Fig. S1F are identical,

$$K_{{}^aC_d \to C_d} = K_{{}^aC_D \to C_D} = K_{{}^aC^o \to C^o} = K_{{}^aC^O \to C^O} = K_{{}^aC_d^O \to C_d^O} = K_{{}^aC_D^O \to C_D^O}$$
$$= K_{{}^aC_d^o \to C_d^o} = K_{{}^aC_D^o \to C_D^o} = K_{{}^aC \to C}$$

$$K_{{}^aO^o \to O^o} = K_{{}^aO_d^o \to O_d^o} = K_{{}^aO_D^o \to O_D^o} = K_{{}^aC \to C}$$

$$K_{{}^aD_D \to D_D} = K_{{}^aD_D^o \to D_D^o} = K_{{}^aD_D^O \to D_D^O} = K_{{}^a(OD)_D^O \to (OD)_D^O} = K_{{}^aC \to C}$$

$$K_{C_d^o \to C^o} = K_{C_d^O \to C^O} = K_{O_d^o \to O^o} = K_{{}^aC_d^o \to {}^aC^o} = K_{{}^aC_d^O \to {}^aC^O} = K_{{}^aO_d^o \to {}^aO^o}$$

$$= K_{{}^aC_d \to {}^aC} = K_{C_d \to C}$$

$$K_{C_D^o \to C_d^o} = K_{C_D^O \to C_d^O} = K_{O_D^o \to O_d^o} = K_{{}^aC_D^o \to {}^aC_d^o} = K_{{}^aC_D^O \to {}^aC_d^O} = K_{{}^aO_D^o \to {}^aO_d^o}$$
$$= K_{{}^aC_D \to {}^aC_d} = K_{C_D \to C_d}$$

$$K_{{}^aD_D \to {}^aC_D} = K_{D_D^o \to C_D^o} = K_{D_D^O \to C_D^O} = K_{{}^aD_D^o \to {}^aC_D^o} = K_{{}^aD_D^O \to {}^aC_D^O} = K_{(OD)_D^O \to O_D^O}$$

$$= K_{{}^a(OD)_D^O \to {}^aO_D^O} = K_{D_D \to C_D}$$

$$K_{C_d^o \to C_d} = K_{C_D^o \to C_D} = K_{D_D^o \to D_D} = K_{{}^aC^o \to {}^aC} = K_{{}^aC_d^o \to {}^aC_d} = K_{{}^aC_D^o \to {}^aC_D}$$

$$= K_{{}^aD_D^o \to {}^aD_D} = K_{C^o \to C}$$

$$K_{C_d^O \to C_d^o} = K_{C_D^O \to C_D^o} = K_{D_D^O \to D_D^o} = K_{{}^aC^O \to {}^aC^o} = K_{{}^aC_d^O \to {}^aC_d^o} = K_{{}^aC_D^O \to {}^aC_D^o}$$

$$= K_{{}^aD_D^O \to {}^aD_D^o} = K_{C^o \to C^o}$$

$$K_{O_d^O \to C_d^O} = K_{O_D^O \to C_D^O} = K_{(OD)_D^O \to D_D^O} = K_{{}^aO^O \to {}^aC^O} = K_{{}^aO_d^O \to {}^aC_d^O}$$

$$= K_{{}^aO_D^O \to {}^aC_D^O} = K_{{}^a(OD)_D^O \to {}^aD_D^O} = K_{O^O \to C^O}.$$

For the forward rates, this is not the case because of cooperativity, and we have

$$K_{C^o \to C_d^o} = K_{C^O \to C_d^O} = K_{O^o \to O_d^o} = K_{C_d \to C_D} = K_{C_d^o \to C_D^o} = K_{C_d^O \to C_D^O}$$
$$= K_{O_d^o \to O_D^o} = K_{C \to C_d}$$

$$K_{{}^aC^o \to {}^aC_d^o} = K_{{}^aC^O \to {}^aC_d^O} = K_{{}^aO^o \to {}^aO_d^o} = K_{{}^aC_d \to {}^aC_D} = K_{{}^aC_d^o \to {}^aC_D^o}$$

$$= K_{{}^aC_d^O \to {}^aC_D^O} = K_{{}^aO_d^o \to {}^aO_D^o} = K_{{}^aC \to {}^aC_d}$$

$$K_{C_D^o \to D_D^o} = K_{C_D^O \to D_D^O} = K_{O_D^o \to (OD)_D^o} = K_{C_D \to D_D}$$

$$K_{{}^aC_D^o \to {}^aD_D^o} = K_{{}^aC_D^O \to {}^aD_D^O} = K_{{}^aO_D^o \to {}^a(OD)_D^o} = K_{{}^aC_D \to {}^aD_D}$$

$$K_{C_d \to C_d^o} = K_{C_D \to C_D^o} = K_{D_D \to D_D^o} = K_{{}^aC_d \to {}^aC_d^o} = K_{{}^aC_D \to {}^aC_D^o} = K_{{}^aD_D^o \to {}^aD_D^o}$$
$$= K_{C^o \to C^o} = K_{C \to C^o}$$

$$K_{{}^aC_d \to {}^aC_d^o} = K_{{}^aC_D \to {}^aC_D^o} = K_{{}^aD_D \to {}^aD_D^o} = K_{{}^aC^o \to {}^aC^o} = K_{{}^aC_d^o \to {}^aC_d^o}$$

$$= K_{{}^aC_D^o \to {}^aC_D^o} = K_{{}^aD_D^o \to {}^aD_D^o} = K_{{}^aC \to {}^aC^o}$$

$$K_{C_d^o \to O_d^o} = K_{C_D^o \to O_D^o} = K_{D_D^o \to (OD)_D^o} = K_{C^o \to O^o}$$

$$K_{{}^aC_d^o \to {}^aO_d^o} = K_{{}^aC_D^o \to {}^aO_D^o} = K_{{}^aD_D^o \to {}^a(OD)_D^o} = K_{{}^aC^o \to {}^aO^o},$$

The current is defined from the fraction of channels in an open state and the conductance of the channels as

$$I = G \times \left(O^O + O_d^O + O_D^O + {}^aO^O + {}^aO_d^O + {}^aO_D^O \right).$$

Voltage and ion concentrations were the same for all experiments and were therefore not explicitly modeled (absorbed in the conductance G).

Fit of the Kinetic Models to the Experimental Data. The 32-state kinetic model of ASIC comprised 17 free parameters: 3 for protonation of the AcP (pH_{50}^a, n_a, and k_a; see Eq. **S14**), 3 for the protonation of the activation sites (pH_{50}^o, n_o, and k_o; see Eq. **S16**), and 3 for the protonation of the desensitization sites (pH_{50}^d, n_d, and k_d; see Eq. **S15**), 1 for each of channel opening, closing, desensitization, and recovery (f_O, b_O, f_D, and b_D; Eqs. **S17** and **S18**), and 4 cooperativity coefficients (α_O, α_D, β_O, and β_D; Eqs. **S19–S22**).

Each mutant was described by three parameters, each changing one of the parameters describing the protonation of the AcP,

$$pH_{50}^a \Rightarrow pH_{50}^a + \Delta pH_{50}^a \quad \text{with} \quad \Delta pH_{50}^a > 0$$

$$n_d \Rightarrow \varepsilon \times n_d \quad \text{with} \quad 0 < \varepsilon < 1$$

$$k_d \Rightarrow \gamma \times k_d.$$

As we fitted the model to data for the WT channel and two mutants, this added six parameters. Finally, the data used came from

54

six different cells (one for activation and one for desensitization for the WT and both mutant channels), which added six parameters describing the overall conductance of ASICs for each cell. This gave a total of 29 free parameters.

The model was fit to measured currents from the activation (step from conditioning pH to different acidic pH; see Fig. 1C) and desensitization protocols (step from different conditioning pH to an acidic pH; blue arrow in Fig. 1D). Specifically, we used currents from seven activation and six desensitization steps for the WT, five activation and eight desensitization steps for the AcP11 mutant, and seven activation and six desensitization steps for the AcP14 mutant. The model was fitted to all of the traces simultaneously, using the Data2Dynamics software (34) with a deterministic optimization

procedure repeated more than 50 times from different starting parameters obtained from a Latin hypercube sampling (40).

Kinetic Model with Protonation of AcP Essential for Activation or Desensitization. The above model was modified to describe a situation where protonation of the AcP is an essential component of either activation or desensitization, i.e., the channel can only activate or desensitize if the AcP is protonated. In the former case, this was simply represented by removing the open states without the AcP protonated (O^O, O_d^O, O_D^O, and OD_D^O) whereas, for the latter (AcP essential for desensitization), we removed the desensitized states without AcP protonated (D_D, D_D^o, D_D^O, and OD_D^O).
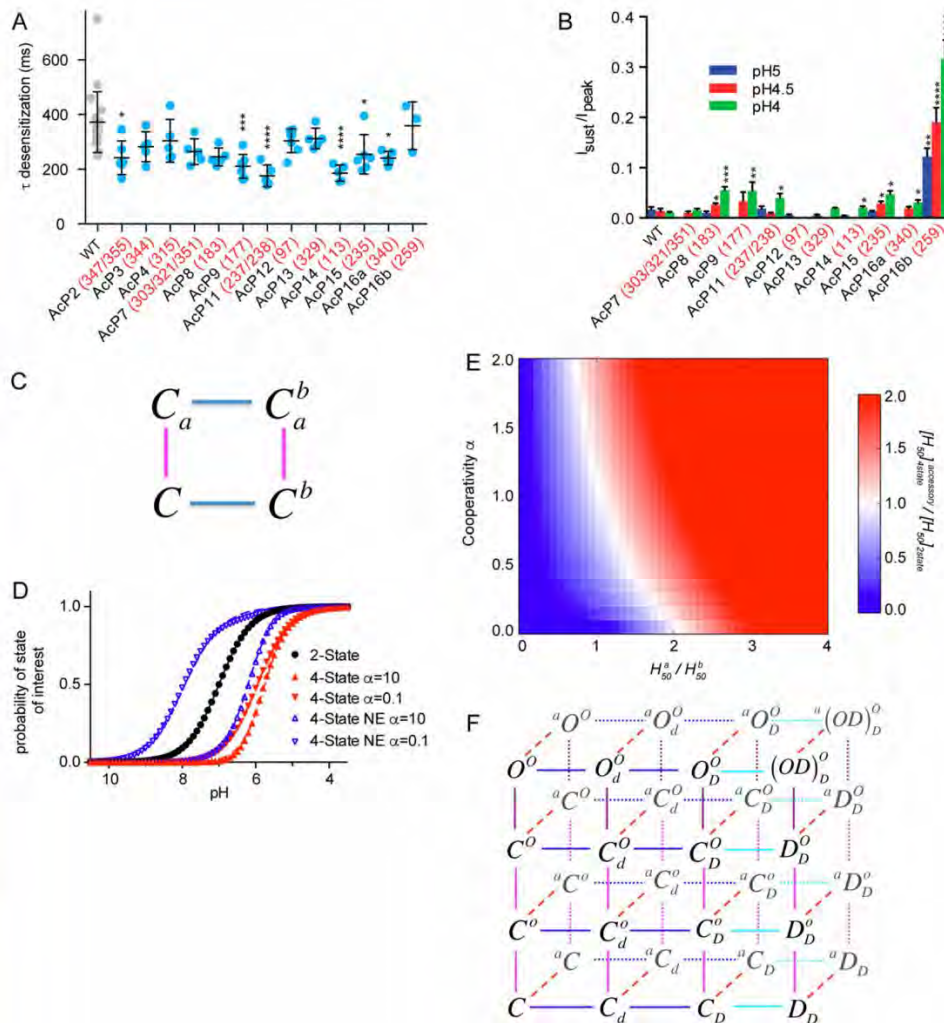
Fig. S1. ASIC modeling and properties of AcP mutants. (*A*) Desensitization kinetics of AcP mutants. The current decay phase of ASIC currents was fitted to a single exponential; $n = 3–19$. The red numbers in the labels indicate the residues mutated in addition to the mutations already present in the preceding mutant (with a lower number of mutations; generally on the left). (*B*) Sustained current/peak current amplitude (I_{sust}/I_{peak}) ratio of AcP mutants determined at pH 5, 4.5, and 4, as indicated; $n = 3–18$. (*C* and *D*) Illustration of the effect of a neutralization mutation on the pH50 and Hill coefficient in (*C*) a four-state model with two protonation sites. The neutralization mutation is modeled as one of the sites being always protonated and corresponds to a two-state kinetic model. Results for the two-state models (corresponding to the mutant) were obtained from Eq. **S9** and are shown as black circles, to which a Hill function was fitted (black line) yielding a pH50 = 7.0 and Hill coefficient $n = 1$. WT channels correspond to a four-state model (Eqs. **S2–S5**) with one of the protonation transitions (transition from C_a to C_a^b) having the exact same parameters as in the two-state model (black circles). If both protonations are essential for the observed transition, the state of interest is C_a^b; therefore we plot $P(C_a^b)$ obtained from Eq. **S5**. In this case, WT channels (red triangles) have lower pH50 and higher (or equal) Hill coefficient than the mutant (black circles), both for positive (red upward triangles) and negative (red downward triangles) cooperativity between the two protonation sites. As before, pH50 and Hill coefficients were obtained from the fit of a Hill function (red lines). Finally, if protonation a is accessory to the transition of interest (NE, not essential), the states of interest correspond to C_a^b and C^b; therefore we plot $P(C^b) + P(C_a^b)$ obtained from Eqs. **S4** and **S5**. In this case, the WT channel can have a pH50 that is either larger (downward blue triangles) or smaller (upward blue triangles) than the mutant channel. Note that, as shown analytically in Eq. **S13**, the Hill coefficient of the WT channel is smaller (respectively larger) than that of the mutant for negative (respectively positive) cooperativity. (*E*) $[H_{50}]_{4state}^{accessory}/[H_{50}]_{2state}$ (i.e., the ratio of the $[H_{50}]$ of the four-state model where protonation of site a is accessory vs. the $[H_{50}]$ of the mutant in which site a has been mutated to a residue mimicking protonation) is shown as a function of $[H_{50}^a]/[H_{50}^b]$ and α (Eq. **S12**). Red regions indicate $[H_{50}]_{4state}^{accessory} > [H_{50}]_{2state}$ (pH50 is increased by the mutation) and blue indicates $[H_{50}]_{4state}^{accessory} < [H_{50}]_{2state}$ (pH50 is decreased by the mutation). (*F*) Model used for fitting experimental traces of WT, AcP11, and AcP14 activation and SSD, as described in *SI Materials and Methods*. The model is composed of 32 states corresponding to three sets of protonation sites (o = activation, d = de-sensitization, and a = AcP) and four conformations [C = closed, O = open, D = closed-desensitized, and (OD) = open-desensitized].

56
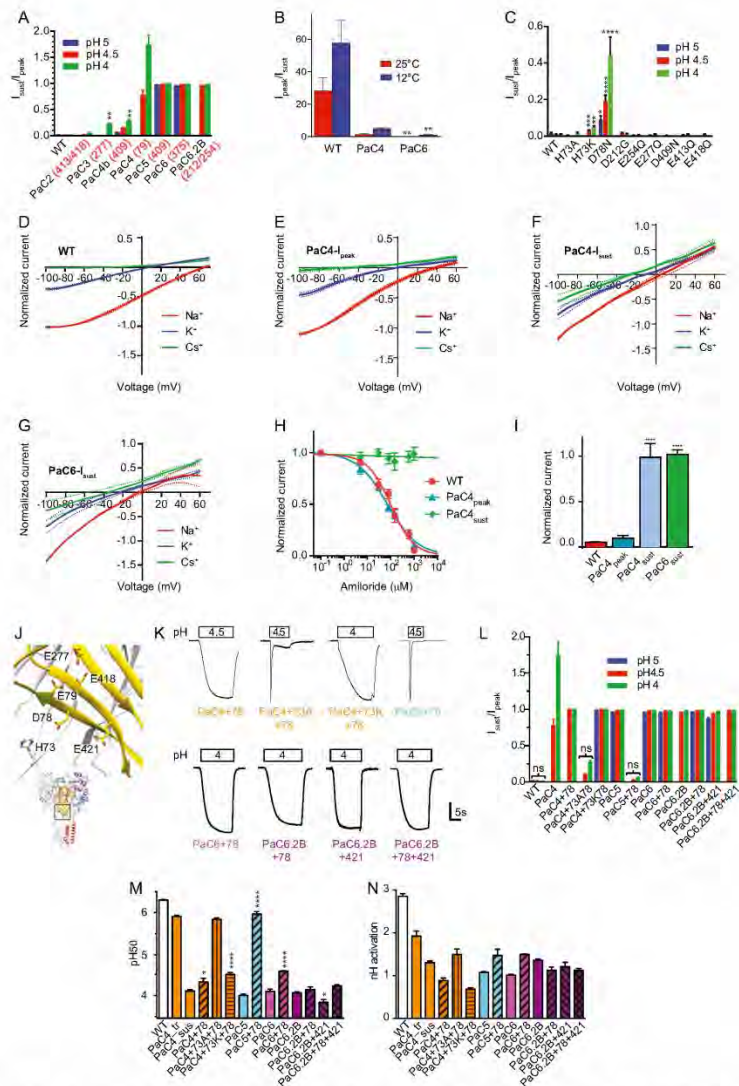
Fig. S2. Properties of palm mutants. (*A*) I_{sust}/I_{peak} ratio of combined palm mutants; *n* = 3–18. (*B*) The I_{peak}/I_{sust} ratio is plotted for WT, PaC4, and PaC6 at the indicated temperatures. Data were recorded at pH 4 from a conditioning pH of 7.4 (*n* = 7–10). (*C*) I_{sust}/I_{peak} ratio of single palm mutants; *n* = 4–28. Mutations to Cys of E79 and E421 have been shown to induce an I_{sust}/I_{peak} ratio of 5 ± 1% and 1 ± 1%, respectively (21). For bar graphs of I_{sust}/I_{peak}, note that, for some mutants, the I_{sust}/I_{peak} ratio was not measured at all three pH values. (*D–G*) Current–voltage relationship of (*D*) ASIC1a WT-I_{peak}, (*E*) PaC4-I_{peak}, (*F*) PaC4-I_{sust}, and (*G*) PaC6-I_{sust} in the presence of either Na$^+$ (red), K$^+$ (blue), or Cs$^+$ (green) in the extracellular solution. The holding potential was −60 mV, and 90-ms voltage ramps from −100 mV to +80 mV were applied. The pH 5-induced ramp current was calculated as the difference between the ramp current obtained during the acidification (during the peak or the sustained phase) and the ramp current measured during the conditioning period at pH 7.4. For each cell, the pH 5-induced currents with extracellular Na$^+$-, K$^+$-, and Cs$^+$-containing solution were normalized to the amplitude measured with Na$^+$ at −80 mV. Dotted lines represent SEM of independent experiments (*n* = 3–11). (*H*) The pH 5.5-induced current as a function of amiloride concentration, normalized to the control condition. IC$_{50}$ values obtained from the fits were 125 ± 43 µM (WT-I_{peak}) and 65 ± 13 µM (PaC4-I_{peak}); *n* = 6. (*I*) Effect of 1 mM amiloride on WT and mutant currents as indicated. The $I_{amiloride}/I_{control}$ ratio obtained at pH 5.5 is shown; *n* = 6–8. (*J*) Structural image showing residues pointing to the wrist that were mutated. Note that D78 is oriented toward H73 of a neighboring subunit. (*K*) Representative current traces of palm mutants in which residues H73, D78, and/or E421 were mutated in the background of various PaC mutants. H73 was mutated to Ala or Lys, because mutation to Asn resulted in very small currents. The vertical bar corresponds to the following current amplitude, in microamperes: 0.6 (PaC4+78), 0.5 (PaC4+73A+78), 0.45 (PaC4+73K+78), 5 (PaC5+78), 2 (PaC6+78), 0.6 (PaC6.2B+78), 0.2 (PaC6.2B+421), and 1 (PaC6.2B+78+421). The color of the label refers, as the color of bars in *L–N*, to the PaC mutant on which the mutant is based. (*L*) I_{sust}/I_{peak} of the indicated mutants; *n* = 6–28. (*M* and *N*) The pH50 and nH of activation of palm–wrist mutants; *n* = 6–129. The color indicates the palm mutant on which the mutant is based; the pattern refers to the added mutations. Statistically significant differences from WT or the corresponding palm mutant on which palm–wrist mutants are based (*M* and *N*; i.e., PaC4+78 is compared with PaC4_tr, etc.) are indicated as *$P < 0.05$, **$P < 0.01$, ***$P < 0.001$, and ****$P < 0.0001$. For *A*, *C*, and *L*, all values close to 1 and higher were different from the WT I_{sust}/I_{peak}; for other values as indicated with the asterisks.

57
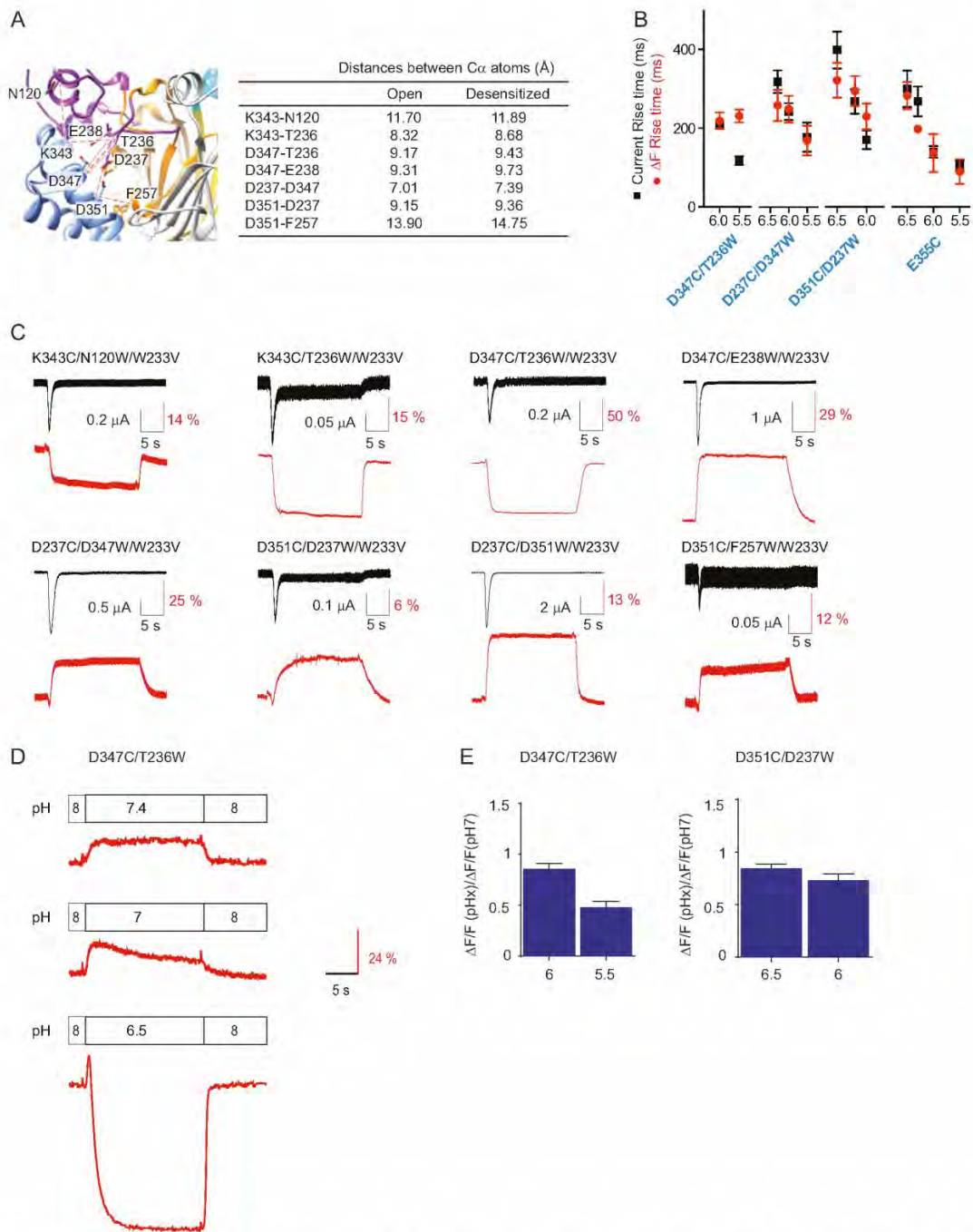
Fig. S3. VCF experiments of the AcP. (*A*) (*Left*) Close-up view of the AcP showing the residues of pairs that gave rise to fluorescence signals. (*Right*) Distances (in angstroms) between the Cα atoms of the corresponding residues, measured in homology models of the open [4NTW (8)] and desensitized [4NYK (6)] structures. (*B*) Current and ΔF kinetics at various stimulation pH conditions. Comparison of current activation and ΔF kinetics (of the first ΔF component) of selected mutants measured at different pH; $n = 3$–12. ΔF and current signals were correlated (Table S2) in all conditions except pH5.5 for D347C/T236W[first] and pH6.3 for E355C[first]. (*C*) Representative current (black) and fluorescence (red) traces of triple mutants in response to extracellular acidification to pH 6. They represent the double mutants used in the VCF part of the study, in which in addition the mutation W233V was introduced to verify that this nearby Trp residue had not influenced the ΔF signals. The conditioning pH for these experiments was 7.4. The traces are representative of 4 to 9 oocytes. Note that all these mutants gave consistent ΔF and current signals, except for D351C/F257W/W233V, which produced small signals that were not present in all oocytes tested. (*D* and *E*) Possible errors in the measurement of the kinetics of ΔF signals containing two components, and correction of the rise time values. (*D*) Representative ΔF traces of the D347C/T236W mutant obtained under different pH changes, to illustrate the overlap of the negative ΔF component over the positive component at more acidic pH conditions. (*E*) ΔF amplitude ratio of the first ΔF component at the indicated pH and its amplitude at pH 7 (where the signal was maximal); $n = 6$–21. These ratios were used to correct the rise time values as indicated in *SI Materials and Methods*.

58
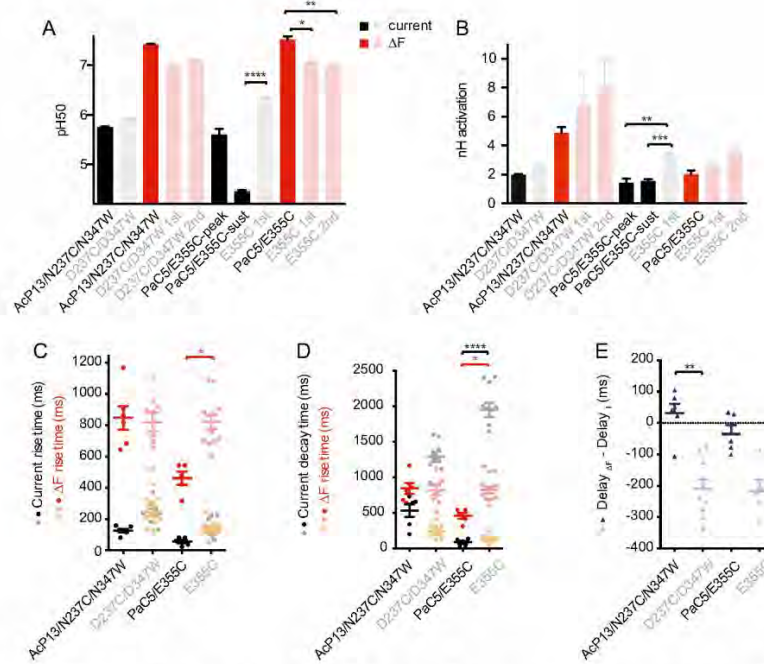
Fig. S4. Combined neutralization and VCF mutations. The figure shows pH and kinetic parameters of the combined mutants AcP13/N237C/N347W and PaC5/E355C (red and black symbols and bars) and compares them to these mutants in the WT background, D237C/D347W and E355C (gray and faintly colored symbols and bars). (A and B) The pH50 and nH of current activation (black and gray) and ΔF (red tones) of the Cys and Cys/Trp mutants combined with the mutant AcP13 or PaC5, compared with values obtained with the Cys and Cys/Trp mutants alone (n= 4–7). (C) Current and ΔF rise time. (D) Current decay time and ΔF rise time. Orange symbols in C and D represent the first ΔF component. (E) Delay$_{\Delta F}$ – Delay$_I$ of the same mutants (n = 5–12). *P < 0.05; **,P < 0.01; ***P < 0.001, and ****P < 0.0001 for the comparison between AcP13/N237C/N347W and D237C/D347W, and between PaC5/E355C and E355C; for mutants with two ΔF components, only the kinetics of the second ΔF components were compared.

Table S1. $\Delta F/F$ amplitude of mutants

Mutant	Ratio $\Delta F/F$ amplitude, %	n
D237C[C]	−6.83 ± 2.13	8
D351C[C]	0.4 ± 0.92	5
K343C	1.20 ± 0.43	4
K343C[C]	0.3 ± 0.05	3
D347C	1.08 ± 0.31	8
T236C	37.89 ± 6.78	8
E355C	7.27 ± 1.25	3
K343C/N120W[C]	−8.07 ± 1.22	6
K343C/T236W	−8.48 ± 2.74	3
D347C/T236W	−7.80 ± 2.43	4
D347C/E238W	39.94 ± 19.88	3
D237C/D347W[C]*	22.56 ± 12.17	6
D351C/D237W[C]	6.51 ± 1.28	6
D351C/F257W[C]	9.36 ± 1.15	5
D237C/D351W[C]	16.63 ± 4.87	7
AcP13/N237C	7.91 ± 0.68	4
AcP13/N237C/N347W	8.13 ± 1.27	13
PaC5/E355C	8.58 ± 1.41	11

The absolute $\Delta F/F$ values, obtained at pH 6, are indicated. Mutant channels were labeled with AlexaFluor488, except where indicated with a superscript "C," in which case channels were labeled with CF488A.
*The pH is 6.2 instead of 6 in four of six experiments.

59

Table S2. Steepness factor of linear regression of kinetics

Mutant	pH	Steepness Factor
A. Rise time$_{\Delta F}$ vs. rise time$_{current}$ at pH6		
K343C/N120W		2.30 ± 0.27
K343C/T236W		2.91 ± 0.27
D347C/T236W first		**1.05 ± 0.08**
D347C/T236W second		2.73 ± 0.17
D347C/E238W		3.45 ± 0.18
D237C/D347W first		**1.03 ± 0.08**
D237C/D347W second		3.15 ± 0.39
D351C/D237W first		**1.28 ± 0.15**
D351C/D237W second		1.43 ± 0.23
D351C/F257W		3.00 ± 0.16
D237C/D351W		2.72 ± 0.34
E355C first		**0.90 ± 0.11**
E355C second		5.11 ± 0.67
T236C		2.73 ± 0.25
B. Rise time$_{\Delta F}$ vs. rise time$_{current}$ at indicated pH value		
D347C/T236W first	5.5	**1.85 ± 0.20**
D351C/D237W first	6.5	**0.79 ± 0.09**
	6.2	**1.10 ± 0.09**
D237C/D347W first	6.3	**0.82 ± 0.09**
	5.5	**0.79 ± 0.20**
E355C first	6.5	**0.82 ± 0.14**
	6.3	**0.71 ± 0.10**
	5.5	**0.77 ± 0.10**
C. Rise time$_{\Delta F}$ vs. decay time$_{current}$ at pH6		
K343C/N120W		0.60 ± 0.09
K343C/T236W		**1.13 ± 0.09**
D347C/T236W first		0.23 ± 0.02
D347C/T236W second		0.62 ± 0.05
D347C/E238W		0.67 ± 0.05
D237C/D347W first		0.18 ± 0.02
D237C/D347W second		0.61 ± 0.06
D351C/D237W first		0.15 ± 0.02
D351C/D237W second		0.19 ± 0.02
D351C/F257W		**0.81 ± 0.07**
D237C/D351W		0.40 ± 0.04
E355C first		0.06 ± 0.00
E355C second		0.41 ± 0.02
T236C		0.32 ± 0.03

For mutant categories A and B, for each mutant and pH condition, ΔF rise time values were plotted for individual experiments as a function of the current rise time. For mutant category C, for each mutant and pH condition, ΔF rise time values were plotted for individual experiments as a function of the current decay time. The „steepness factor" for the mutants in this table corresponds to the steepness of linear regressions to these data points; the indicated error is the error of the linear regression; n is as indicated in the legends of Fig. 3 and Fig. S3B. ΔF and current kinetics were considered as correlated for a given mutant and pH condition if the steepness of the linear regression was not more than a factor of 0.75 different from 1, and thus between 0.75 and 1.33 (highlighted in bold).

60

Table S3. Test for possible intrinsic pH dependence of fluorophores

Mutant	Ratio $\Delta F/F_{desensitized-to-open}/\Delta F/F_{closed-to-open}$ protocol, %
T236C	-0.8 ± 3.1
E355C	9.8 ± 2.8
K343C/ N120W[C]	28.4 ± 1.9
K343C/ T236W	26.9 ± 7.5
D347C/ T236W	17.86 ± 1.9
D347C/ E238W	16.9 ± 4.6
D351C/ D237W[C]	-11.9 ± 10.0
D351C/ F257W[C]	31.5 ± 9.4
D237C/D347W[C]*	26.0 ± 5.0
D237C/D351W[C]	0.2 ± 3.9

To test for a possible intrinsic pH dependence of the fluorophore in the experiment, labeled channels were desensitized by exposing them for 30 s to pH 6.8, before switching to the stimulation pH 6. In this protocol, pH 6 did not induce currents. If a ΔF signal is measured in this protocol, either it reflects an electrically silent transition or it is due to the intrinsic pH dependence of the fluorophore at its location in the protein. Shown here is the ratio of the $\Delta F/F$ of the desensitized-to-open protocol (i.e., pH 6.8 to pH 6) to the $\Delta F/F$ of the closed-to-open protocol (i.e., pH 7.4 to pH 6) as a percentage; $n = 3–8$. A low ratio indicates that there is no intrinsic pH dependence of the fluorophore, and a higher ratio indicates the presence of either electrically silent transitions or of an intrinsic pH dependence of the fluorophore in the experimental conditions. This ratio was measured with the fluorophore AlexaFluor488 or, where indicated with a superscript "C," with CF488A.
*For the mutant D237C/D347W, the indicated values are from two experiments at pH 6. At pH 6.2, the ratio was 17.3 ± 9.2 ($n = 4$). The ratio was not measured for the combined VCF/PaC or APc mutants, because they still showed currents after exposure to conditioning pH ≤ 6.8.

Other Supporting Information Files

Dataset S1 (XLSX)

3.2 Project 2: Conformational changes in the lower palm and wrist domains

Prepared manuscript for publication: Rapid and slow conformational changes in the lower palm and wrist region associated with ASIC1a gating transitions

Authors: Sabrina Vullo, Nicolas Ambrosio and Stephan Kellenberger

Proton binding events in different extracellular domains lead to several conformational changes that are probably propagated through the lower palm domain and wrist to the transmembrane domains, where the pore and channel gates reside. The wrist constitutes the structural junction that directly connects the palm to the transmembrane domains and provides the pathway through which the ions flow into the pore. Therefore, structural changes in this region likely play a critical role in transmitting an activation signal to the channel gate. In this study, we used the voltage-clamp fluorometry technique to investigate the conformational changes occurring in the lower palm domain and in the wrist during channel activation and desensitization. Our results showed fast conformational changes in the wrist with the same timing as channel activation, whereas the palm domain undergoes slow conformational changes consistent with a role in channel desensitization. Moreover, the introduction of an engineered fluorescence quencher at different channel domains revealed structural rearrangements occurring between two distinct ASIC subunits and correlated with specific channel transitions.

In summary, our studies suggest that proton binding to the extracellular domain of ASIC1a induces conformational changes in the lower palm and in wrist regions most likely important for transmitting the transduction signal to the channel gate. Our findings provide new insights on the basic mechanisms controlling ASIC activity and may be relevant for other ENaC/DEG family members.

My contribution to the manuscript:

I made a certain number of mutations, screened $^2/_3$ of the 86 tested mutants in VCF, performed and analyzed a large amount of experiments, made all the figures and wrote a first draft of the manuscript. The second part of the screening and analysis of the experiments have been performed by the master student Nicolas Ambrosio.

Rapid and slow conformational changes in the lower palm and wrist region associated with ASIC1a gating transitions

Sabrina Vullo, Nicolas Ambrosio and Stephan Kellenberger*

Department of Pharmacology and Toxicology, University of Lausanne, 1011 Lausanne

* To whom correspondence should be addressed: Stephan Kellenberger, Department of Pharmacology and Toxicology, University of Lausanne, Rue du Bugnon 27, CH-1011 Lausanne, Switzerland; Stephan.Kellenberger@unil.ch; Phone ++4121 692 5422, Fax ++4121 692 5355.

Abstract

Acid-Sensing Ion Channels (ASICs) are trimeric proton-gated and Na^+-conducting channels that are widely expressed in neurons of the central and peripheral nervous systems and play important physiological and pathological roles as pH sensors. Although chicken ASIC1a structures have been solved in the closed, open and desensitized states, the mechanisms by which protonation of extracellular titratable residues promotes channel opening are still poorly defined. The extracellular part of ASIC subunits is connected at its central domain, the palm, via two short and flexible segments forming the "wrist" to the transmembrane domains that contain the ion pore and the channel gates. In this study, we used voltage-clamp fluorometry to investigate the conformational changes occurring in the lower palm domain and in the wrist during channel activation and desensitization. Strategically placed fluorophores reported slow conformational changes related to channel desensitization in the palm, and fast conformational changes, likely associated with channel opening, in the wrist. Introduction of quenching groups at several positions within the thumb, palm and β-ball domains, in combination with fluorophores placed in the palm, allowed the detection of fluorescence changes with different kinetics, depending on the positioning of the quenching group. This identified inter-subunit rearrangements in this region with the timing of channel opening and desensitization. Our findings highlight the importance of the palm and wrist in transmitting the activation signal to the ASIC pore, and lay a basis for future studies aimed at modulating these channels.

Introduction

Ion channels gated by extracellular ligands are integral membrane proteins that control many signaling processes in our body. To open an ion channel, specific ligands bind to the extracellular domain leading thereby to the opening of channel pore located in the membrane, rendering it permeable to small ions. This involves a signal transmission within the ion channel, from the ligand binding site to the channel pore (Hille, 2001). For classical ligand-gated ion channels it was shown that the binding of the ligand changes the conformation of the channel protein, and that this conformational change leads to the opening of the channel pore (Nemecz et al., 2016). Acid-sensing ion channels (ASICs) are a special kind of ion channels, since protons – as opposed to small molecules – are their activating ligands (Kellenberger and Schild, 2015; Waldmann et al., 1997b). Protons will not bind to one defined binding site within each channel subunit; rather, an increase in proton concentration (=lowering of pH) will change the protonation state of residues whose pKa is between the pH before and after the solution change. Such changes in the charge of amino acid side chains likely induce conformational changes leading to channel opening. The molecular mechanisms of ASIC activation are currently not known. ASICs are Na^+-conducting ion channels of the central and peripheral nervous system. Since they are involved in the expression of fear, neurodegeneration after ischemic stroke, learning and pain sensation, they are attractive potential drug targets. A better understanding of the molecular mechanisms of ASIC function is needed for the design and development of appropriate ASIC inhibitors or activators. For this reason, we have set out to investigate possible mechanisms of signaling between proton-sensing sites and the pore of ASIC1a.

Four different ASIC genes are known that give rise to 6 different subunits in rodents, ASIC1a, ASIC1b, ASIC2a, ASIC2b, ASIC3 and ASIC4. The subunits are widely expressed in the nervous system, with ASIC1b and ASIC3 mostly in the PNS, ASIC4 mostly in the CNS, ASIC1a, -2a and -2b in both CNS and PNS. The channel properties (pH dependence, kinetics) depend on the subunit composition (Kellenberger and Schild, 2015; Wemmie et al., 2013). ASICs respond to a sustained extracellular acidification with a transient current of a duration of tens of milliseconds to seconds, because after opening, these channels enter a non-conducting desensitized state. Therefore, ASICs can exist in three different functional states, closed, open and desensitized. Crystal structures of chicken ASIC1a were published in conformations that most likely correspond to the closed (Yoder et al., 2018), toxin-opened (Baconguis et al., 2014; Baconguis and Gouaux, 2012; Dawson et al., 2012), and the desensitized state (Gonzales et al., 2009; Jasti et al., 2007). Functional ASICs are trimers of homologous or identical subunits (Bartoi et al., 2014). Each subunit consists of intracellular N- and C-terminal ends, not resolved

in the crystal structures, two transmembrane α-helices, and a large ectodomain, whose shape was compared to a hand holding a small ball, with individual parts named palm, knuckle, β-ball (scaffolding, β-strand-rich, central part), as well as the thumb and finger that contain several α-helices and are located at the outside of the channel protein (Fig. 1A). The palm forms the continuation of the transmembrane helices. Extracellular ions access the pore via fenestrations located just above the plasma membrane, and the extracellular vestibule, located above the pore. The transition zone between the transmembrane part and the palm is called the wrist. Farther up, the three palm domains enclose another cavity, the central vestibule. Each ASIC channel contains in addition three acidic pockets, which are enclosed by the thumb, finger and β-ball of one, and the palm of a neighboring subunit. The comparison of the crystal structures shows that the extended acidic pockets, seen in the closed state, collapse upon opening. In the open state, the lower palm and transmembrane segments (TM)2 move away from each other, and the extracellular vestibule and the pore are substantially widened. Upon desensitization, these domains adapt a conformation that is close to, but not identical with that of the closed state (Yoder et al., 2018). Except for these differences, no changes in the ectodomain were observed between the toxin-opened and desensitized conformations. The acidic pocket contains many acidic residues, and it was suggested that acidification allows its collapse, and that this conformational change induces the opening of the pore (Jasti et al., 2007). Functional studies showed that the acidic pocket contributes to ASIC activation, that it is however not essential, and that other domains such as the palm and the wrist likely also contribute to pH sensing (Krauson and Carattino, 2016; Krauson et al., 2013; Liechti et al., 2010; Lynagh et al., 2018; Paukert et al., 2008; Vullo et al., 2017). The lower palm domains of the three residues move towards each other during desensitization, and preventing this movement impairs desensitization (Roy et al., 2013).

If proton sensors in the acidic pocket, palm or domains located farther up are protonated, a possible path for transmitting this information to the pore is via the palm domain, which is covalently linked to the transmembrane segments. As mentioned above, several studies have provided a strong link between the palm and desensitization. Glu418 of the palm was however also identified as contributing to activation (Krauson et al., 2013; Liechti et al., 2010). Two loops located just above the lower palm domain, the β1-β2 and β11-β12 loops, interact with each other and co-determine the ASIC current kinetics, supporting an involvement of these loops in activation and desensitization (Coric et al., 2003; Li et al., 2010a, b; Springauf et al., 2011). The wrist forms the interface between the transmembrane and extracellular channel parts

and provides the fenestrations through which ions gain access to the pore. In addition, the wrist may also itself contribute to the pH-dependent gating, since each subunit contains three His residues, His70, His72 and His73, of which His73 is in close proximity of Asp78 of a neighboring subunit. Combined mutation of some of these residues was shown to suppress ASIC currents without much affecting the cell surface expression (Paukert et al., 2008). Aromatic interactions between the wrist and the β-turn, a small linker connecting the β9 strand of the palm to the α4 helix of the thumb, are required to preserve the function of the channel (Li et al., 2009).

The crystal structures provide important information for the understanding of molecular mechanisms of the control of ASIC activity. They do however not explain the transitions between the functional states, nor do they identify the forces that drive the conformational changes leading to the transitions. We used here voltage-clamp fluorometry (VCF) to study the kinetics of conformational changes in the palm and wrist regions, in order to gain information on their possible involvement in activation and desensitization. We show that conformational changes occurring in the β1-β2 linker of the palm are likely involved in channel desensitization. The introduction of a quencher group at several positions close to this linker reveals structural rearrangements of different ASIC domains associated with both activation and desensitization. The lower palm – wrist axis undergoes significant structural changes upon extracellular acidification, consistent with a role in ASIC activation.

Results

Conformational changes in the β1-β2 linker of the palm. Residues of interest in human ASIC1a were mutated to Cys, and the mutant channels were expressed in *Xenopus laevis* oocytes. Prior to the experiment, oocytes were exposed to maleimide derivatives of AlexaFluor488 or CF488A to attach the fluorophore to the engineered Cys residues. We used then VCF, which allows the simultaneous measurement of ionic currents and of fluorescent signals. We have previously shown that exposure of WT ASIC1a to the maleimide derivatives of these two fluorophores does not lead to fluorescence changes upon acidification (Bonifacio et al., 2014), indicating that the fluorophores are attached to the engineered Cys residues. Three fluorophore docking positions in the β1-β2 linker, A81, S83 and Q84, yielded robust fluorescence changes (ΔF, Fig. 1A-B). The ΔF signals indicate that conformational changes occur. The ΔF may be due to changes in solvent exposure of the fluorophore, or to changes of the exposure to nearby quenching groups (Pantazis and Olcese, 2012). A candidate quenching

group in the vicinity of these residues is Tyr417 (Fig. 1A). When Tyr417 was mutated to Val in the background of these Cys mutants, the ΔF signal was lost in the background of A81C and S83C, and showed an apparent, but not significant decrease in Q84C/Y417V (Fig. 1B-D), indicating that the ΔF signal in the single mutants A81C and S83C is due to a change in distance or orientation relative to Tyr417, and that this may be partially the case for Q84C. The three single mutants displayed a negative ΔF, suggesting that the fluorophore attached to the Cys mutants approached Tyr417 when the pH was changed. To determine during which functional transition these conformational changes occurred, we measured the kinetics of the currents and of the ΔF signals. Figure 1E plots the rise time (time between reaching 10% and 90% of the maximal amplitude) of the ΔF onset (red symbols), the current appearance (black), and the decay time of the current desensitization (blue). The data show that the ΔF onset was slower than the current appearance but faster than the current decay, indicating that the movements occur after channel opening but before desensitization. The conformational changes that generate the ΔF may therefore prepare ASIC desensitization. In addition, the pH dependence of the ΔF signals of the single cysteine mutants showed an alkaline shift compared to that of current activation, and overlapped the pH dependence of SSD (Fig. S1). Tyr417 is located on the β strand 12 of the palm. Our observation suggests a relatively slow distance change between the $\beta1$-$\beta2$ linker and β strand 12, which is consistent with the known role of this structure in desensitization.

Intersubunit conformational changes involved in ASIC1a gating transitions. We took then advantage of the double mutants in the $\beta1$-$\beta2$ linker and β strand 12 to determine the timing and direction of distance changes between fluorophores attached to A81C, S83C or Q84C and engineered Trp residues introduced at different positions, and acting as fluorescence quenchers. A total number of 30 triple mutants was tested within this region, 11 of which showed a specific fluorescence signal. Trp residues were placed in the $\beta5$-$\beta6$ linker of the β-ball (R206, K208, M210), in the β-turn (T289), the thumb-palm $\alpha5$-$\beta10$ linker (D357, Q358, E359) and the $\beta10$-strand of the palm (L369). Of these four groups, the quenching occurs between residues of the same subunit for Trp residues introduced in the $\beta5$-$\beta6$ linker, while the quenching occurs across subunits for the other three groups (Fig. 2A). Representative traces of these mutants show that many of the ΔF were negative and sustained, while some were positive, and several combined, with negative and positive components (Fig. 2B). The analysis of the current and ΔF rise times identifies four pairs in which the ΔF is faster or of the same speed as the current appearance,

A81C/Y417V/L369, S83C/Y417V/T289W, S83C/Y417V/E359W and S83C/Y417V/L369W (Fig. 2C). For almost all these mutants, there is no significant difference in the delay between current and fluorescence appearance (Fig. 2E). For most of the triple mutants, the ΔF onset is faster than the current decay (Fig. 2D). It is likely that during these gating transitions, both partners, *i.e.* the fluorophore and the engineered Trp, move. In this case, the kinetics of the appearance of the ΔF depends on the relative movement of both partners. In the single mutants S83C and Q84C, the similar time course of the ΔF onset kinetics with those of current decay indicates that the fluorophore and the quencher move towards each other with the kinetics of current decay. If they both move in the same direction, but one faster than the other, the kinetics of the ΔF reflect this difference in speed. The fast ΔF kinetics observed with the four triple mutants indicate that at least one of the partners (A81/L369, S83/T289, S83/E359, S83/L369) moves with the speed of activation. Overall, we observe more negative signals, thus mostly approaching between Cys-Trp partners. The most rapid ΔF signals reflect an approaching of the α5-β10 linker (Glu359), the β10 strand (Leu369) and the β-turn (Thr289) towards the β1-β2 linker. Slower signals indicate an approaching between the β1-β2 linker and Tyr417 of β strand 12, and the closer part of the β5-β6 linker, whereas the distance between Ala81 and Met210 (β5-β6 linker) and Gln358 (located close to the α5-β10 helix) increases.

Fast conformational changes in the wrist. Both potential signaling pathways from the putative pH sensors to the pore, which occur via the palm domain or via the β-turn-TM1 interaction of residues Trp287 and Tyr71, involve the wrist. We have placed fluorophores at different positions in wrist and upper pore region, and found for several of them ΔF signals (Fig. 3A-B). Several mutants (E63C, H70C, Y71C, H72C, T419C and K424C) showed composite ΔF signals, with positive and negative components. The kinetics of single component ΔF signals, and of the faster component of two-component ΔF signals in this area had either the same timing as the current appearance (H70C, Y71C, H72C, T419C, K424C, I428C) or were faster (E63C, A425C ($p < 0.05$ and $p < 0.001$, respectively); Fig. 3C). For some of them, the fluorescence signal appeared before the current activation (Fig. 3E). We have previously measured fast ΔF signals in different ASIC1a domains, however, had not used the perfusion system that measures current and ΔF at approximately the same part of the oocyte surface (Bonifacio et al., 2014; Gwiazda et al., 2015a). Some of these mutants were re-measured for kinetic comparison of ΔF and current kinetics (*Methods*). Comparison with these mutants (Fig. S2) shows that the ΔF kinetics of the fast wrist mutants were similar to those of fast residues

further distal of the pore (finger, knuckle and acidic pocket) identified in these previous studies (Bonifacio et al., 2014; Gwiazda et al., 2015a; Vullo et al., 2017).

As a measure of how the ΔF onset kinetics relate to those of current appearance, we determined at pH6 the ratio rise time ΔF/rise time I (compare Fig. 2F-3G-S2C). The analysis shows that the conformational changes in the more distant parts occur with a similar timing as the wrist mutants and as the four "fast" triple mutants in the region of the palm $\beta 1$-$\beta 2$ linker.

We have previously found with mutants in most ASIC domains, even for mutants showing rapid ΔF kinetics, that the pH_{50} of the ΔF signal was more alkaline than the pH_{50} of the current amplitude, and was for many mutants close to the midpoint of SSD, the pHD_{50} (Bonifacio et al., 2014; Vullo et al., 2017). In the tested wrist mutants, the pH_{50} of the current was significantly different from that of the WT, and the pHD_{50} was in all mutants very close to the WT value (Fig. 3F). These values were all determined on mutants that had been labeled with the fluorophore. The pH_{50} of the ΔF signal was in E63C similar to the pHD_{50} of the current, it was in several mutants between the current pHD_{50} and pH_{50} values, and in some of them (H72C, T419C, K424C, A425C) closer to the pH_{50}, or even lower than this value.

Discussion

The crystal structures of cASIC1a in complex with the gating modifier Psalmotoxin-1 or Mit-Toxin reveal structural rearrangements of the three channel subunits that displace the $\beta 1$ and $\beta 12$ strands of the palm domain toward the membrane and the TM1 and TM2a away from the central vertical axis of the channel. Here, we investigated the conformational changes in the lower palm and wrist regions of hASIC1a following extracellular acidification from functional experiments. Environmental-sensitive fluorophores attached to cysteine residues in these regions reported fluorescence changes of different types and related with specific functional transitions.

Conformational changes in the β1-β2 linker prepare channel desensitization

Our VCF experiments have shown that the loop connecting the palm and the β-ball domains undergoes dynamic structural changes upon extracellular acidification, given by the presence of negative ΔF signals. We found that the presence of these signals was mostly due to quenching events by the close Tyr417, located in the β12 strand. Since quenching events depend on changes in distance and orientation between fluorophore and quencher, a negative fluorescence emission would indicate a displacement of the residues located in this linker toward the β12

strand. Analysis of the timing of the observed movements indicates that they are slower than channel activation but faster than desensitization, suggesting that these residues likely prepare channel desensitization. In addition, we found that the pH dependence of the ΔF signals exactly overlaps that of the SSD. In agreement with our observations, comparison between crystal structures indicate that residues in the β1-β2 linker approach the β12 strand when the channel transits from the open to the desensitized state (Baconguis and Gouaux, 2012; Gonzales et al., 2009).

The role of the β1-β2 linker in channel desensitization has been investigated in several functional studies. Coric *et al.* made chimeric channels between rat and fish ASIC1, whose desensitization kinetics are much faster than those of rat, to identify residues that contribute to this functional transition. They found that a tract of three residues (Ser83-Gln84-Leu85, human protein) in the β1-β2 linker was responsible for the faster desensitization kinetics in fish ASIC1a (Coric et al., 2003). Similarly, other mutagenesis and functional studies have shown that mutation of residues located in this linker impaired the rate of desensitization and in some cases led to the development of a sustained current component (Li et al., 2010b, c; Springauf et al., 2011). Together these studies support the notion that residues in the β1-β2 linker facilitate the transition from the open to the desensitized state.

Intersubunit fluorescence quenching points to conformational changes involved in proton-dependent gating of ASIC1a

The β1-β2 linker faces the palm domain of a neighboring subunit, which is directly connected to the α5 of the thumb domain through a flexible loop. To infer information about the structural rearrangements in this region, a Trp quencher was introduced at several positions in double mutants lacking the endogenous quencher Tyr417. Analysis of the types and the timing of the detected fluorescence changes indicates that residues of the α5-β10 strand loop, the β-turn and the β strand 10 approach the β1-β2 linker of an adjacent subunit during and immediately after channel activation, suggesting that structural changes in these regions may be involved in channel opening and in the transition from the open to desensitized state. All the observed movements are faster than channel desensitization and may have a role in the closing of the palm domains toward the central axis after channel protonation (Della Vecchia et al., 2013; Roy et al., 2013).

The structural dynamics of these regions has also been observed by applying normal mode analysis (Yang et al., 2009). This study provides evidence for structural rearrangements

associated to the β1-β2 linker and to the β-turn. The authors suggest that these motions may be important for transmitting the transduction signal to the channel gate.

Slower movements were observed in our VCF study in the β5-β6 linker of the β-ball domain, bringing the residues Lys208 and Arg206 close to the β1-β2 linker, and the residue Met210 away from it. Comparison of the crystal structures shows a decreased distance between the β10 strand and the β1-β2 linker of the palm domain and between the β-turn and the β1-β2 linker, occurring during channel opening, thus in agreement with our findings. Small or no structural changes of the α5 helix-β10 loop and β5-β6 linker were, however, observed between the open and desensitized structures (Baconguis et al., 2014; Gonzales et al., 2009). This discrepancy of the prediction of an absence of conformational changes from the crystal structures, and evidence of conformational changes by VCF, may be due to the fact that the crystal structures show a cASIC1a channel opened by toxins. It is possible, that the toxin-bound open conformation does not correspond to the proton-opened conformation. The importance of intersubunit interactions in this region was highlighted in a recent functional study conducted by Yoder and Gouaux (Yoder et al., 2018). They showed that introduction of a disulfide bridge between the end of the α5 helix of the thumb and the β1-β2 linker of the palm of a neighboring subunit keeps the channel in an expanded conformation, thus preventing channel opening, consistent with the presence of structural rearrangement in this region during channel activity.

In summary, these results report conformational changes involved in both activation and desensitization and provide insights about the structural rearrangements occurring between different ASIC subunits.

Fluorescence changes in the post-TM1 and pre-TM2 loops report conformational changes related with channel opening

The wrist region is formed by two small linkers that directly connect the β1 and β12 strands of the palm domain to the TM1 and TM2, respectively. This region constitutes also the conduction pathway utilized by ions to enter the channel. We hypothesized that the post-TM1 and pre-TM2 linkers undergo structural reorganization upon channel proton binding and that these motions may transmit the transduction signal to the gate to activate the channel.

Fluorophores attached to several cysteine residues in the wrist reported fluorescence signals characterized by the presence of two distinct components with opposite polarity. The first component was always of bigger amplitude compared to the second one and was faster or of the same timing as the current activation. We have previously observed ΔF signals with two

components in the acidic pocket (Vullo et al., 2017). With the acidic pocket mutants, the first component of the ΔF signal was however in all cases much smaller than the second component. Consistent with a role in channel opening, the pH dependence of the fluorescence signals was for about half of the mutants in the wrist close to the pH dependence of current activation. In a previous study conducted by Passero and colleagues, it was shown that the segment preceding the TM2 domain undergoes structural rearrangements upon extracellular acidification associated with channel opening (Passero et al., 2009). This study, however, was limited to only one residue, Glu427, and did not provide information about the conformational changes of adjacent regions.

A functional study has shown that combined neutralization of titratable residues in the loop preceding the TM1 domain produced proton-insensitive channels that were normally expressed at the cell surface (Paukert et al., 2008). Moreover, disruption of the aromatic interaction between the post-TM1 segment and the β-turn reduced channel proton affinity or abolished channel function (Li et al., 2009), suggesting that this region may be critically involved in ASIC proton sensing.

A recent study indicates that the wrist of ASIC1a is a drug target site. The authors identified residues in the wrist as likely binding sites for channel inhibition by ibuprofen (Lynagh et al., 2017b). The wrist has a role in the regulation of ENaC channels as well. A functional study has shown that the extent of ENaC Na^+ self-inhibition was reduced by selected cysteine mutations of residues within the wrist (Shi et al., 2012).

In summary, our study reveals dynamic conformational changes in the post-TM1 and pre-TM2 regions associated with channel activation, and intersubunit interactions in the palm domain consistent with a role in both activation and desensitization. Our findings add important insights on the structural changes underlying ASIC gating and may open a new path for future studies aimed at modulating these channels.

Materials and Methods

Molecular biology

The human ASIC1a cDNA construct was cloned into a pSP65 vector containing 5'- and 3'-untranslated sequences for expression in *Xenopous* oocytes. Point mutations were introduced by site-directed mutagenesis using KAPA HiFi HotStart PCR polymerase (KAPA Biosystems). All mutations were verified by direct sequencing (Synergen Biotech). Complementary RNAs were synthetized *in vitro* using mMESSAGE mMACHINE SP6 kit (Ambion/Applied Biosystems).

Oocyte expression

Surgical removal of oocytes was carried out as described previously (Liechti et al., 2010). Healthy oocytes stages V and VI were collected from adult female *Xenopous laevis* in accordance with the Swiss federal law on animal welfare and approved by the committee on animal experimentation of the Canton de Vaud. Oocytes were injected with 0.02-1 µg/µL of cRNA encoding hASIC1a WT and mutants. Oocytes used for VCF experiments were incubated after cRNA injection for 1h in Modified Barth's Solution (MBS) containing 10 mM 3-maleimidopropionic acid (Bachem) to modify free cysteine residues of proteins natively expressed on the cell membrane, and then maintained at 19°C in MBS, composed of (mM): 85 NaCl, 1 KCl, 2.4 NaHCO$_3$, 0.33 Ca(NO$_3$)$_2$, 0.82 MgSO$_4$, 0.41 CaCl$_2$, 10 HEPES and 4.08 NaOH.

Electrophysiology

Two-electrode voltage clamp experiments were conducted at room temperature (20-25°C) 1-2 days after cRNA injection. All oocytes used for TEVC and VCF experiments had been previously labelled in the dark with 5 µM CF488 maleimide (Biotium) or AlexaFluor488 maleimide (Invitrogen) at room temperature for 15 min. Oocytes were placed in a RC-26Z recording chamber (Warner Instruments) and impaled with glass electrodes filled with 1M KCl and continuously perfused by gravity at a rate of 5 to 15mL/min. A specially designed chamber was used to measure the ΔF and current kinetics from about the same oocytes surface, as described previously (Vullo et al., 2017). Macroscopic currents were measured at a holding potential of -40 mV with a TEV-200A amplifier (Dagan Corporation). Data were recorded with Chartmaster software (HEKA Electronics) at a sampling rate of 1 ms and low-pass filtering at

2 kHz. Standard recording solutions contained (mM): 110 NaCl, 2 CaCl$_2$, and 10 HEPES for pH $\geq$ 6.8. For solutions with a pH < 6.8, HEPES was replaced by 10 mM MES. The pH was adjusted using NaOH and HCl.

Fluorescence measurements

A total number of 85 fluorophore-labelled cysteine mutants had been tested in VCF. Out of 56 cysteine residues in the lower palm, wrist and transmembrane domain, 11 yielded a robust fluorescence signal. Concerning the triple mutants, we tested a total number of 30 mutants located among the palm, thumb and β-ball domains; out of them, 11 showed a specific fluorescence signal. The VCF setup was equipped with an Intensilight mercury lamp (C-HGFI; Nikon), a 40x Nikon oil-immersion objective to detect the fluorescence signal emitted by fluorophore-labelled oocytes. The optical signal was then converted into current units by a photodiode (S1336-18BQ; Hamamatsu Photonics) coupled to the head stage of an amplifier (List-EPC-7; HEKA). A low-pass eight-pole Bessel filter was used to amplify and filter the signal at 50 Hz. Changes in fluorescence intensity (ΔF) were normalized to the total fluorescence signal (F). Specificity of the fluorescence signals was assessed by exposing the oocytes to a slight acidic pH, which allows the direct channel transition from the closed to the desensitized state, and then stimulated with an acidic pH 6. Cysteine mutants that gave rise to a specific fluorescence signal showed no or very small fluorescence signal after application of this protocol. As a measure of the specificity of the signal, we calculated the ratio of the ΔF/F relative to the transition desensitized to open to the ΔF/F for the transition closed to open, and expressed this ratio as a percentage. The lower is the ratio, the higher is the specificity of the fluorescence signal. In this study we included only mutants that showed a ΔF/F$_{D-O}$/ΔF/F$_{C-O}$ lower than 35%.

Data analysis and statistics

Data were collected from at least two oocyte batches isolated from different animals for each mutant. Experimental data were analyzed with the software Fitmaster (HEKA Electronics) and with Origin PRO software (OriginLab Corp, Northampton, USA). Concentration response curve were fit to the Hill function: $[(I = I_{max}/(1+ (10^{-pH}{}_{50}/10^{-pH})^{nH}]$, where I$_{max}$ is the maximal current, pH$_{50}$ is the pH at which maximal of the current is achieved, and nH is the Hill coefficient. SSD curves were fitted with an analogous equation.

The results are presented as mean ± SEM. They represent the mean of n independent experiments on different oocytes. Statistical analysis was done with t-test where two conditions were compared, or with One-way ANOVA followed by Dunnett's or Tukey multiple comparisons test for comparison of >2 conditions (Graphpad Prism 6). ΔF and current kinetics were considered as correlated for a given mutant and pH condition if the steepness of the linear regression of a plot of the rise time of ΔF as a function of the rise time of the current kinetics was between 0.75 and 1.33.

References

Baconguis, I., Bohlen, C.J., Goehring, A., Julius, D., and Gouaux, E. (2014). X-ray structure of Acid-sensing ion channel 1-snake toxin complex reveals open state of a Na^+-selective channel. Cell *156*, 717-729.

Baconguis, I., and Gouaux, E. (2012). Structural plasticity and dynamic selectivity of acid-sensing ion channel-spider toxin complexes. Nature *489*, 400-405.

Bartoi, T., Augustinowski, K., Polleichtner, G., Grunder, S., and Ulbrich, M.H. (2014). Acid-sensing ion channel (ASIC) 1a/2a heteromers have a flexible 2:1/1:2 stoichiometry. Proc Natl Acad Sci U S A *111*, 8281-8286.

Bonifacio, G., Lelli, C.I., and Kellenberger, S. (2014). Protonation controls ASIC1a activity via coordinated movements in multiple domains. J Gen Physiol *143*, 105-118.

Coric, T., Zhang, P., Todorovic, N., and Canessa, C.M. (2003). The extracellular domain determines the kinetics of desensitization in acid-sensitive ion channel 1. J Biol Chem *278*, 45240-45247.

Dawson, R.J., Benz, J., Stohler, P., Tetaz, T., Joseph, C., Huber, S., Schmid, G., Hugin, D., Pflimlin, P., Trube, G.*, et al.* (2012). Structure of the Acid-sensing ion channel 1 in complex with the gating modifier Psalmotoxin 1. Nat commun *3*, 936.

Della Vecchia, M.C., Rued, A.C., and Carattino, M.D. (2013). Gating transitions in the palm domain of ASIC1a. The Journal of biological chemistry *288*, 5487-5495.

Gonzales, E.B., Kawate, T., and Gouaux, E. (2009). Pore architecture and ion sites in acid-sensing ion channels and P2X receptors. Nature *460*, 599-604.

Gwiazda, K., Bonifacio, G., Vullo, S., and Kellenberger, S. (2015). Extracellular Subunit Interactions Control Transitions between Functional States of Acid-sensing Ion Channel 1a. J Biol Chem *290*, 17956-17966.

Hille, B. (2001). Ion channels of excitable membranes, 3rd edn (Sunderland: Sinauer Associates).

Jasti, J., Furukawa, H., Gonzales, E.B., and Gouaux, E. (2007). Structure of acid-sensing ion channel 1 at 1.9 A resolution and low pH. Nature *449*, 316-323.

Kellenberger, S., and Schild, L. (2015). International Union of Basic and Clinical Pharmacology. XCI. Structure, Function, and Pharmacology of Acid-Sensing Ion Channels and the Epithelial Na^+ Channel. Pharmacological reviews *67*, 1-35.

Krauson, A.J., and Carattino, M.D. (2016). The Thumb Domain Mediates Acid-sensing Ion Channel Desensitization. The Journal of biological chemistry *291*, 11407-11419.

Krauson, A.J., Rued, A.C., and Carattino, M.D. (2013). Independent contribution of extracellular proton binding sites to ASIC1a activation. The Journal of biological chemistry *288*, 34375-34383.

Li, T., Yang, Y., and Canessa, C.M. (2009). Interaction of the aromatics Tyr-72/Trp-288 in the interface of the extracellular and transmembrane domains is essential for proton gating of acid-sensing ion channels. J Biol Chem *284*, 4689-4694.

Li, T., Yang, Y., and Canessa, C.M. (2010a). Asn415 in the beta11-beta12 linker decreases proton-dependent desensitization of ASIC1. The Journal of biological chemistry *285*, 31285-31291.

Li, T., Yang, Y., and Canessa, C.M. (2010b). Leu85 in the beta1-beta2 linker of ASIC1 slows activation and decreases the apparent proton affinity by stabilizing a closed conformation. The Journal of biological chemistry *285*, 22706-22712.

Li, T., Yang, Y., and Canessa, C.M. (2010c). Two residues in the extracellular domain convert a nonfunctional ASIC1 into a proton-activated channel. Am J Physiol Cell Physiol *299*, C66-73.

Liechti, L.A., Berneche, S., Bargeton, B., Iwaszkiewicz, J., Roy, S., Michielin, O., and Kellenberger, S. (2010). A combined computational and functional approach identifies new residues involved in pH-dependent gating of ASIC1a. The Journal of biological chemistry *285*, 16315-16329.

Lynagh, T., Mikhaleva, Y., Colding, J.M., Glover, J.C., and Pless, S.A. (2018). Acid-sensing ion channels emerged over 600 Mya and are conserved throughout the deuterostomes. Proc Natl Acad Sci U S A *115*, 8430-8435.

Lynagh, T., Romero-Rojo, J.L., Lund, C., and Pless, S.A. (2017). Molecular Basis for Allosteric Inhibition of Acid-Sensing Ion Channel 1a by Ibuprofen. J Med Chem *60*, 8192-8200.

Nemecz, A., Prevost, M.S., Menny, A., and Corringer, P.J. (2016). Emerging Molecular Mechanisms of Signal Transduction in Pentameric Ligand-Gated Ion Channels. Neuron *90*, 452-470.

Pantazis, A., and Olcese, R. (2012). Relative transmembrane segment rearrangements during BK channel activation resolved by structurally assigned fluorophore-quencher pairing. J Gen Physiol *140*, 207-218.

Passero, C.J., Okumura, S., and Carattino, M.D. (2009). Conformational changes associated with proton-dependent gating of ASIC1a. J Biol Chem *284*, 36473-36481.

Paukert, M., Chen, X., Polleichtner, G., Schindelin, H., and Grunder, S. (2008). Candidate amino acids involved in H^+ gating of acid-sensing ion channel 1a. J Biol Chem *283*, 572-581.

Roy, S., Boiteux, C., Alijevic, O., Liang, C., Berneche, S., and Kellenberger, S. (2013). Molecular determinants of desensitization in an ENaC/degenerin channel. FASEB J *27*, 5034-5045.

Shi, S., Carattino, M.D., and Kleyman, T.R. (2012). Role of the wrist domain in the response of the epithelial sodium channel to external stimuli. The Journal of biological chemistry *287*, 44027-44035.

Springauf, A., Bresenitz, P., and Grunder, S. (2011). The interaction between two extracellular linker regions controls sustained opening of acid-sensing ion channel 1. The Journal of biological chemistry *286*, 24374-24384.

Vullo, S., Bonifacio, G., Roy, S., Johner, N., Berneche, S., and Kellenberger, S. (2017). Conformational dynamics and role of the acidic pocket in ASIC pH-dependent gating. Proc Natl Acad Sci U S A *114*, 3768-3773.

Waldmann, R., Champigny, G., Bassilana, F., Heurteaux, C., and Lazdunski, M. (1997). A proton-gated cation channel involved in acid-sensing. Nature *386*, 173-177.

Wemmie, J.A., Taugher, R.J., and Kreple, C.J. (2013). Acid-sensing ion channels in pain and disease. Nature reviews Neuroscience *14*, 461-471.
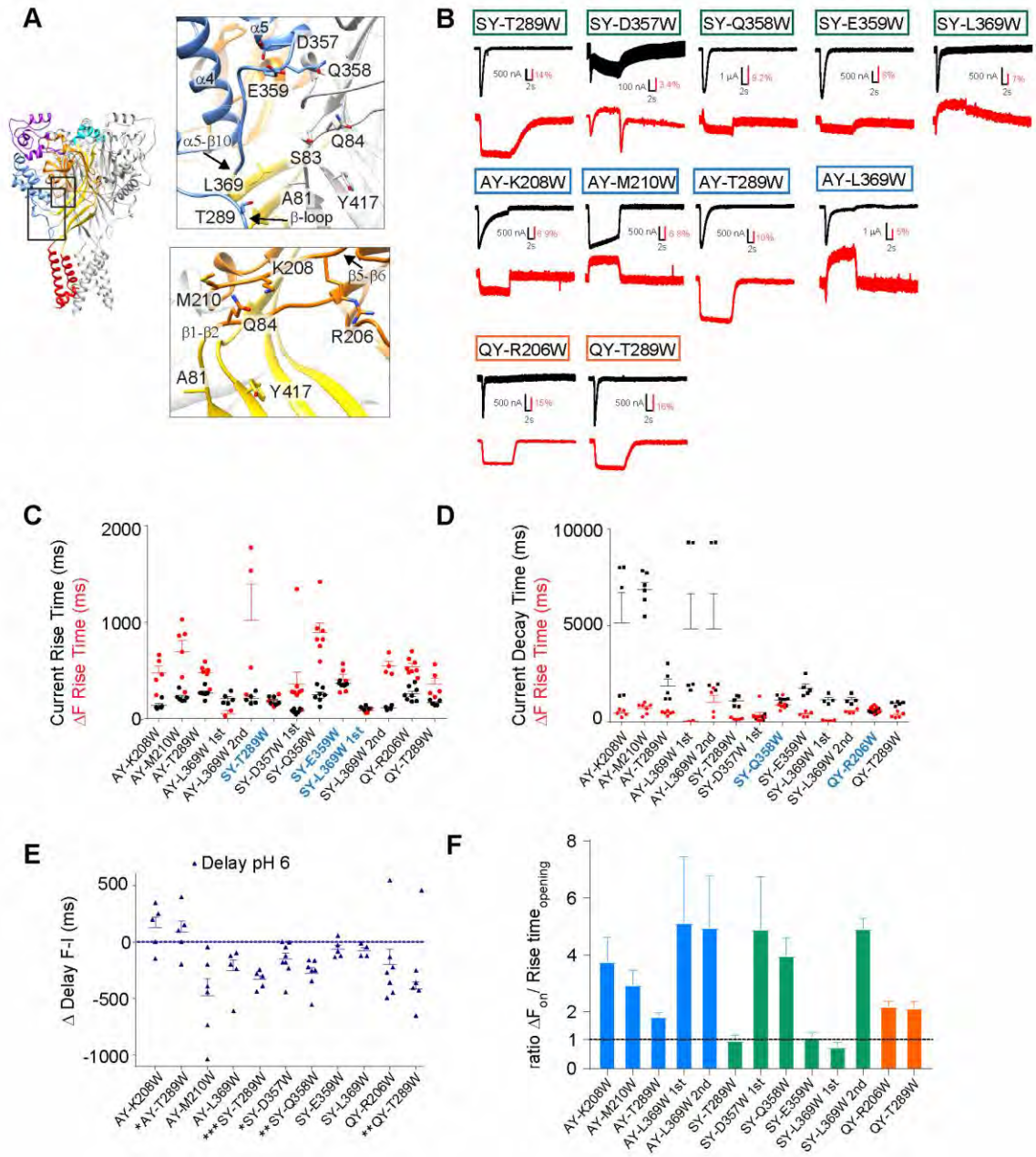
Yang, H., Yu, Y., Li, W.G., Yu, F., Cao, H., Xu, T.L., and Jiang, H. (2009). Inherent dynamics of the acid-sensing ion channel 1 correlates with the gating mechanism. PLoS Biol *7*, e1000151.

Yoder, N., Yoshioka, C., and Gouaux, E. (2018). Gating mechanisms of acid-sensing ion channels. Nature *555*, 397-401.
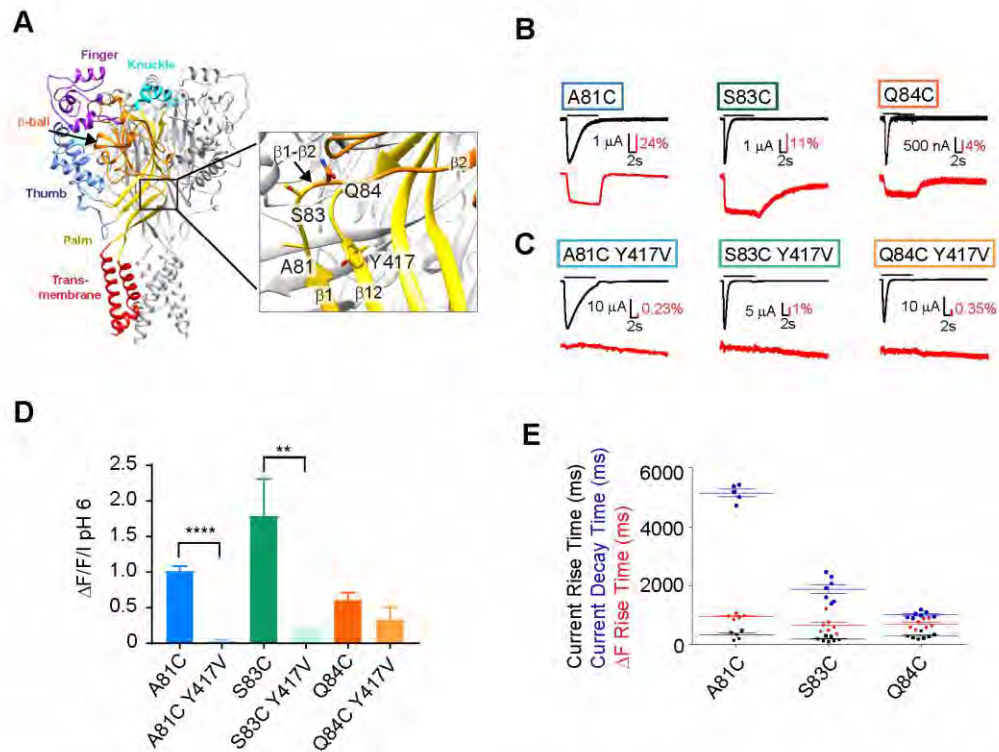
Figure 1. Structural rearrangements in the β1-β2 linker prepare channel desensitization.
A. Close-up view of β1-β2 linker, showing the residues mutated to cysteine: Ala81 and Ser83 in the β1 of the palm domain and Gln84 in the β2 of the β-ball domain. The Tyr417 is located in the β strand 12 of the palm domain. B-C. Representative current and fluorescence traces recorded from oocytes expressing the single cysteine mutants (B) and the corresponding mutants in which the endogenous fluorescence quencher Tyr417 was mutated to Val (C). Single cysteine mutants were measured in a special oocyte chamber to allow the simultaneous measurement of current and ΔF signal from about the same oocyte surface. Double cysteine mutants lacking the Tyr417 were measured in a RC-26Z recording chamber were the oocyte is entirely exposed to the acidic solution. ASIC current was induced by application of an acidic pH 6 for 10 s. D. ΔF/F normalized to pH 6 induced current is indicated for each individual cysteine mutant and in combination with Y417V (n = 4-5) **P <0.01, ****P <0.0001, determined with ANOVA followed by Tukey post-test. E. Scatter graph showing the current rise time (black), the current decay time (blue) and the fluorescence onset (red) after application of an acidic pH 6 from a conditioning pH 7.4 (n= 5-7). Error bars represent SEM.

A

α5
α4
D357
Q358
E359
α5-β10
L369
S83
Q84
Y417
A81
T289
β-loop

K208
β5-β6
M210
Q84
R206
β1-β2
A81
Y417

B

SY-T289W | SY-D357W | SY-Q358W | SY-E359W | SY-L369W
500 nA / 2s / 14% | 100 nA / 2s / 3.4% | 1 μA / 2s / 8.2% | 500 nA / 2s / 8% | 500 nA / 2s / 7%

AY-K208W | AY-M210W | AY-T289W | AY-L369W
500 nA / 2s / 8.9% | 500 nA / 2s / 8.8% | 500 nA / 2s / 10% | 1 μA / 2s / 5%

QY-R206W | QY-T289W
500 nA / 2s / 15% | 500 nA / 2s / 16%

C

Current Rise Time (ms) / ΔF Rise Time (ms)

AY-K208W, AY-M210W, AY-T289W, AY-L369W 1st, AY-L369W 2nd, SY-T289W, SY-D357W 1st, SY-Q358W 1st, SY-E359W, SY-L369W 1st, SY-L369W 2nd, QY-R206W, QY-T289W

D

Current Decay Time (ms) / ΔF Rise Time (ms)

AY-K208W, AY-M210W, AY-T289W, AY-L369W 1st, AY-L369W 2nd, SY-T289W, SY-D357W 1st, SY-Q358W, SY-E359W, SY-L369W 1st, SY-L369W 2nd, QY-R206W, QY-T289W

E

Δ Delay F-I (ms)

Delay pH 6

AY-K208W, *AY-T289W, AY-M210W, AY-L369W, ***SY-T289W, *SY-D357W, **SY-Q358W, SY-E359W, SY-L369W, QY-R206W, **QY-T289W

F

ratio ΔF$_{on}$ / Rise time$_{opening}$

AY-K208W, AY-M210W, AY-T289W, AY-L369W 1st, AY-L369W 2nd, SY-T289W, SY-D357W 1st, SY-Q358W, SY-E359W, SY-L369W 1st, SY-L369W 2nd, QY-R206W, QY-T289W

Figure 2. Quenching between thumb, β-ball and palm domains uncovers intersubunit conformational changes. A. close-up view of residues located in the thumb, β-ball and palm domains. Domains are shown in color in one of the two represented subunits, and in grey in the other. B. Representative recordings of simultaneous current (black traces) and fluorescence signals (red traces) of cysteine mutants in which Tyr417 was mutated to valine (V), and an engineered quencher has been introduced in different channel domains. ASIC currents were elicited by extracellular acidification to pH 6 for 10s. C-D. Scatter dot plots comparing the rise time of the channel activation (black, C), the current decay time (black, D) and the fluorescence appearance (red) after application of a stimulating pH 6 from a conditioning pH 7.4. Correlation between the ΔF and current signal is indicated by labeling in bold turquoise (*n*= 2-9). E. Scatter graph showing the difference in timing appearance between ΔF and current delay for each triple mutant upon acidification from pH 7.4 to pH 6, n = 4-8. (*P < 0.05; **P < 0.01; ***P < 0.001; ****P < 0.0001; different from 0). F. Ratio of the rise time of the ΔF onset divided by the rise time of the current opening ($rt_{\Delta Fon}/rt_{opening}$) at pH6 for each triple mutant. Note that a higher ratio corresponds to a slower conformational change (*n*= 2-8). Error bars represent SEM.
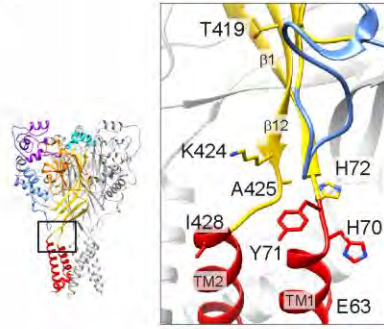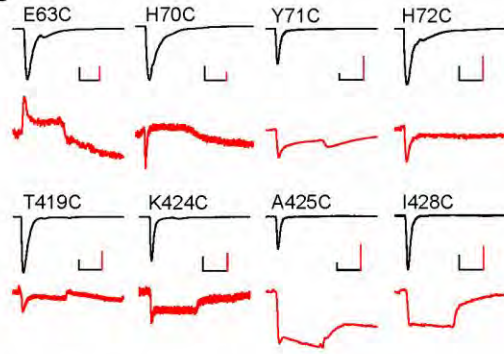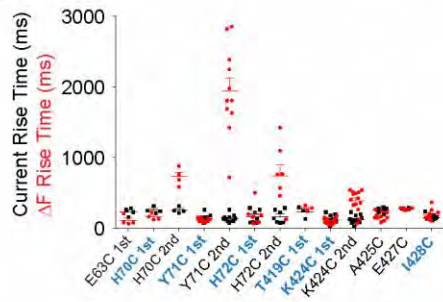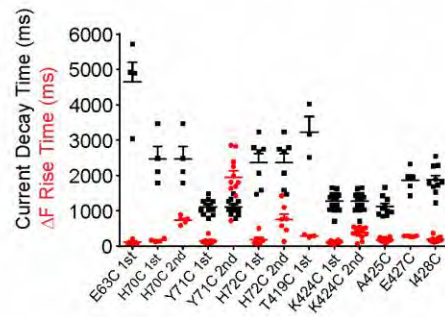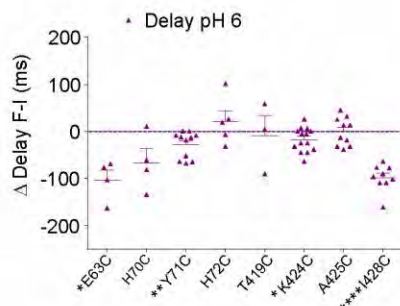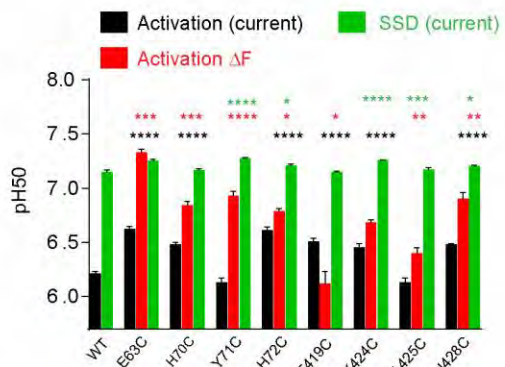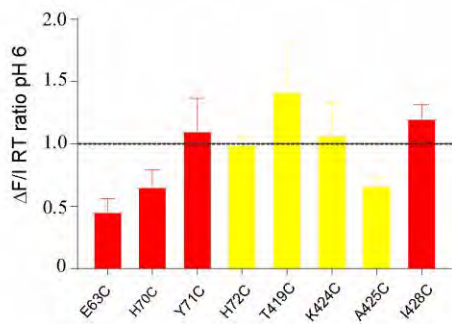
Figure 3. Conformational changes in the wrist are associated with channel activation. A. Close-up view of the wrist region showing the residues that were mutated to cysteine. B. Representative current (black traces) and fluorescence signals (red traces) recorded from oocytes clamped at -40 in response to extracellular acidification from pH 7.4 to pH 6. The acidic pH was applied for 10s for all mutants except H70C where the stimulation lasted 20s. Horizontal line corresponds to 5s, the vertical line for the current (black) corresponds to: 1 µA for the mutants Y71C and T419C; 5 µA for the mutants H72C, K424C, A425C and I428C; 10 µA for the mutants E63C and H70C. The red vertical line corresponds to (%): 3 for the mutant E63C, 5.75 for H70C, 7 for Y71C, 19 for H72C, 8 for T419C, 10 for K424C, 14 for A425C, 5 for I428C. C-D. Scatter graphs comparing the current rise time (black, C) and decay time (black, D) with the fluorescence onset (red) obtained by exposing the oocyte channels to an acidic pH 6 from a conditioning pH 7.4. The duration of the acidic stimulation was as mentioned in (B). Correlation between the ΔF and current signal is indicated by labeling in bold turquoise (n=3-14). E. Scatter dot plot showing the difference in current and fluorescence delay of appearance measured at pH 6 (n=3-14). (*P < 0.05; **P < 0.01; ***P < 0.001; ****P < 0.0001; different from 0). F. pH of half-maximal amplitude (pH_{50}) for current activation (black), ΔF (red), and current SSD (green). Conditioning pH was 7.4 for the current and 8 for the fluorescence. Black stars indicate statistical significance between the pH_{50} of current activation of ASIC1a WT and the mutants; green stars between the pH_{50} SSD of the WT and mutants; red stars between the pH_{50} of current activation of each mutant and the pH_{50} of fluorescence for the same mutant. (*P < 0.05; **P < 0.01; ***P < 0.001; ****P < 0.0001) (n=4-8). G. Ratio of the rise time of the ΔF onset divided by the rise time of the current opening ($rt_{\Delta Fon}/rt_{opening}$) for each mutant. A higher ratio corresponds to a slower conformational change. Error bars represent SEM, n=3-14.
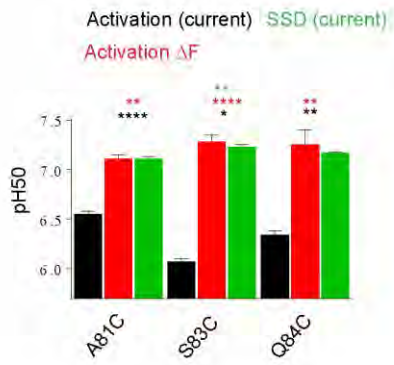
Figure S1. pHD$_{50}$ of single cysteine mutants in the β1-β2 linker correlates with the pH$_{50}$ of ΔF signals. pH$_{50}$ of current activation (black), ΔF (red), and current SSD (green). Conditioning pH was 7.4 for experiments in which the pH dependence of the current was determined, and 8 for experiments in which the pH dependence of the fluorescence was measured. Black stars indicate statistically significant differences between the pH$_{50}$ of current activation of ASIC1a WT and the mutants; green stars between the pH$_{50}$ SSD of the WT and mutants; red stars between the pH$_{50}$ of current activation of each mutant and the pH$_{50}$ of fluorescence for the same mutant. (*P < 0.05; **P < 0.01; ***P < 0.001; ****P < 0.0001) (n=5-6).
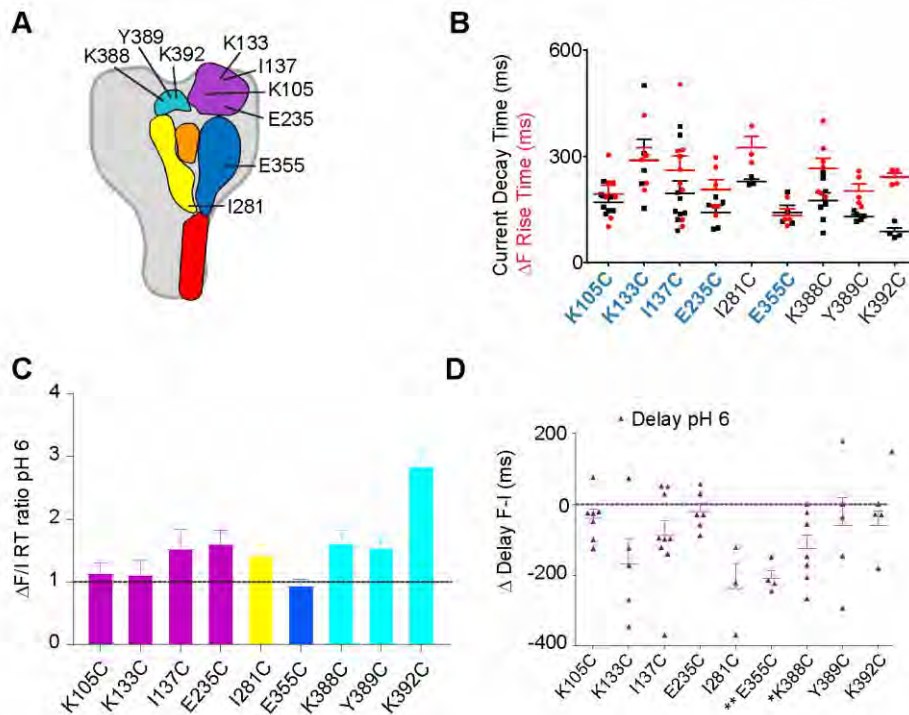
Figure S2. Fast conformational changes detected in different ASIC domains. A. Cartoon representation showing an individual ASIC subunit with five distinct domains and the residues that had been mutated to cysteine: finger (pink), knuckle (turquoise), β-ball (orange), thumb (blue), palm (yellow), transmembrane domain (red). B. Scatter dot plots comparing the rise time of the channel activation (black) and the fluorescence appearance (red) after application of a stimulating pH 6 from a conditioning pH 7.4. Correlation between the ΔF and current signal is indicated by labeling in bold turquoise (n=3-9). C. Ratio of the rise time of the ΔF onset divided by the rise time of the current opening ($rt_{\Delta Fon}/rt_{opening}$) for each mutant. A higher ratio corresponds to a slower conformational change. n=3-9. D. Scatter graph showing the difference in timing appearance between ΔF and current delay for each triple mutant upon acidification from pH 7.4 to pH 6, n=3-9.). (*P < 0.05; **P < 0.01; ***P < 0.001; ****P < 0.0001; different from 0). Error bars represent SEM.

3.3 Project 3: Other

Article not included in the thesis report: Extracellular Subunit Interactions Control Transitions between Functional States of Acid-sensing Ion Channel 1a

Authors: Gwiazda K., Bonifacio G., **Vullo S.**, Kellenberger S., J Biol Chem., 2015

My contribution to the manuscript:

I performed the control experiments in voltage-clamp fluorometry asked by the reviewers and I contributed to the writing of the manuscript.

4. General Discussion

4.1 Role of the acidic pocket and palm in pH sensing

4.1.1 Proton sensing in the acidic pocket fine-tunes channel pH dependence

In the first part of the project, we determined the contribution of the acidic pocket and palm domain to channel activation and desensitization. Note that, in the discussion, amino acid numbering refers to human ASIC1a and the numbers [1,2] shown in superscript refer to the projects n. 1 (Vullo et al., 2017) and n. 2 (paragraph 3.2).

To understand the role of the acidic pocket in pH sensing by ASIC1a, we combined up to 16 titratable residues (Asp, Glu and His) narrowly distributed within the acidic pocket to Asn or Gln to mimic a protonated state. Channels harboring multiple amino acid substitutions at selected positions still produced transient current upon acidic stimulation ([1]Fig. 1E-C). However, the concentration-response curve for channel activation was for almost all mutants shifted by about 0.5 units to more acidic values compared to the WT channels ([1]Fig. 1E). Moreover, we observed a decreased cooperativity during channel activation in acidic pocket mutants containing more than seven neutralizing mutations (nH equal to ~1.5 in these mutants, compared to ~3 in the WT) ([1]Fig. 1E). In contrast, the pH dependence of SSD was shifted to more alkaline values and the nH was for most of the mutants similar to that of WT channels ([1]Fig. 1F). What is the significance of a diminished proton sensitivity in the acidic pocket? Neutralization mutations of all Asp and Glu within the acidic pocket mimic a protonated state. This situation would correspond to a gain of function of the channel, since it implies a lower proton concentration to activate the channel. As a consequence, we would expect a shift of the pH dependence of activation of a given mutant to more alkaline values, as observed in other proton-gated channels (Posson et al., 2013). However, we found that neutralizing mutations within the acidic pocket increased the proton concentration required to activate the channels. For a better interpretation of our results, we built a kinetic model that could explain how these

mutations altered in an unexpected way the pH dependence of activation of these mutants. Our kinetic model identified the contribution of three different protonation sites: 1) sites in the acidic pocket, 2) sites leading to channel activation and 3) sites leading to channel desensitization. The model was fitted to activation and SSD curves and to experimental traces. From these data, the modeling suggested that a decrease of the pH dependence of activation, together with a decrease of nH, was expected if protonation in the acidic pocket was considered as non-essential for channel activation and contributing with a negative cooperativity to open the channel. Based on our data, we concluded, thus, that acidic residues in the acidic pocket have an inhibitory role in channel activation and they are not essential proton sensors.

Residues in the acidic pocket have been investigated in previous studies. Due to the presence of several carboxyl groups, Jasti and colleagues proposed the acidic pocket as "the" ASIC proton-binding site (Jasti et al., 2007). However, channels bearing neutralizing mutations of Asp347 and Asp351 in this region showed an acidic shift of the concentration-response curve, but retained proton sensitivity, suggesting that additional residues contribute to proton sensing. Liechti and colleagues identified in this region one acidic residue as potential pH sensor, Asp347 (Liechti et al., 2010). This residue has been extensively investigated in our VCF experiments (see below).

In another study, Krauson and coworkers have shown that two mutants in the acidic pocket, E238C and D347C, reduced proton apparent affinity after chemical modification by MTSET, without, however, suppressing channel function, indicating that neither of these sites is indispensable for proton gating (Krauson et al., 2013).

Other studies have found that nonconservative mutations in the acidic pocket dramatically lowered the apparent proton affinity, suggesting that probably these mutations introduce structural changes in this site that may have effects that are independent of H^+ sensing (Li et al.,

2009; Ramaswamy et al., 2013). Taken together, these studies indicate that protonation events in the acidic pocket are not essential for ASIC function, but contribute to channel activation. Interestingly, several mutagenesis and functional studies have identified many pH sensors in different ASIC domains. Liechti *et al.* combined computational and functional approaches to examine the contribution of acidic residues to ASIC proton sensing based on their predicted pK_a values in the desensitized cASIC1a structure. Their analysis identified several residues in the palm, thumb and β-ball domains that contribute to proton gating, suggesting that multiple binding sites are necessary for activation (Liechti et al., 2010).

ASIC pH sensors have also been found in the lower palm. Functional studies employed the cysteine accessibility method and site-directed mutagenesis to examine the mechanism of activation of ASIC1a by extracellular protons. The authors have shown that non-titratable substitutions at positions Glu79 and Glu418 resulted in channels with reduced proton affinity for activation, suggesting that they might be involved in the channel opening (Krauson et al., 2013; Liechti et al., 2010). Other mutagenesis studies have identified other pH sensors in the wrist and TM domain (see paragraph *4.2.2*). All these studies support the notion that ASIC gating does not depend on the protonation/deprotonation of few residues, but, rather, protonation of multiple residues in different ASIC domains contributes to pH-dependent gating.

4.1.2 Protonation events in the palm domain are required for normal desensitization

The palm domain has a central role in channel gating. From a structural view, conformational changes in this region participate in all ASIC functional transitions (Cushman et al., 2007; Roy et al., 2013; Yoder et al., 2018). Consistent with this structural evidence, experimental studies have shown that mutations in this domain significantly affected the kinetics and the extent of desensitization (Coric et al., 2003; Cushman et al., 2007; Roy et al., 2013).

To determine the contribution of the palm domain to ASIC1a proton sensing, we combined neutralizing mutations of six acidic residues located in this region and two nearby residues in the β-ball domain. All acidic residues investigated in this work are conserved in almost every ASIC that produces a proton-induced current, but not in other acid-insensitive ENaC/DEG family members (Jasti et al., 2007), suggesting that they might be involved in channel activation. To our surprise, conservative mutations of acidic residues in the palm did not alter channel activation, but had, rather, a profound effect on channel desensitization, manifested as the appearance of a sustained current component for mutants containing up to four neutralizing mutations, and as complete disappearance of the transient component for mutants with more than four mutations. What is the origin of the complete loss of ASIC peak current and the appearance of a sustained current component? We hypothesized that the disappearance of the transient ASIC component was not due a loss of channel activation, but, rather, to a fast transition from the open to the desensitized state. To test this hypothesis, the acid-induced ASIC current of the mutated channels was measured at lower temperature (~12°C). Indeed, it is known that, in contrast to activation, ASIC desensitization strongly depends on temperature. Channel exposure to cold temperature potentiates current amplitude by slowing the desensitization rate (Askwith et al., 2001). When mutated channels in the palm domain were stimulated by an acidic pH at low temperature, we observed an increased current amplitude and, most important, the appearance of a transient ASIC current component ([1]Fig. 2D), confirming that residues in this region are importantly involved in the transduction mechanism that allows the transition from the open to the desensitized state.

Interestingly, we observed that the sustained current of the combined mutants in the palm showed distinct properties compared to the transient current, such as reduced proton sensitivity (the pH dependence of activation was shifted to more acidic values, [1]Fig. 2E), partial loss of Na^+/K^+ selectivity ([1]Fig. S2D-G) and loss of inhibition by the pore blocker amiloride ([1]Fig.

S2H). The origin of this different type of opening is unclear; probably, the introduction of uncharged amino acids within this region alters some electrostatic interactions between channel subunits, resulting in different conformational changes that may increase the diameter of the pore. This different type of opening is reminiscent of the sustained opening induced by PcTx1 in complex with cASIC1a at pH 7.25 (see paragraph *1.2.2*).

In summary, our data strongly suggest that, in order to occur, normal channel desensitization requires protonation events of multiple acidic residues in the palm domain, and that disruption or alterations of potential intra and/or intersubunit interactions may allow a new type of opening, generating a current whose gating properties are profoundly different from the transient ASIC current. The importance of the palm domain in channel desensitization has also been investigated in several other studies; many of them are discussed in the paragraph *1.2.3*.

4.2 Investigation of ASIC1a conformational changes using voltage-clamp fluorometry

4.2.1 Quenching events underlie some of the fluorescence changes and uncover conformational changes in different ASIC domains

The acidic pocket is an important regulatory site of ASIC1a. Its importance is highlighted by the fact that it constitutes the binding site of a potent animal toxin, PcTx1, that modulates the channel. A better understanding of the structural rearrangements in this region would provide, thus, important insights on the molecular mechanisms controlling ASIC activity. This part of the study aims at investigating the conformational changes in this region and their correlation with specific channel transitions.

We found that single cysteine mutants labelled with a thiol-reactive fluorophore showed small or no detectable fluorescence changes upon acidic stimulation. In order to detect changes in

fluorescence, we generated Cysteine-Tryptophan (Cys-Trp) pairs, with the engineered Cys used as docking site for the fluorophore and the Trp as a quencher of the fluorescence. As expected, we observed that the proximity of a Trp residue to a fluorescent probe generated ΔF signals. Since the fluorescence signal of single Cys residues belonging to these pairs was of very small amplitude and no fluorescence change was detected from labeled oocytes expressing hASIC1a WT (Bonifacio et al., 2014), we concluded that the observed change in fluorescence emission was generated by changes in distance between the fluorophore and the engineered Trp. We extensively used this approach to elucidate the structural rearrangement occurring in this region. This analysis of the different ΔF signals has shown that the acidic pocket undergoes structural rearrangements that bring the outer end of the $\alpha 5$ helix of the thumb close to the $\alpha 1$ helix of the finger domain (negative ΔF signals in K343C/N120W and K343C/T236W), while the inner part moves away from the β-ball domain (positive ΔF signals in D351C/F257W) ([1]Fig. 4A-C) (Vullo et al., 2017). Comparison of the kinetics of current and fluorescence signals in terms of rise time indicated that these movements occur during channel desensitization or prepare this transition ([1]Fig. 3E-H). A movement of the inner end of the $\alpha 5$ helix of the thumb domain was also shown in a functional study where the formation of a disulfide bond between the residues E355C in the thumb domain and R175C in the palm domain arrested the channel in a closed state. In agreement with our study, measurements with the luminescence resonance energy transfer (LRET) technique showed a decreased distance between thumb and finger domains in the desensitized compared to closed state. This technique does not provide, however, any information about the kinetics of the movements, but it provides, rather, the changes in distance between the fluorophores (Ramaswamy et al., 2013).

One of the most striking features observed in our Cys-Trp pairs located in the acidic pocket was the appearance of a "biphasic" fluorescence change upon acidic stimulation, as shown for example in the double mutant D237C/D347W ([1]Fig. 4A). Comparison of the kinetics of current

and fluorescence signals in these mutants indicated that the rise time of the first small ΔF component correlated or was faster than the rise time of the current appearance ([1]Fig. 3G), suggesting that most likely these conformational changes contribute to channel opening. In contrast, the second bigger fluorescence component was slower than current activation but faster or of the same timing as the current desensitization ([1]Fig. 3H), suggesting that these movements either prepare or occur during channel desensitization. Interpretation of the slow ΔF component indicates a sequence of extended movements that displace the finger loop toward the $\alpha 1$ helix of the finger during channel desensitization ([1]Fig. 4C), while the first rapid ΔF signals suggest a tilting of the finger loop that would bring the residue Asp237, located at the lower end of the loop, close to the $\alpha 5$ helix of the thumb domain, and the residue Thr236, located higher up, farther away from the $\alpha 5$ helix ([1]Fig. 4C).

The presence of structural rearrangements in the thumb and finger domains have also been investigated in a study that applied normal mode analysis (NMA) to predict the collective dynamics underlying ASIC gating mechanism. The authors, not only reported conformational changes in these domains, but suggested also that H^+ binding enhances the interaction between the thumb and finger domains, and that this attraction constitutes the initial driving force for transmitting the extracellular domain movements to the channel gate (Yang et al., 2009).

The pH dependence of the ΔF signals in our experiments, including also the rapid ΔF components, was for all mutants more alkaline than the pH dependence of current activation and, for most mutants, close to the pH dependence of SSD ([1]Fig. 3I), a feature that was observed in a previous study. Cha and Bezanilla investigated the structural rearrangements occurring in *Shaker* K^+ channels expressed in *Xenopous* oocytes. In their study, the fluorophore tetramethylrhodamine-5-maleimide (TMRM) was attached at different transmembrane segments to report voltage-dependent changes in fluorescence emission during channel activity. Analysis of the VCF data showed a leftward shift by 15-20 mV of the fluorescence-dependent

curve compared to that of the current voltage-dependence. They observed, however, that the kinetics of the fluorescence changes correlated with the time constants of the current activation, suggesting that these movements are related to channel opening (Cha and Bezanilla, 1997).

In our study, the fact that mutants whose ΔF signals correlated with the channel opening do not share the same pH dependence of activation does not exclude the possibility that these residues are involved in channel opening. Channel opening, indeed, requires a complex sequence of movements upon pH change, which may suggest the presence of several intermediate channel states, or conformations, each of them characterized by a different pH dependence. In this scenario, we could speculate that the channel state that determines the pH dependence of the opening would correspond to the last transition, and that our conformational changes take place during an earlier channel transition whose pH dependence is defined by more alkaline values.

In summary, we have shown that the acidic pocket undergoes structural rearrangements that contribute to both activation and desensitization of the channel.

Proton binding to multiple ASIC domains induces conformational changes that are probably transmitted to the channel pore through the flexible wrist. The palm domain undergoes several conformational changes during channel activity (Yoder et al., 2018) and represents, probably, a key region for transferring gating motions to the channel gate. We initially investigated the presence of structural rearrangements in the β1-β2 linker, which connects the palm to the β-ball domain. This region undergoes marked conformational changes in the open-desensitized transition (Baconguis and Gouaux, 2012) and plays a critical role in channel function and regulation (more details on these studies are provided in the paragraph *1.2.3*).

Fluorophore-labelled oocytes expressing the mutants A81C, S83C and Q84C yielded large negative fluorescence signals after exposure to an acidic pH, suggesting that these residues undergo structural rearrangements during channel activity ([2]Fig. 1C). We found that the observed fluorescence change was mostly due to fluorescence quenching events, since single

cysteine mutants lacking the Tyr417 in the β12 strand showed a dramatically reduced ΔF amplitude after application of an acidic pH ([2]Fig. 1D). The presence of negative fluorescence signals, whose kinetics were slower than current appearance but faster than current decay, indicates that the single cysteine mutants approach the β12 strand after channel activation and before channel desensitization. In agreement with our VCF data, comparison between cASIC1a structures indicates a decreased distance between the residues in the β1-β2 linker and Tyr417 in the desensitized structure with regard to the open crystal structure (Baconguis et al., 2014; Gonzales et al., 2009).

Several functional studies indicate the presence of conformational changes in the palm domain during ASIC activity. A study conducted by Roy and coworkers investigated the role of residues located in the four strands of the lower palm domain of hASIC1a and their conformational changes during channel gating. They found that the MTSET modification rate of engineered cysteine residues pointing to the central vestibule was decreased when the chemical reagent was applied during the desensitized state, suggesting that the lower palm domains of the three subunits undergo a closing movement that stabilizes the desensitized state. Moreover, substitution of almost any residue in the lower palm affected the pH dependence of SSD and the time course of desensitization, resulting for some mutants in the appearence of a sustained current or in a completely nondesensitizing current, suggesting that residues in the palm domain stabilize the desensitized state (Roy et al., 2013). A similar study using cysteine accessibility method and site-directed mutagenesis has shown that residues Glu79 and Gu418 were better accessible by the MTSET reagent in the desensitized state compared to closed state, indicating that the palm domain assumes an expanded conformation at resting pH and resides in a contracted conformation upon extracellular acidification (Della Vecchia et al., 2013). Other studies have shown that the β1-β2 linker and β11-β12 linker interact with each other, and

highlighted the importance of these two linkers for desensitization; these studies are discussed in more detail in the paragraph *1.2.3*.

In order to get insights on the presence and the direction of conformational changes of neighbouring domains, we have added a Trp residue at various positions to double mutants lacking the Tyr417 to restore the ΔF signal. The resulting triple mutants yielded significant fluorescence changes of different types ([2]Fig. 2B). Analysis of the types and the timing of the detected fluorescence changes indicates that residues of the α5-β10 strand loop, the β-turn and the β strand 10 approach the β1-β2 linker of an adjacent subunit during and immediately after channel activation, suggesting that structural changes in these regions are likely involved in the transition from the open to desensitized state (Fig. 9). Slower movements were observed in the β5-β6 linker of the β-ball domain, bringing the residues Lys208 and Arg206 close to the β1-β2 linker, and the residue Met210 away from it (Fig. 9).
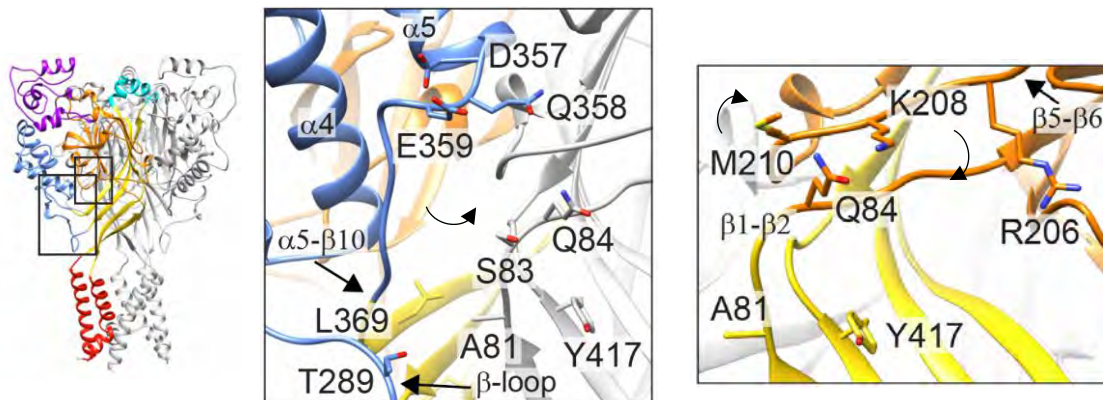
Figure 9. Close-up view of residues located in the thumb (blue), β-ball (orange) and palm (yellow) domains. Residues located in a neighbouring subunit are shown in grey (central panel).

Consistent with the presence of structural rearrangements in this region, Yoder and Gouaux have shown in an experiment that introduction of a disulfide bridge between the end of the α5 helix of the thumb and the β1-β2 linker of the palm of a neighbouring subunit keeps the channel in an expanded conformation and prevents channel opening, supporting the notion that

intersubunit interactions in this region are important to control ASIC activity (Yoder et al., 2018).

In agreement with the crystal structures, our studies show a decreased distance between the β10 strand and the β1-β2 linker of the palm domain and between the β-turn and the β1-β2 linker, occurring during channel opening. The structures show, however, small or no structural changes associated to the α5 helix-β10 loop and β5-β6 linker in the open and desensitized states (Baconguis et al., 2014; Gonzales et al., 2009). This discrepancy may be explained by the fact that the crystal structures show a cASIC1a channel open by toxins; it is possible, thus, that the toxin-bound open conformation does not correspond to the acid-opened conformation.

A certain flexibility of the β1-β2 linker and the β-turn has also been shown by applying NMA. This study provided evidence for bending and twisting motions associated to the β1-β2 linker, while the β-turn undergoes to swinging vibration. The authors suggested that these motions are important to regulate ASIC activity (Yang et al., 2009).

In summary, our results report conformational changes involved in both activation and desensitization and provide insights about the structural rearrangements occurring between different ASIC subunits.

4.2.2 Conformational changes in the wrist accompany channel opening

The wrist constitutes the structural junction between the ECD and TM domains and provides the fenestrations through which ions gain access to the pore. Conformational changes in this region may thus be of crucial importance for transferring the activation signal to the channel gate. The only VCF study investigating the structural changes in this region was conducted by Passero and colleagues. The authors reported that the loop preceding the TM2 domain undergoes structural rearrangements concomitantly with the pore opening. However, this study

was limited to the residue Glu427, leaving open the question of whether and how other residues in this region could be involved in channel gating (Passero et al., 2009).

In our study, we employed the VCF technique to detect conformational changes in the wrist and transmembrane domain. Analyses of the VCF experiments showed that six fluorophore-labelled cysteine mutants in this region exhibited conformational changes characterized by the presence of a double fluorescence change, reminiscent of that observed in some mutants in the acidic pocket and in the triple mutants of the palm domain ([2]Fig. 3B). However, in contrast to the previously observed ΔF signals, the first component of the ΔF signal of the wrist mutants was always of bigger amplitude, probably reflecting a more extended movement, compared to the second component. It is possible that the movements observed in our study might serve to stabilize the open conformation and facilitate ions entering the channel.

Analysis of the current and fluorescence kinetics of our VCF experiments indicates that residues in the wrist undergo conformational changes most likely involved in channel opening. The absence of a quencher reference within this region, however, limits the interpretation concerning the direction of the observed movements. In support of a role in channel opening, we found that half of the mutants show a pH dependence of ΔF signals close to the pH dependence of the current activation ([2]Fig. 3F).

Yang and colleagues employed NMA to predict the structural changes occurring in this region during channel activity. Interestingly, they found that conformational changes in the wrist and β-turn were associated with motions of the channel gate, suggesting that these regions are most likely involved in ASIC gating mechanisms (Yang et al., 2009). These results are, thus, in agreement with our findings.

This structural evidence is supported by functional studies investigating the contribution of several residues located in this region to ASIC proton sensing. Paukert and colleagues screened more than 40 conserved, charged amino acids in the ECD to determine a possible contribution

to ASIC H^+ gating. Surprisingly, almost none of the single neutralizing mutations strongly impaired proton activation. However, combination of neutralizing mutations of the residues His72 and His73 in the wrist produced proton-insensitive channels without affecting their surface expression, suggesting that they could be involved in ASICs proton sensing (Paukert et al., 2008). The findings of Paukert and colleagues show, therefore, that the wrist does not only transduce a signal, but can be a pH sensing region by itself. In another study, it has been shown that the aromatic interaction between Tyr71 and Trp287, located in the wrist and β-turn loop, is essential for conferring proton sensitivity to the channel, since individual mutation of both residues into non-aromatic amino acids reduces or abolishes channel proton affinity and in some cases lowers the channel expression at the cell surface, indicating that the interaction between the β-turn and the TM1 domain is important for ASIC activation (Jing et al., 2011; Li et al., 2009).

Taken together, these studies indicate that the wrist is an important component of the ASIC proton sensing machinery and plays probably a key role in communicating conformational changes to the channel gate. In this context and from these functional evidence, we might speculate that the wrist constitutes the most important pH sensor and that the other H^+ sites are involved in the regulation of the channel activity.

4.2.3 A proposed gating model

ASIC1a contains a large number of titratable residues in the extracellular region that could serve as proton binding sites; however, several works have shown that a limited number of them are functionally relevant. Different studies have identified residues whose mutation suppressed ASIC current or altered its main properties in the thumb, finger, β-ball and palm domains, but also in the wrist and TM domain (Della Vecchia et al., 2013; Li et al., 2009; Liechti et al., 2010; Lynagh et al., 2018; Paukert et al., 2008; Sherwood et al., 2009).

At present, the molecular mechanisms by which protonation controls ASIC activity remain poorly understood. Protonation events in multiple ASIC domains initiate conformational changes that are in turn transmitted to the channel gate. What conformational changes drive ASIC activity? And which domains are mostly involved in this mechanism? Crystal structures, together with functional studies using different approaches, have greatly contributed to answering these questions. The information coming from all these studies allow us to propose a possible scenario for ASICs gating mechanism (Fig. 10).

<u>Channel activation</u>: the crystal structures suggest that proton binding in several ASIC domains induces the collapse of the acidic pocket enabling the formation of carboxyl-carboxylate pairings that stabilizes the interface between thumb, finger and palm domains (Baconguis et al., 2014; Yoder et al., 2018). Our experiments have however shown that the acidic pocket is not required for channel activation but it has, rather, a modulatory role. Consistent with a role in channel activation, we detected big structural changes in the wrist associated with channel opening, in agreement with previous studies (Passero et al., 2009; Vullo et al., 2017; Yang et al., 2009).

Superposition of the closed, open and desensitized cASIC1a structures suggests a conserved structural scaffold defined by the upper palm and knuckle domains, which adopt the same conformation among the different channel transitions. Experiments with fluorophore-quencher pairing and voltage-clamp fluorometry have shown, however, structural changes associated to ASIC upper domains during channel activity, consisting in an outward movement of the finger and knuckle domains from the β-ball domain (Bonifacio et al., 2014; Gwiazda et al., 2015b).

<u>Channel desensitization</u>: among ASIC domains, the palm has definitely a central role in the mechanism of desensitization. Functional studies have shown that transition to this functional state involves substantial rearrangements culminating in a closing movement of the palm domains toward the central axis (Krauson et al., 2013; Roy et al., 2013). Structural evidence

suggest that transition from open to desensitized conformation involves a swap in sidechain orientation of the Leu415 and Asn416 (Yoder et al., 2018); it was hypothesized that these movements underlie the mechanism of channel desensitization by serving as a molecular clutch that decouples the collapsed acidic pocket from the lower palm and allows the transmembrane domains to relax back, restoring a non-conducting channel pore (Yoder et al., 2018). VCF and LRET measurements reported conformational changes in the acidic pocket related with channel desensitization, consisting in the thumb α5 helix approaching the finger and moving away from the β-ball domain (Fig. 10) (Ramaswamy et al., 2013; Vullo et al., 2017)

-Resting state: at physiological pH values most acidic amino acids are in the deprotonated state. The ASIC structure in the resting state shows that, due to the electrostatic repulsion of negatively charged residues, the thumb is located away from the β-ball and finger domains, resulting in an expanded conformation of the acidic pocket, whereas the TM domains assume a constricted conformation that shuts the gate preventing passage of the ions (Yoder et al., 2018).
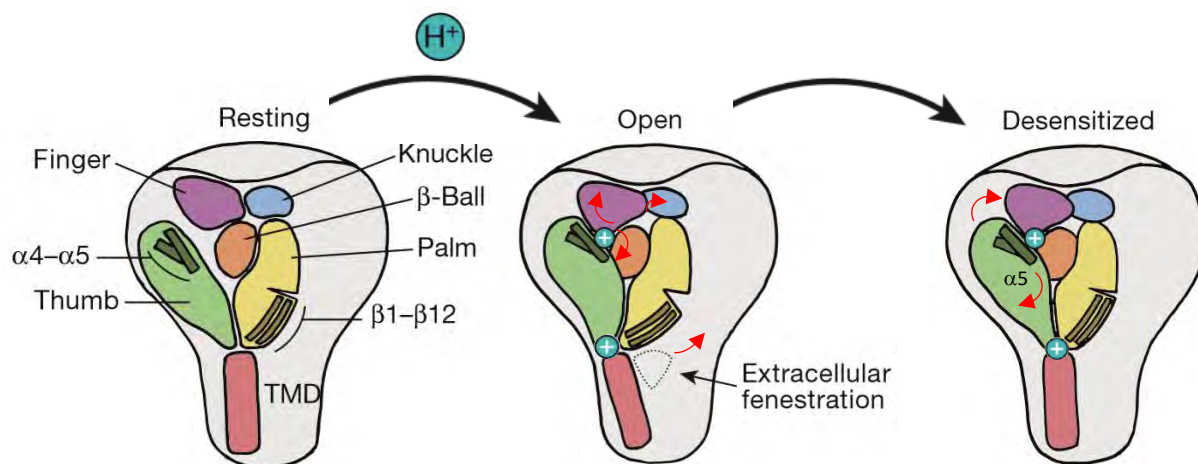
Figure 10. Hypothesized conformational changes during ASIC1a gating. Red arrows indicate evidence from VCF, NMA and LRET studies. (Adapted from (Yoder et al., 2018)).

5. Perspectives

Despite the large amount of information concerning the structural and molecular aspects of ASIC channels, there is still a considerable gap in understanding how protonation events lead to channel opening. At present, it seems that ASIC activity depends on protonation of multiple residues and that conformational changes in different domains are necessary to control channel activity. My work has provided new important insights with regard to both structural and functional aspects that govern channel function; however, it has not provided a clear picture of the mechanisms that control ASIC transitions. Future works go, therefore, in this direction, focusing on the two following steps:

-Identification of proton sensor residues involved in ASIC activation.

Constant pH molecular dynamics simulations will be carried out to identify candidate pH sensors relevant for ASIC activation. This analysis will be restricted to residues located in the lower palm and transmembrane domains that are expected to have a pKa between 7.4 and 6, a pH range in which these residues will likely change their protonation status. The role of these potential candidates will be then investigated in functional experiments.

-Investigation of conformational changes that drive ASIC activation and desensitization

The VCF technique has proven to be a very useful technique to report conformational changes during channel activity. Unfortunately, however, the large size of current fluorophores and their low membrane permeability, may lead to an uncertainty of the interpretation of the observed fluorescence changes, and limit the investigation of conformational changes to the extracellular part of the channel. A promising approach to overcome this limitation could be the use of fluorescent unnatural amino acids (fUAAs) (Pless and Ahern, 2013), which can be incorporated anywhere within the protein, providing insights about conformational changes associated with TM or intracellular domain. In addition, they are smaller than fluorophores traditionally used in VCF; the channel is thus less perturbed and the interpretation of conformational changes is

more reliable. This approach has already been successfully used in several studies (Kalstrup and Blunck, 2013; Wulf and Pless, 2018).

6. References

Adams, C.M., Anderson, M.G., Motto, D.G., Price, M.P., Johnson, W.A., and Welsh, M.J. (1998). Ripped Pocket and Pickpocket, Novel Drosophila Deg/Enac Subunits Expressed in Early Development and in Mechanosensory Neurons. Journal of Cell Biology *140*, 143-152.

Akopian, A.N., Chen, C.C., Ding, Y.N., Cesare, P., and Wood, J.N. (2000). A new member of the acid-sensing ion channel family. Neuroreport *11*, 2217-2222.

Alijevic, O., and Kellenberger, S. (2012). Subtype-specific modulation of acid-sensing ion channel (ASIC) function by 2-guanidine-4-methylquinazoline. The Journal of biological chemistry *287*, 36059-36070.

Askwith, C.C., Benson, C.J., Welsh, M.J., and Snyder, P.M. (2001). DEG/ENaC ion channels involved in sensory transduction are modulated by cold temperature. Proc Natl Acad Sci U S A *98*, 6459-6463.

Babini, E., Paukert, M., Geisler, H.S., and Grunder, S. (2002). Alternative splicing and interaction with di- and polyvalent cations control the dynamic range of acid-sensing ion channel 1 (ASIC1). J Biol Chem *277*, 41597-41603.

Baconguis, I., Bohlen, C.J., Goehring, A., Julius, D., and Gouaux, E. (2014). X-ray structure of Acid-sensing ion channel 1-snake toxin complex reveals open state of a Na^+-selective channel. Cell *156*, 717-729.

Baconguis, I., and Gouaux, E. (2012). Structural plasticity and dynamic selectivity of acid-sensing ion channel-spider toxin complexes. Nature *489*, 400-405.

Bargeton, B., and Kellenberger, S. (2010). The contact region between three domains of the extracellular loop of ASIC1a is critical for channel function. The Journal of biological chemistry *285*, 13816-13826.

Baron, A., Schaefer, L., Lingueglia, E., Champigny, G., and Lazdunski, M. (2001). Zn^{2+} and H^+ are coactivators of acid-sensing ion channels. J Biol Chem *276*, 35361-35367.

Bartoi, T., Augustinowski, K., Polleichtner, G., Grunder, S., and Ulbrich, M.H. (2014). Acid-sensing ion channel (ASIC) 1a/2a heteromers have a flexible 2:1/1:2 stoichiometry. Proc Natl Acad Sci U S A *111*, 8281-8286.

Bassler, E.L., Ngo-Anh, T.J., Geisler, H.S., Ruppersberg, J.P., and Grunder, S. (2001). Molecular and functional characterization of acid-sensing ion channel (ASIC) 1b. J Biol Chem *276*, 33782-33787.

Blanchard, M.G., Rash, L.D., and Kellenberger, S. (2012). Inhibition of voltage-gated Na^+ currents in sensory neurones by the sea anemone toxin APETx2. Br J Pharmacol *165*, 2167-2177.

Bohlen, C.J., Chesler, A.T., Sharif-Naeini, R., Medzihradszky, K.F., Zhou, S., King, D., Sanchez, E.E., Burlingame, A.L., Basbaum, A.I., and Julius, D. (2011). A heteromeric Texas coral snake toxin targets acid-sensing ion channels to produce pain. Nature *479*, 410-414.

Bonifacio, G., Lelli, C.I., and Kellenberger, S. (2014). Protonation controls ASIC1a activity via coordinated movements in multiple domains. J Gen Physiol *143*, 105-118.

Boscardin, E., Alijevic, O., Hummler, E., Frateschi, S., and Kellenberger, S. (2016). The function and regulation of acid-sensing ion channels (ASICs) and the epithelial Na(+) channel (ENaC): IUPHAR Review 19. Br J Pharmacol *173*, 2671-2701.

Canessa, C.M., Horisberger, J.-D., and Rossier, B.C. (1993). Epithelial sodium channel related to proteins involved in neurodegeneration. Nature *361*, 467-470.

Canessa, C.M., Schild, L., Buell, G., Thorens, B., Gautschi, I., Horisberger, J.-D., and Rossier, B.C. (1994). Amiloride-sensitive epithelial Na^+ channel is made of three homologous subunits. Nature *367*, 463-467.

Caterina, M.J., Leffler, A., Malmberg, A.B., Martin, W.J., Trafton, J., Petersen-Zeitz, K.R., Koltzenburg, M., Basbaum, A.I., and Julius, D. (2000). Impaired nociception and pain sensation in mice lacking the capsaicin receptor. Science *288*, 306-313.

Cha, A., and Bezanilla, F. (1997). Characterizing voltage-dependent conformational changes in the shaker K^+ channel with fluorescence. Neuron *19*, 1127-1140.

Chalfie, M., and Wolinsky, E. (1990a). The identification and supression of inherited neurodegeneration in Caenorhabditis elegans. Nature *345*, 410-416.

Chalfie, M., and Wolinsky, E. (1990b). The identification and supression of inherited neurodegeneration in Caenorhabditis elegans Nature *345*, 410-416.

Chang, S.S., Grunder, S., Hanukoglu, A., Rosler, A., Mathew, P.M., Hanukoglu, I., Schild, L., Lu, Y., Shimkets, R.A., Nelson-Williams, C*., et al.* (1996). Mutations in subunits of the epithelial sodium channel cause salt wasting with hyperkalaemic acidosis, pseudohypoaldosteronism type 1. Nat Genet *12*, 248-253.

Chatterjee, A., Guo, J., Lee, H.S., and Schultz, P.G. (2013). A genetically encoded fluorescent probe in mammalian cells. J Am Chem Soc *135*, 12540-12543.

Chen, X., and Grunder, S. (2007). Permeating protons contribute to tachyphylaxis of the acid-sensing ion channel (ASIC) 1a. J Physiol *579*, 657-670.

Chen, X., Kalbacher, H., and Grunder, S. (2005). The Tarantula Toxin Psalmotoxin 1 Inhibits Acid-sensing Ion Channel (ASIC) 1a by Increasing Its Apparent H^+ Affinity. J Gen Physiol *126*, 71-79.

Chen, X., Kalbacher, H., and Grunder, S. (2006). Interaction of acid-sensing ion channel (ASIC) 1 with the tarantula toxin psalmotoxin 1 is state dependent. J Gen Physiol *127*, 267-276.

Chen, X., Polleichtner, G., Kadurin, I., and Grunder, S. (2007). Zebrafish acid-sensing ion channel (ASIC) 4, characterization of homo- and heteromeric channels, and identification of regions important for activation by H+. The Journal of biological chemistry *282*, 30406-30413.

Choi, D.W. (1988). Glutamate neurotoxicity and diseases of the nervous system. Neuron *1*, 623-634.

Chu, X.P., Papasian, C.J., Wang, J.Q., and Xiong, Z.G. (2011). Modulation of acid-sensing ion channels: molecular mechanisms and therapeutic potential. Int J Physiol Pathophysiol Pharmacol *3*, 288-309.

Chu, X.P., Wemmie, J.A., Wang, W.Z., Zhu, X.M., Saugstad, J.A., Price, M.P., Simon, R.P., and Xiong, Z.G. (2004). Subunit-dependent high-affinity zinc inhibition of acid-sensing ion channels. J Neurosci *24*, 8678-8689.

Collier, D.M., and Snyder, P.M. (2009). Extracellular chloride regulates the epithelial sodium channel. The Journal of biological chemistry *284*, 29320-29325.

Coric, T., Passamaneck, Y.J., Zhang, P., Di Gregorio, A., and Canessa, C.M. (2008). Simple chordates exhibit a proton-independent function of acid-sensing ion channels. FASEB J *22*, 1914-1923.

Coric, T., Zhang, P., Todorovic, N., and Canessa, C.M. (2003). The extracellular domain determines the kinetics of desensitization in acid-sensitive ion channel 1. J Biol Chem *278*, 45240-45247.

Coryell, M.W., Wunsch, A.M., Haenfler, J.M., Allen, J.E., Schnizler, M., Ziemann, A.E., Cook, M.N., Dunning, J.P., Price, M.P., Rainier, J.D*., et al.* (2009). Acid-sensing ion channel-1a in the amygdala, a novel therapeutic target in depression-related behavior. J Neurosci *29*, 5381-5388.

Coryell, M.W., Ziemann, A.E., Westmoreland, P.J., Haenfler, J.M., Kurjakovic, Z., Zha, X.M., Price, M., Schnizler, M.K., and Wemmie, J.A. (2007). Targeting ASIC1a reduces innate fear and alters neuronal activity in the fear circuit. Biological psychiatry *62*, 1140-1148.

Coscoy, S., de Weille, J.R., Lingueglia, E., and Lazdunski, M. (1999). The pre-transmembrane 1 domain of acid-sensing ion channels participates in the ion pore. J Biol Chem *274*, 10129-10132.

Cushman, K.A., Marsh-Haffner, J., Adelman, J.P., and McCleskey, E.W. (2007). A conformation change in the extracellular domain that accompanies desensitization of acid-sensing ion channel (ASIC) 3. J Gen Physiol *129*, 345-350.

Dawson, R.J., Benz, J., Stohler, P., Tetaz, T., Joseph, C., Huber, S., Schmid, G., Hugin, D., Pflimlin, P., Trube, G*., et al.* (2012). Structure of the Acid-sensing ion channel 1 in complex with the gating modifier Psalmotoxin 1. Nat commun *3*, 936.

de la Rosa, D.A., Krueger, S.R., Kolar, A., Shao, D., Fitzsimonds, R.M., and Canessa, C.M. (2003). Distribution, subcellular localization and ontogeny of ASIC1 in the mammalian central nervous system. J Physiol *546*, 77-87.

Delaunay, A., Gasull, X., Salinas, M., Noel, J., Friend, V., Lingueglia, E., and Deval, E. (2012). Human ASIC3 channel dynamically adapts its activity to sense the extracellular pH in both acidic and alkaline directions. Proc Natl Acad Sci U S A *109*, 13124-13129.

Della Vecchia, M.C., Rued, A.C., and Carattino, M.D. (2013). Gating transitions in the palm domain of ASIC1a. The Journal of biological chemistry *288*, 5487-5495.

Deval, E., Baron, A., Lingueglia, E., Mazarguil, H., Zajac, J.M., and Lazdunski, M. (2003). Effects of neuropeptide SF and related peptides on acid sensing ion channel 3 and sensory neuron excitability. Neuropharmacol *44*, 662-671.

Deval, E., Salinas, M., Baron, A., Lingueglia, E., and Lazdunski, M. (2004). ASIC2b-dependent regulation of ASIC3, an essential acid-sensing ion channel subunit in sensory neurons via the partner protein PICK-1. The Journal of biological chemistry *279*, 19531-19539.

Diochot, S., Baron, A., Rash, L.D., Deval, E., Escoubas, P., Scarzello, S., Salinas, M., and Lazdunski, M. (2004). A new sea anemone peptide, APETx2, inhibits ASIC3, a major acid-sensitive channel in sensory neurons. EMBO J *23*, 1516-1525.

Diochot, S., Baron, A., Salinas, M., Douguet, D., Scarzello, S., Dabert-Gay, A.S., Debayle, D., Friend, V., Alloui, A., Lazdunski, M*., et al.* (2012). Black mamba venom peptides target acid-sensing ion channels to abolish pain. Nature *490*, 552-555.

Donier, E., Rugiero, F., Jacob, C., and Wood, J.N. (2008). Regulation of ASIC activity by ASIC4--new insights into ASIC channel function revealed by a yeast two-hybrid assay. Eur J Neurosci *28*, 74-86.

Du, J., Reznikov, L.R., Price, M.P., Zha, X.-M., Lu, Y., Moninger, T.O., Wemmie, J.A., and Welsh, M.J. (2014). Protons are a neurotransmitter that regulates synaptic plasticity in the lateral amygdala. Proceedings of the National Academy of Sciences of the United States of America.

Duan, B., Wu, L.J., Yu, Y.Q., Ding, Y., Jing, L., Xu, L., Chen, J., and Xu, T.L. (2007). Upregulation of acid-sensing ion channel ASIC1a in spinal dorsal horn neurons contributes to inflammatory pain hypersensitivity. J Neurosci *27*, 11139-11148.

Duvarci, S., and Pare, D. (2014). Amygdala microcircuits controlling learned fear. Neuron *82*, 966-980.

Eastwood, A.L., and Goodman, M.B. (2012). Insight into DEG/ENaC channel gating from genetics and structure. Physiology (Bethesda) *27*, 282-290.

Er, S.Y., Cristofori-Armstrong, B., Escoubas, P., and Rash, L.D. (2017). Discovery and molecular interaction studies of a highly stable, tarantula peptide modulator of acid-sensing ion channel 1. Neuropharmacology *127*, 185-195.

Escoubas, P., DeWeille, J.R., Lecoq, A., Diochot, S., Waldmann, R., Champigny, G., Moinier, D., Ménez, A., and Lazdunski, M. (2000). Isolation of a tarantula toxin specific for a class of proton-gated Na$^+$ channels. J Biol Chem *275*, 25116-25121.

Feldman, D.H., Horiuchi, M., Keachie, K., McCauley, E., Bannerman, P., Itoh, A., Itoh, T., and Pleasure, D. (2008). Characterization of acid-sensing ion channel expression in oligodendrocyte-lineage cells. Glia *56*, 1238-1249.

Gandhi, C.S., and Olcese, R. (2008). The voltage-clamp fluorometry technique. Methods Mol Biol *491*, 213-231.

Garcia-Anoveros, J., Derfler, B., Nevillegolden, J., Hyman, B.T., and Corey, D.P. (1997). BNaC1 and BNaC2 constitute at new family of human neuronal sodium channels related to degenerins and epithelial sodium channels. Proc Natl Acad Sci USA *94*, 1459-1464.

Garty, H., and Palmer, L.G. (1997). Epithelial sodium channels: function, structure, and regulation. Physiol Rev *77*, 359-396.

Gonzales, E.B., Kawate, T., and Gouaux, E. (2009). Pore architecture and ion sites in acid-sensing ion channels and P2X receptors. Nature *460*, 599-604.

Gründer, S., Geissler, H.-S., Bässler, E.-L., and Ruppersberg, J.P. (2000). A new member of acid-sensing ion channels from pituitary gland. Neuroreport *11*, 1607-1611.

Gwiazda, K., Bonifacio, G., Vullo, S., and Kellenberger, S. (2015a). Extracellular Subunit Interactions Control Transitions between Functional States of Acid-sensing Ion Channel 1a. J Biol Chem *290*, 17956-17966.

Gwiazda, K., Bonifacio, G., Vullo, S., and Kellenberger, S. (2015b). Extracellular Subunit Interactions Control Transitions Between Functional States of Acid-sensing Ion Channel 1a. The Journal of biological chemistry.

Hansson, J.H., Nelson-Williams, C., Suzuki, H., Schild, L., Shimkets, R., Lu, Y., Canessa, C., Iwasaki, T., Rossier, B., and Lifton, R.P. (1995). Hypertension caused by a truncated epithelial sodium channel gamma subunit: Genetic heterogeneity of Liddle syndrome. Nature Genet *11*, 76-82.

Harding, A.M., Kusama, N., Hattori, T., Gautam, M., and Benson, C.J. (2014). ASIC2 subunits facilitate expression at the cell surface and confer regulation by PSD-95. PloS one *9*, e93797.

Hille, B. (2001). Ion channels of excitable membranes, 3rd edn (Sunderland: Sinauer Associates).

Hong, K., Mano, I., and Driscoll, M. (2000). In vivo structure-function analyses of *Caenorhabditis elegans* MEC-4, a candidate mechanosensory ion channel subunit. J Neurosci *20*, 2575-2588.

Hu, Y.L., Mi, X., Huang, C., Wang, H.F., Song, J.R., Shu, Q., Ni, L., Chen, J.G., Wang, F., and Hu, Z.L. (2017). Multiple H(+) sensors mediate the extracellular acidification-induced [Ca(2+)]i elevation in cultured rat ventricular cardiomyocytes. Scientific reports *7*, 44951.

Immke, D.C., and McCleskey, E.W. (2001). Lactate enhances the acid-sensing Na^+ channel on ischemia-sensing neurons. Nat Neurosci *4*, 869-870.

Immke, D.C., and McCleskey, E.W. (2003). Protons open acid-sensing ion channels by catalyzing relief of Ca^{2+} blockade. Neuron *37*, 75-84.

Inoue, J., Iwaoka, T., Tokunaga, H., Takamune, K., Naomi, S., Araki, M., Takahama, K., Yamaguchi, K., and Tomita, K. (1998). A family with Liddles-syndrome caused by a new missense mutation in the β subunit of the epithelial sodium channel. J Clin Endocrinol Metabol *83*, 2210-2213.

Jahr, H., van Driel, M., van Osch, G.J., Weinans, H., and van Leeuwen, J.P. (2005). Identification of acid-sensing ion channels in bone. Biochem Biophys Res Commun *337*, 349-354.

Jasti, J., Furukawa, H., Gonzales, E.B., and Gouaux, E. (2007). Structure of acid-sensing ion channel 1 at 1.9 A resolution and low pH. Nature *449*, 316-323.

Jiang, N., Wu, J., Leng, T., Yang, T., Zhou, Y., Jiang, Q., Wang, B., Hu, Y., Ji, Y.H., Simon, R.P.*, et al.* (2016). Region specific contribution of ASIC2 to acidosis-and ischemia-induced

neuronal injury. Journal of cerebral blood flow and metabolism : official journal of the International Society of Cerebral Blood Flow and Metabolism.

Jing, L., Jiang, Y.Q., Jiang, Q., Wang, B., Chu, X.P., and Zha, X.M. (2011). The interaction between the first transmembrane domain and the thumb of ASIC1a is critical for its N-glycosylation and trafficking. PLoS One *6*, e26909.

Kalstrup, T., and Blunck, R. (2013). Dynamics of internal pore opening in K(V) channels probed by a fluorescent unnatural amino acid. Proc Natl Acad Sci U S A *110*, 8272-8277.

Kellenberger, S., Gautschi, I., and Schild, L. (1999). A single point mutation in the pore region of the epithelial Na$^+$ channel changes ion selectivity by modifying molecular sieving. Proc Natl Acad Sci U S A *96*, 4170-4175.

Kellenberger, S., and Schild, L. (2002). Epithelial sodium channel/degenerin family of ion channels: A variety of functions for a shared structure. Physiol Rev *82*, 735-767.

Kellenberger, S., and Schild, L. (2015). International Union of Basic and Clinical Pharmacology. XCI. Structure, Function, and Pharmacology of Acid-Sensing Ion Channels and the Epithelial Na$^+$ Channel. Pharmacological reviews *67*, 1-35.

Kennedy, M.B. (1995). Origin of PDZ (DHR, GLGF) domains. Trends in biochemical sciences *20*, 350.

Krauson, A.J., and Carattino, M.D. (2016). The Thumb Domain Mediates Acid-sensing Ion Channel Desensitization. The Journal of biological chemistry *291*, 11407-11419.

Krauson, A.J., Rued, A.C., and Carattino, M.D. (2013). Independent contribution of extracellular proton binding sites to ASIC1a activation. The Journal of biological chemistry *288*, 34375-34383.

Kreple, C.J., Lu, Y., Taugher, R.J., Schwager-Gutman, A.L., Du, J., Stump, M., Wang, Y., Ghobbeh, A., Fan, R., Cosme, C.V.*, et al.* (2014). Acid-sensing ion channels contribute to synaptic transmission and inhibit cocaine-evoked plasticity. Nat Neurosci.

Krishtal, O.A., and Pidoplichko, V.I. (1980). A receptor for protons in the nerve cell membrane. Neuroscience *5*, 2325-2327.

Kusama, N., Gautam, M., Harding, A.M., Snyder, P.M., and Benson, C.J. (2013). Acid-sensing ion channels (ASICs) are differentially modulated by anions dependent on their subunit composition. Am J Physiol Cell Physiol *304*, C89-101.

Kusama, N., Harding, A.M., and Benson, C.J. (2010). Extracellular chloride modulates the desensitization kinetics of acid-sensing ion channel 1a (ASIC1a). The Journal of biological chemistry *285*, 17425-17431.

Li, T., Yang, Y., and Canessa, C.M. (2009). Interaction of the aromatics Tyr-72/Trp-288 in the interface of the extracellular and transmembrane domains is essential for proton gating of acid-sensing ion channels. J Biol Chem *284*, 4689-4694.

Li, T., Yang, Y., and Canessa, C.M. (2010a). Asn415 in the beta11-beta12 linker decreases proton-dependent desensitization of ASIC1. The Journal of biological chemistry *285*, 31285-31291.

Li, T., Yang, Y., and Canessa, C.M. (2010b). Leu85 in the beta1-beta2 linker of ASIC1 slows activation and decreases the apparent proton affinity by stabilizing a closed conformation. The Journal of biological chemistry *285*, 22706-22712.

Li, T., Yang, Y., and Canessa, C.M. (2010c). Two residues in the extracellular domain convert a nonfunctional ASIC1 into a proton-activated channel. Am J Physiol Cell Physiol *299*, C66-73.

Li, T., Yang, Y., and Canessa, C.M. (2011). Outlines of the pore in open and closed conformations describe the gating mechanism of ASIC1. Nat commun *2*, 399.

Liechti, L.A., Berneche, S., Bargeton, B., Iwaszkiewicz, J., Roy, S., Michielin, O., and Kellenberger, S. (2010). A combined computational and functional approach identifies new

residues involved in pH-dependent gating of ASIC1a. The Journal of biological chemistry *285*, 16315-16329.

Lin, S.-H., Chien, Y.-C., Chiang, W.-W., Liu, Y.-Z., Lien, C.-C., and Chen, C.-C. (2015). Genetic mapping of ASIC4 and contrasting phenotype to ASIC1a in modulating innate fear and anxiety. Eur J Neurosci *41*, 1553-1568.

Lingueglia, E., Champigny, G., Lazdunski, M., and Barbry, P. (1995). Cloning of the amiloride-sensitive FMRFamide peptide-gated sodium channel. Nature *378*, 730-733.

Lingueglia, E., de Weille, J.R., Bassilana, F., Heurteaux, C., Sakai, H., Waldmann, R., and Lazdunski, M. (1997). A modulatory subunit of acid sensing ion channels in brain and dorsal root ganglion cells. J Biol Chem *272*, 29778-29783.

Lingueglia, E., Voilley, N., Waldmann, R., Lazdunski, M., and Barbry, P. (1993). Expression cloning of an epithelial amiloride-sensitive Na^+ channel. FEBS Lett *318*, 95-99.

Liu, M.G., Li, H.S., Li, W.G., Wu, Y.J., Deng, S.N., Huang, C., Maximyuk, O., Sukach, V., Krishtal, O., Zhu, M.X.*, et al.* (2016). Acid-sensing ion channel 1a contributes to hippocampal LTP inducibility through multiple mechanisms. Scientific reports *6*, 23350.

Lorinczi, E., Bhargava, Y., Marino, S.F., Taly, A., Kaczmarek-Hajek, K., Barrantes-Freer, A., Dutertre, S., Grutter, T., Rettinger, J., and Nicke, A. (2012). Involvement of the cysteine-rich head domain in activation and desensitization of the P2X1 receptor. Proc Natl Acad Sci U S A *109*, 11396-11401.

Lynagh, T., Flood, E., Boiteux, C., Wulf, M., Komnatnyy, V.V., Colding, J.M., Allen, T.W., and Pless, S.A. (2017a). A selectivity filter at the intracellular end of the acid-sensing ion channel pore. eLife *6*.

Lynagh, T., Mikhaleva, Y., Colding, J.M., Glover, J.C., and Pless, S.A. (2018). Acid-sensing ion channels emerged over 600 Mya and are conserved throughout the deuterostomes. Proc Natl Acad Sci U S A *115*, 8430-8435.

Lynagh, T., Romero-Rojo, J.L., Lund, C., and Pless, S.A. (2017b). Molecular Basis for Allosteric Inhibition of Acid-Sensing Ion Channel 1a by Ibuprofen. J Med Chem *60*, 8192-8200.

Mannuzzu, L.M., Moronne, M.M., and Isacoff, E.Y. (1996). Direct physical measure of conformational rearrangement underlying potassium channel gating. Science *271*, 213-216.

Mansoor, S.E., Dewitt, M.A., and Farrens, D.L. (2010). Distance mapping in proteins using fluorescence spectroscopy: the tryptophan-induced quenching (TrIQ) method. Biochemistry *49*, 9722-9731.

Mazzuca, M., Heurteaux, C., Alloui, A., Diochot, S., Baron, A., Voilley, N., Blondeau, N., Escoubas, P., Gelot, A., Cupo, A.*, et al.* (2007). A tarantula peptide against pain via ASIC1a channels and opioid mechanisms. Nat Neurosci *10*, 943-945.

Nemecz, A., Prevost, M.S., Menny, A., and Corringer, P.J. (2016). Emerging Molecular Mechanisms of Signal Transduction in Pentameric Ligand-Gated Ion Channels. Neuron *90*, 452-470.

Pantazis, A., and Olcese, R. (2012). Relative transmembrane segment rearrangements during BK channel activation resolved by structurally assigned fluorophore-quencher pairing. J Gen Physiol *140*, 207-218.

Passero, C.J., Okumura, S., and Carattino, M.D. (2009). Conformational changes associated with proton-dependent gating of ASIC1a. J Biol Chem *284*, 36473-36481.

Paukert, M., Babini, E., Pusch, M., and Grunder, S. (2004). Identification of the Ca^{2+} blocking site of acid-sensing ion channel (ASIC) 1: implications for channel gating. J Gen Physiol *124*, 383-394.

Paukert, M., Chen, X., Polleichtner, G., Schindelin, H., and Grunder, S. (2008). Candidate amino acids involved in H^+ gating of acid-sensing ion channel 1a. J Biol Chem *283*, 572-581.

Peigneur, S., Beress, L., Moller, C., Mari, F., Forssmann, W.G., and Tytgat, J. (2012). A natural point mutation changes both target selectivity and mechanism of action of sea anemone toxins. FASEB J *26*, 5141-5151.

Peng, Z., Li, W.G., Huang, C., Jiang, Y.M., Wang, X., Zhu, M.X., Cheng, X., and Xu, T.L. (2015). ASIC3 Mediates Itch Sensation in Response to Coincident Stimulation by Acid and Nonproton Ligand. Cell reports *13*, 387-398.

Pfister, Y., Gautschi, I., Takeda, A.N., van Bemmelen, M., Kellenberger, S., and Schild, L. (2006). A gating mutation in the internal pore of ASIC1a. The Journal of biological chemistry *281*, 11787-11791.

Pignataro, G., Simon, R.P., and Xiong, Z.G. (2007). Prolonged activation of ASIC1a and the time window for neuroprotection in cerebral ischaemia. Brain *130*, 151-158.

Pless, S.A., and Ahern, C.A. (2013). Unnatural amino acids as probes of ligand-receptor interactions and their conformational consequences. Annu Rev Pharmacol Toxicol *53*, 211-229.

Posson, D.J., Thompson, A.N., McCoy, J.G., and Nimigean, C.M. (2013). Molecular interactions involved in proton-dependent gating in KcsA potassium channels. J Gen Physiol *142*, 613-624.

Price, M.P., Snyder, P.M., and Welsh, M.J. (1996). Cloning and expression of a novel human brain Na^+ channel. J Biol Chem *271*, 7879-7882.

Quintana, P., Soto, D., Poirot, O., Zonouzi, M., Kellenberger, S., Muller, D., Chrast, R., and Cull-Candy, S.G. (2015). Acid-sensing ion channel 1a drives AMPA receptor plasticity following ischaemia and acidosis in hippocampal CA1 neurons. J Physiol (Lond).

Ramaswamy, S.S., MacLean, D.M., Gorfe, A.A., and Jayaraman, V. (2013). Proton-mediated conformational changes in an acid-sensing ion channel. The Journal of biological chemistry *288*, 35896-35903.

Rossier, B.C., Pradervand, S., Schild, L., and Hummler, E. (2002). Epithelial sodium channel and the control of sodium balance: Interaction between genetic and environmental factors. Annu Rev Physiol *64*, 877-897.

Roy, S., Boiteux, C., Alijevic, O., Liang, C., Berneche, S., and Kellenberger, S. (2013). Molecular determinants of desensitization in an ENaC/degenerin channel. FASEB J *27*, 5034-5045.

Rudokas, M.W., Varga, Z., Schubert, A.R., Asaro, A.B., and Silva, J.R. (2014). The Xenopus oocyte cut-open vaseline gap voltage-clamp technique with fluorometry. Journal of visualized experiments : JoVE.

Salinas, M., Besson, T., Delettre, Q., Diochot, S., Boulakirba, S., Douguet, D., and Lingueglia, E. (2014). Binding site and inhibitory mechanism of the mambalgin-2 pain-relieving peptide on acid-sensing ion channel 1a. The Journal of biological chemistry *289*, 13363-13373.

Samways, D.S., Harkins, A.B., and Egan, T.M. (2009). Native and recombinant ASIC1a receptors conduct negligible Ca^{2+} entry. Cell Calcium *45*, 319-325.

Schild, L., Schneeberger, E., Gautschi, I., and Firsov, D. (1997). Identification of amino acid residues in the alpha, beta, and gamma subunits of the epithelial sodium channel (ENaC) involved in amiloride block and ion permeation. J Gen Physiol *109*, 15-26.

Schroeder, C.I., Rash, L.D., Vila-Farres, X., Rosengren, K.J., Mobli, M., King, G.F., Alewood, P.F., Craik, D.J., and Durek, T. (2014). Chemical synthesis, 3D structure, and ASIC binding site of the toxin mambalgin-2. Angew Chem Int Ed Engl *53*, 1017-1020.

Schurr, A. (2002). Lactate, glucose and energy metabolism in the ischemic brain (Review). Int J Mol Med *10*, 131-136.

Sherwood, T., Franke, R., Conneely, S., Joyner, J., Arumugan, P., and Askwith, C. (2009). Identification of protein domains that control proton and calcium sensitivity of ASIC1a. The Journal of biological chemistry *284*, 27899-27907.

Sherwood, T.W., and Askwith, C.C. (2008). Endogenous arginine-phenylalanine-amide-related peptides alter steady-state desensitization of ASIC1a. The Journal of biological chemistry *283*, 1818-1830.

Sherwood, T.W., Lee, K.G., Gormley, M.G., and Askwith, C.C. (2011). Heteromeric acid-sensing ion channels (ASICs) composed of ASIC2b and ASIC1a display novel channel properties and contribute to acidosis-induced neuronal death. J Neurosci *31*, 9723-9734.

Shi, S., Carattino, M.D., and Kleyman, T.R. (2012). Role of the wrist domain in the response of the epithelial sodium channel to external stimuli. The Journal of biological chemistry *287*, 44027-44035.

Sluka, K.A., Winter, O.C., and Wemmie, J.A. (2009). Acid-sensing ion channels: A new target for pain and CNS diseases. Curr Opin Drug Discov Devel *12*, 693-704.

Smith, M.L., von Hanwehr, R., and Siesjo, B.K. (1986). Changes in extra- and intracellular pH in the brain during and following ischemia in hyperglycemic and in moderately hypoglycemic rats. Journal of cerebral blood flow and metabolism : official journal of the International Society of Cerebral Blood Flow and Metabolism *6*, 574-583.

Smith, R.N., and Gonzales, E.B. (2014). Protons and Psalmotoxin-1 reveal nonproton ligand stimulatory sites in chicken acid-sensing ion channel: Implication for simultaneous modulation in ASICs. Channels (Austin) *8*, 49-61.

Springauf, A., Bresenitz, P., and Grunder, S. (2011). The interaction between two extracellular linker regions controls sustained opening of acid-sensing ion channel 1. The Journal of biological chemistry *286*, 24374-24384.

Stefani, E., and Bezanilla, F. (1998). Cut-open oocyte voltage-clamp technique. Methods in enzymology *293*, 300-318.

Sun, D., Yu, Y., Xue, X., Pan, M., Wen, M., Li, S., Qu, Q., Li, X., Zhang, L., Li, X.*, et al.* (2018). Cryo-EM structure of the ASIC1a-mambalgin-1 complex reveals that the peptide toxin mambalgin-1 inhibits acid-sensing ion channels through an unusual allosteric effect. Cell discovery *4*, 27.

Sutherland, S.P., Benson, C.J., Adelman, J.P., and McCleskey, E.W. (2001). Acid-sensing ion channel 3 matches the acid-gated current in cardiac ischemia-sensing neurons. Proc Natl Acad Sci USA *98*, 711-716.

van Bemmelen, M.X., Huser, D., Gautschi, I., and Schild, L. (2015). The Human Acid-Sensing Ion Channel ASIC1a: Evidence for a Homotetrameric Assembly State at the Cell Surface. PLoS One *10*, e0135191.

Virkki, L.V., Murer, H., and Forster, I.C. (2006). Voltage clamp fluorometric measurements on a type II Na$^+$-coupled Pi cotransporter: shedding light on substrate binding order. J Gen Physiol *127*, 539-555.

Voilley, N., de Weille, J., Mamet, J., and Lazdunski, M. (2001). Nonsteroid anti-inflammatory drugs inhibit both the activity and the inflammation-induced expression of acid-sensing ion channels in nociceptors. Journal of Neuroscience *21*, 8026-8033.

Vukicevic, M., and Kellenberger, S. (2004). Modulatory effects of acid-sensing ion channels on action potential generation in hippocampal neurons. Am J Physiol Cell Physiol *287*, C682-690.

Vukicevic, M., Weder, G., Boillat, A., Boesch, A., and Kellenberger, S. (2006). Trypsin Cleaves Acid-sensing Ion Channel 1a in a Domain That Is Critical for Channel Gating. J Biol Chem *281*, 714-722.

Vullo, S., Bonifacio, G., Roy, S., Johner, N., Berneche, S., and Kellenberger, S. (2017). Conformational dynamics and role of the acidic pocket in ASIC pH-dependent gating. Proc Natl Acad Sci U S A *114*, 3768-3773.

Waldmann, R., Bassilana, F., Deweille, J., Champigny, G., Heurteaux, C., and Lazdunski, M. (1997a). Molecular cloning of a non-inactivating proton-gated Na^+ channel specific for sensory neurons. J Biol Chem *272*, 20975-20978.

Waldmann, R., Champigny, G., Bassilana, F., Heurteaux, C., and Lazdunski, M. (1997b). A proton-gated cation channel involved in acid-sensing. Nature *386*, 173-177.

Wang, Q., and Lynch, J.W. (2012). A comparison of glycine- and ivermectin-mediated conformational changes in the glycine receptor ligand-binding domain. The international journal of biochemistry & cell biology *44*, 335-340.

Wemmie, J.A., Askwith, C.C., Lamani, E., Cassell, M.D., Freeman, J.H., Jr., and Welsh, M.J. (2003). Acid-sensing ion channel 1 is localized in brain regions with high synaptic density and contributes to fear conditioning. J Neurosci *23*, 5496-5502.

Wemmie, J.A., Chen, J., Askwith, C.C., Hruska-Hageman, A.M., Price, M.P., Nolan, B.C., Yoder, P.G., Lamani, E., Hoshi, T., Freeman, J.H.*, et al.* (2002). The Acid-Activated Ion Channel ASIC Contributes to Synaptic Plasticity, Learning, and Memory. Neuron *34*, 463-477.

Wemmie, J.A., Coryell, M.W., Askwith, C.C., Lamani, E., Leonard, A.S., Sigmund, C.D., and Welsh, M.J. (2004). Overexpression of acid-sensing ion channel 1a in transgenic mice increases acquired fear-related behavior. Proc Natl Acad Sci U S A *101*, 3621-3626.

Wemmie, J.A., Price, M.P., and Welsh, M.J. (2006). Acid-sensing ion channels: advances, questions and therapeutic opportunities. Trends Neurosci *29*, 578-586.

Wemmie, J.A., Taugher, R.J., and Kreple, C.J. (2013). Acid-sensing ion channels in pain and disease. Nature reviews Neuroscience *14*, 461-471.

Wiemuth, D., Sahin, H., Falkenburger, B.H., Lefevre, C.M., Wasmuth, H.E., and Grunder, S. (2012). BASIC--a bile acid-sensitive ion channel highly expressed in bile ducts. FASEB J *26*, 4122-4130.

Wu, P.-Y., Huang, Y.-Y., Chen, C.-C., Hsu, T.-T., Lin, Y.-C., Weng, J.-Y., Chien, T.-C., Cheng, I.H., and Lien, C.-C. (2013). Acid-sensing ion channel-1a is not required for normal hippocampal LTP and spatial memory. J Neurosci *33*, 1828-1832.

Wulf, M., and Pless, S.A. (2018). High-Sensitivity Fluorometry to Resolve Ion Channel Conformational Dynamics. Cell reports *22*, 1615-1626.

Xiong, Z.G., Zhu, X.M., Chu, X.P., Minami, M., Hey, J., Wei, W.L., MacDonald, J.F., Wemmie, J.A., Price, M.P., Welsh, M.J.*, et al.* (2004). Neuroprotection in ischemia: Blocking calcium-permeable acid- sensing ion channels. Cell *118*, 687-698.

Yang, H., Yu, Y., Li, W.G., Yu, F., Cao, H., Xu, T.L., and Jiang, H. (2009). Inherent dynamics of the acid-sensing ion channel 1 correlates with the gating mechanism. PLoS Biol *7*, e1000151.

Yoder, N., and Gouaux, E. (2018). Divalent cation and chloride ion sites of chicken acid sensing ion channel 1a elucidated by x-ray crystallography. PLoS One *13*, e0202134.

Yoder, N., Yoshioka, C., and Gouaux, E. (2018). Gating mechanisms of acid-sensing ion channels. Nature *555*, 397-401.

Yu, Y., Chen, Z., Li, W.G., Cao, H., Feng, E.G., Yu, F., Liu, H., Jiang, H., and Xu, T.L. (2010). A nonproton ligand sensor in the acid-sensing ion channel. Neuron *68*, 61-72.

Yu, Y., Li, W.G., Chen, Z., Cao, H., Yang, H., Jiang, H., and Xu, T.L. (2011). Atomic level characterization of the nonproton ligand-sensing domain of ASIC3 channels. The Journal of biological chemistry *286*, 24996-25006.

Zha, X.M., Costa, V., Harding, A.M., Reznikov, L., Benson, C.J., and Welsh, M.J. (2009). ASIC2 subunits target acid-sensing ion channels to the synapse via an association with PSD-95. J Neurosci *29*, 8438-8446.

Zha, X.M., Wemmie, J.A., Green, S.H., and Welsh, M.J. (2006). Acid-sensing ion channel 1a is a postsynaptic proton receptor that affects the density of dendritic spines. Proc Natl Acad Sci U S A *103*, 16556-16561.

Zhang, P., Sigworth, F.J., and Canessa, C.M. (2006). Gating of acid-sensitive ion channel-1: release of Ca^{2+} block vs. allosteric mechanism. J Gen Physiol *127*, 109-117.

Ziemann, A.E., Allen, J.E., Dahdaleh, N.S., Drebot, II, Coryell, M.W., Wunsch, A.M., Lynch, C.M., Faraci, F.M., Howard, M.A., 3rd, Welsh, M.J*., et al.* (2009). The amygdala is a chemosensor that detects carbon dioxide and acidosis to elicit fear behavior. Cell *139*, 1012-1021.

Zuo, Z., Smith, R.N., Chen, Z., Agharkar, A.S., Snell, H.D., Huang, R., Liu, J., and Gonzales, E.B. (2018). Identification of a unique Ca(2+)-binding site in rat acid-sensing ion channel 3. Nat commun *9*, 2082.